Investigating the form and function of the mouse blastocyst fluid lumen

Allyson Ryan

Thèse de doctorat de

EMBL Heidelberg et de

L'Université Sorbonne Paris Cité

Préparée à l'Université Paris Diderot

Ecole doctorale Physique en Île-de-France ED564

Laboratoire Matière et Systèmes Complexes

Investigating the Form and Function of the Mouse Blastocyst Fluid Lumen

Par Allyson RYAN

Thèse de doctorat de Physique

Dirigée par François GRANER, PhD

Présentée et soutenue publiquement à l'Université Paris Diderot le 04.07.2019

Président du jury : Jérôme COLLIGNON, PhD, Insitut Jacques Monod

Rapporteurs : Muriel GRAMMONT, PhD, Ens Lyon-Monod et Alexander AULEHLA, PhD, EMBL Heidelberg

Directeur de thèse : François GRANER, PhD, l'Université Paris Diderot

Co-directeurs de thèse : Takashi HIIRAGI, PhD, EMBL Heidelberg

Membre invités : Jacqueline TABLER, PhD, MPI-CBG Dresden

Titre :
Étude de la forme et la fonction de la lumière du blastocyste de souris

Résumé :
La formation de blastocystes de souris implique la formation de lumière et la spécification du destin de cellules. Bien que de nombreuses études aient étudié la façon dont les lignées de cellules de blastocystes sont spécifiées par la génétique et la signalisation, des études sur le rôle potentiel de la lumière du fluide n'ont pas encore été menées. Nous découvrons que le liquide de blastocyste émerge par la sécrétion de vésicules cytoplasmiques dans l'espace intercellulaire en plus du flux trans épithélial. Nous observons que le début de la ségrégation spatiale des épiblastes et des endodermes primitifs suit directement la coalescence de la lumière. Nous montrons notamment que la perturbation de l'expansion de la lumière par des moyens pharmacologiques et biophysiques altère la spécification et la ségrégation spatiale des cellules d'endoderme primitives au sein du blastocyste. Ensemble, nos résultats suggèrent que l'expansion de la lumière du blastocyste joue un rôle critique dans la spécification et le positionnement du destin des cellules. Comme les tissus épithéliaux forment typiquement une lumière, l'expansion de la lumière peut fournir un mécanisme général de contrôle du destin cellulaire dans de nombreux tissus.

Mots clefs :
souris, développement, blastocyste, lumière, signalisation

Title :
Investigating the Form and Function of the Mouse Blastocyst Fluid Lumen

Abstract :
Mouse blastocyst formation involves lumen formation and cell fate specification. While many studies have investigated how the blastocyst cell lineages are specified through genetics and signaling, studies into the potential role of the fluid lumen have yet to be conducted. We discover that blastocyst fluid emerges by secretion of cytoplasmic vesicles to intercellular space in addition to trans-epithelial flow. We observe that the beginning of epiblast and primitive endoderm spatial segregation directly follows lumen coalescence. Notably, we show that perturbing lumen expansion by pharmacological and biophysical means impair the specification and spatial segregation of primitive endoderm cells within the blastocyst. Combined, our results suggest that blastocyst lumen expansion plays a critical role in guiding cell fate specification and positioning. As epithelial tissues typically form lumina, lumen expansion may provide a general mechanism of cell fate control in many tissues.

Keywords :
mouse, development, blastocyst, lumen, signaling

Investigating the Form and Function of the Mouse Blastocyst Fluid Lumen

Allyson Quinn Ryan

4 July 2019

Contents

Acknowledgements

The work presented in this thesis would not have been possible without the support of many, many people. I am immensely grateful to all of you for reasons so varied and extensive that they cannot be done justice here. Therefore, I will keep my statements of thanks brief, but please know that no words would suffice to sum up the past [nearly] four years.

To Dr. Takashi Hiiragi, thank you for giving me the opportunity to pursue my PhD in your group. This has been an invaluable experience not simply for my scientific career, but also for general professional development. I have learned what feels to be an immeasurable amount under your supervision.

To Dr. François Graner, thank you for making it possible for me to undertake the daunting task of completing a PhD. Your advice in both scientific and personal subject matter has greatly influenced how my skills as a scientist have developed. Because of my experiences under your supervision, I am excited about the possibility to push further into interdisciplinary research.

To my coauthors and thesis committee members, you have guided, mentored and encouraged me through the peaks and valleys of this process. As I am acutely aware, there were some particularly *deep* valleys, and I must extend additional gratitude to you for not giving up on me during these times. Furthermore, I would like to acknowledge Dr. Darren Gilmour, who initially encouraged me to pursue a PhD.

To all of the colleagues I have had during my time in the Hiiragi Group, we have shared many memories. As I said, trying to thank you all here would be impossible so I have opted for word association with a special memory for those who I have spent the most time with: Joe (plums), Laura (Singapore), Esther (paella), Dimitri (09:00 Mondays), Hui Ting (tickly dragons) and Prachiti (Flax the Drumstick).

To my loving family, without you I would never have made it anywhere. Therefore, I think this achievement belongs as much to you as it does to me. You have always supported me in my studies but not at the expense of teaching me the value of other things in life (like common sense).

To my friends, 'My Important People', we are all moving on soon (within the next year anyhow). The four of us have been through a lot together and still manage to enjoy science and sort of have social lives...? Let's keep all our fingers and toes crossed that we stay close enough to get each other through whatever comes at us next. So, here is to the next step for each of us! Prost und viel Glück!

Chapter 1

Introduction I: Lumen Formation and Function in Development

Lumina are common multicellular structures found in a wide range of epithelial tissues (Sigurbjörnsdóttir et al., 2014). Lumen formation is broadly classified into two different classes of mechanisms, which will in this thesis be referred to as 'space enclosure' and '*de novo* lumen formation.' Space enclosure is the formation of a separated space within a tissue or organ that either already contains an empty (i.e. there are no cells within the space) space, or is adjacent to an open space (e.g. an extracellular environment that the tissue with 'reach' into). In the field of developmental biology, the formation of the neural tube is arguably the most famous example of space enclosure. To form the neural tube, which is a precursory structure for the Central Nervous System, the neural plate undergoes local tissue thickening to produce neural folds that reach into the extracellular space above the neural plate, navigate toward the embryo's midline and fuse to form the neural tube and other tissues (Gilbert 2000).

While space enclosure is the mechanism underlying the proper morphogenesis of multiple developmental processes, *de novo* lumen formation will be the focus of the bulk of this chapter. *De novo* lumen formation is the emergence of an empty space within or between tissues where that specific volume is initially occupied by cells (i.e. the spatial rearrangement of cells as either individuals or collectives to vacate a certain space). This process is absolutely essential to vertebrate embryonic development as without it, many tube- or cyst-based organ systems (i.e. respiratory, vascular, digestive, excretory, etc.) would undergo improper morphogenesis and the basic functions of such systems would be compromised.

Although it is crucial for development, *de novo* lumen formation has been most extensively studied by cell biologists. The wealth of information characterizing the molecular regulation of *de novo* lumen formation is due largely to studies conducted on MDCK (Madin-Darby canine kidney) cells in 3D *in vitro* culture systems (as it would easily exceed 100 citations to attempt referencing all molecular regulation of polarity establishment and lumen formation studies in MDCK cysts here are three of the most prominent and relevant results for the purposes of this

project – Bryant et al., 2010 and 2014; Martin-Belmonte et al., 2007).

The molecular pathways, particularly those involved in establishing and regulating apicobasal polarity, are tightly regulated during lumen morphogenesis and have been studied extensively (reviewed here – Blasky et al., 2015; Bryant and Mostov, 2008; Martin-Belmonte and Mostov, 2008; Rodriguez-Boulan and Macara, 2014). Briefly, the highly conserved molecular events of *de novo* lumen formation are as follows: membrane organization, junctional assembly and secretory machinery organization. These events will be described for cord hollowing, a more specific form of *de novo* lumen formation, in the following section.

Moving on from the molecular (i.e. subcellular or transcriptional) regulation of lumen formation is indeed important, the remaineder of this introduction will focus almost exclusively on the cell (i.e. membrane domain partitioning) and tissue (i.e. multicellular coordination) levels of organization. It is important to note that the typical morphology of tubular and cystic lumina consists of the apical domain of cells encasing a hollow space that is sealed by junctions, typically tight junctions, formed at the boundaries between apical and basal (basolateral) membrane domains of cells (Bryant and Mostov, 2008). Extending upon this for the case of *de novo* lumen formation, there must be a luminal initiation site (i.e. a membrane subsection that the cell can distinguish as possessing different properties that the rest of its membrane) in order to form a lumen at the correct position within a tissue. In most tissues, the positioning of the initiation site is coordinated through the interplay of cell adhesions and the cell cortex. Intuitively, if the membrane domains that will eventually encapsulate the fluid lumen are to be apical, the initiation site must form opposite to, or at least be excluded from, basal membrane domains. While the initiation site is specific to the *de novo* mechanism, the principle of membrane partitioning hold true for the organization of both space enclosure and *de novo* lumen formation.

1.1 *De Novo* Lumen Formation

There are multiple mechanisms of *de novo* lumen formation. These include, but are not limited to: cord hollowing, cell hollowing and cavitation. Two of these mechanisms, cord hollowing and cell hollowing, can for the purposes of this thesis be considered analogous mechanisms differing in a single prerequisite, which is the number of cells involved in the process. Cord hollowing pertains to multicellular lumen formation; cell hollowing, single cell lumen formation. Cavitation, however, is a markedly different mechanism of *de novo* lumen formation as the empty space is created at the contacts between cells, but through the apoptosis of several cells (Schematic 1).

Schematic 1. *De novo* lumen formation via cavitation creates a new hollow space through the clearance of several apoptotic cells within the boundaries of a junctional seal.

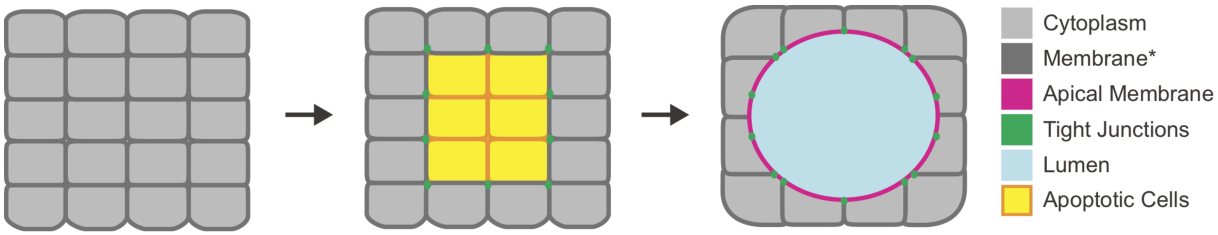

The aforementioned mechanisms of *de novo* lumen formation and some of the more specific molecular (i.e. subcellular) programs underlying each have been nicely reviewed by Sigurbjörnsdóttir et al., 2014; however, the remainder of this chapter will focus solely on the cord hollowing mechanism. Below is a simplified description of classical cord hollowing, henceforth referred to as 'apical cord hollowing (ACH),' to provide sufficient background into the mechanism in order to inform on the reasoning behind the experiments presented in later chapters.

The process of ACH can generalized into three steps (Schematic 2):

1. Cells involved in the lumen formation partition their apolar (i.e. uniform in composition) plasma membrane into apical and basolateral domains and acquire junctions (typically tight junctions) at the borders between the domains.

2. Nascent secretory vesicles and recycling vesicles containing components for lumen expansion are directed to the apical domain to undergo either content secretion or integration into the plasma membrane. Through this and other mechanisms (e.g. osmotic regulation) the lumen begins to open.

3. The lumen continues to expand, and, if applicable, microlumina (i.e. small fluid pockets isolated from the dominating lumen) undergo coalescence until the cyst or tube achieves its final geometry.

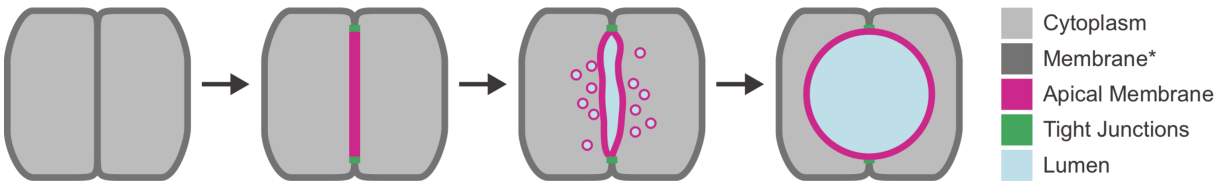

Schematic 2. ACH occurs through the specialization of membrane domains, formation and maturation of junctional boundaries, directed secretion of apical membrane and other lumen components, followed by luminal coalescence and expansion.

The mouse blastocyst lumen is formed *de novo* through cord hollowing-like actions. There are two significant departures from ACH in the context of the mouse blastocyst:

1. The orientation of the apical and basolateral membrane domains of the cells surrounding the lumen is inverted to that of typical cysts and tubes (e.g. MDCK cells).

2. The cell layers surrounding the lumen are not equally distributed (i.e. there is a distinct axis of symmetry created when the blastocyst lumen forms).

These points will be elaborated upon in **Introduction II: Mouse Blastocyst Morphogenesis**.

1.2 Tubulogenesis and Lumen Function in Development

Continuous tube formation and expansion are necessary morphogenetic steps in the embryonic development of multiple organ systems. Many such tubes are formed via the ACH mechanism of *de novo* lumen formation. Depending on the tissue and developmental time, lumina can serve various purposes including inducing, but not limited to: cell shape change, nutrient delivery and absorption, tissue or organ level symmetry breaking and even signaling niches (Gebala et al., 2016; Sobajima et al., 2015; Essner et al., 2005; Durdu et al., 2014). Furthermore, tissue (and sometimes organism) dependent lumen maturation mechanisms can exist. A few examples of such mechanisms include:

1. Rab dependent microvilli maturation and orientation (functional acquisition) during *Mus musculus* intestinal maturation (Sobajima et al., 2015).

2. Genetic control of singular lumen resolution via adhesion remodeling during *Danio rerio* intestinal development (Alvers et al., 2014; Bagnat et al., 2007).

3. Cell lineage spatial domain restriction and cell fate allocation ratio control through apical polarity mediated lumen coalescence during embryonic *Mus musculus* pancreas development (Kesavan et al., 2009).

4. Afadin dependent reorganization and coalescence of apical membrane microdomains lining the lumen of the developing mouse nephron (Yang et al., 2013).

These studies, along with many of the 3D MDCK investigations, begin to point towards a clear commonality of illuminated tissues, which is that failure to reach proper luminal morphology inevitably leads to alterations in tissue function. Investigations into the molecular regulation of polarity programs required for lumen initiation and resolution within the embryonic mouse pancreas revealed an interesting effect of luminal morphology on the fate specification of immediately adjacent cells as well as cells in subsequent tissue layers. This effect was described as a change in the allocation of cell fates i.e. the ratios of cell types within a developing organ system is perturbed due to a failure of luminal resolution (summarized in Schematic 3; Kesavan et al., 2009). The results of the study identified Cdc24 as a regulator for the coalescence of apical membrane microdomains within the developing mouse pancreas. Upon failure to resolve the apical domain on a tissue level, the proportions and spatial positioning of acinar and endocrine cells were altered within the developing organ (i.e. the number of acinar cells increased at the expense of endocrine cells; Kesavan et al., 2009).

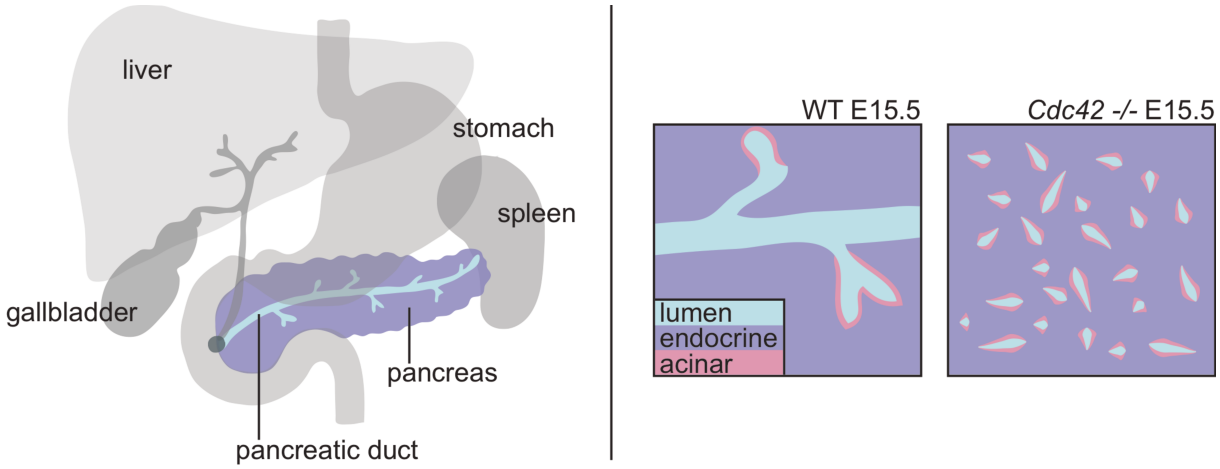

Schematic 3. Resultant luminal morphology dictates cell fate allocation ratios within the developing embryonic mouse pancreas.

During mouse proamniotic lumen formation, PTEN, an apically localized $PIP_{2,3}$ converter, is proposed to be critical to the selection of a dominating luminal rosette (i.e. luminal positioning site) thereby functioning similarly to Cdc24 during pancreatic lumen morphogenesis (Meng et al., 2017). The importance of either selecting a dominant initiation site for lumen formation or resolving all initiation sites into one is common to several, if not most systems that utilize ACH. The formation and resolution of initiation sites is relatively simple in systems with small starting cell numbers (e.g. an MDCK cell doublet in 3D gel culture); however, in systems with increased starting cell number and thus also an increase in the potential number of initiation sites, resolution of competing initiation sites would quickly become time consuming without mechanisms for selection or establishing biases. While these regulatory mechanisms have been described in a few systems, in most cases they remain largely unknown. As can be seen during zebrafish intestinal lumen formation, perturbation of a resolution mechanism can disrupt not only the final geometry of the illuminated tissue...

Despite the fact that the cells surrounding lumina are often highly specialized (i.e. of a specific cell fate or lineage), the potential for lumina to feed into the process of cell fate specification or maintenance has yet to be investigated. If this were to be shown conclusively, it would offer a unifying function of lumina across several systems.

Chapter 2

Introduction II: Mouse Blastocyst Morphogenesis

The majority of this chapter contains context-specific (i.e. mouse pre-implantation embryogenesis specific) information. To aid in the interpretation and understanding of subsequent sections, below is a brief overview of general mechanisms of cell fate specification in embryogenesis. In cellularized embryonic development, there are two main types of cell fate specification: autonomous and conditional specification (Gilbert 2000). Here, autonomous specification is split into two mechanisms ('Determinant' and 'Invariant Cleavage'), which are defined below along with conditional specification (adapted and summarized from Gilbert, 2000 and Davidson, 1990):

1. **Determinant Specification**: a mode of cell commitment (i.e. an irreversible state of differentiation from a previously more potent state) in which the blastomere either inherits a determinant (e.g. a set of maternally deposited transcription factors in the egg cytoplasm) that regulates gene expression to direct either itself or a neighboring cell through a particular path of development.

2. **Invariant Cleavage Specification**: the fertilized egg undergoes an strict cleavage pattern that robustly results in exactly the same distribution of cells in all embryos of that species (i.e. Both the final positions and trajectories of a blastomere and its progeny would be identical between replicates within a single species).

3. **Conditional Specification**: the ability of cells to achieve their respective fates through interactions with other cells. What a cell becomes is, likely, in large measure specified by paracrine factors secreted by its neighbors, cell-cell interactions (e.g. adhesion) and cell-niche interactions. Key to this mechanism is the concept of plasticity (i.e. the ability of a cell to either retain its potency for multiple lineages or to initiate a differentiation path but not yet become terminally committed), which allows a cell to change its prospective lineage based on received cues from its surroundings.

Several popular model organisms for developmental biology studies involve autonomous specification from the first cleavage-stage division (e.g. tunicates; Schematic 4). Through asymmetric deposition of fate and/or axis determining factors and/or mRNAs between blastomere cytoplasm, the embryo is able to robustly develop to blastula stages (Determinant Specification). This can also be coupled with stereotypic cleavage patterns (Invariant Cleavage Specificiation), which can aid further robustness to the final patterning of the blastula.

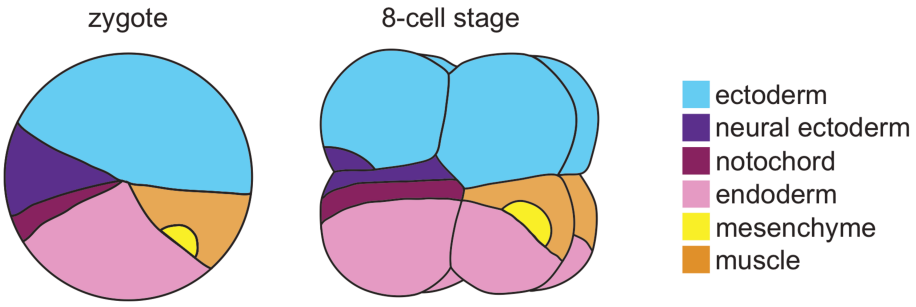

Schematic 4. Distinct regions of the zygotes, and subsequently blastomeres, of organisms that develop via pre-patterning mechanisms (e.g. ascidians; depicted here) are committed to develop into specific tissue types.

While modes of autonomous specification, henceforth referred to as 'pre-patterning', are critical for early embryogenesis in many organisms, some systems (e.g. mammalian preimplantation embryos) rely entirely on conditional specification during embryonic stages (i.e. the organism's embryonic development is self-organized). It should also be acknowledged that even in species which utilize autonomous specification mechanisms, post-blastula and post-gastrulation stage embryos often require conditional specification when cell-interaction geometry (i.e. faces of contact) and determinant diffusion fields become increasingly complex as development progresses.

The following sections will explain proposed cell fate specification models for preimplantation mouse development and the current evidence supporting conditional fate specification (i.e. self-organized) models before delving deeper into individual lineages. It is important to note that while the textbook definition of conditional cell fate specification leans heavily on the importance of paracrine signaling and cell-cell adhesion, other criteria (i.e. cell position, cell microenvironment, etc.) may have equal weight in determining a cell's lineage commitment though these are far less explored possibilities.

2.1 Cell Fate Specification during Blastocyst Formation

Three major models have been proposed for fate patterning during the first lineage segregation event of pre-implantation mouse development – the pre-patterning model, the inside-outside model and the cell polarity model (comprehensively reviewed in Wennekamp et al., 2013). The

pre-patterning model is a classic form of determinant autonomous specification as it is centered around either the asymmetric localization of maternally deposited cytoplasmic factors or sperm entry point. Both the inside-outside (Tarkowski, 1959; Tarkowski and Wróblewska, 1967) and cell polarity (Johnson and Ziomek, 1981) models are forms of conditional specification. The inside-outside model proposes that the position of a blastomere relative to its neighboring cells and the extraembryonic environment (i.e. contact-free surfaces) dictates its downstream differentiation and commitment pathway (Tarkowski, 1959; Tarkowski and Wróblewska, 1967). The cell polarity model, however, proposes that a daughter cell's ability or inability to apically polarize based on division plane is the deciding factor in lineage commitment (Johnson and Ziomek, 1981). Classifying the cell polarity model as a form of conditional specification may be seen as controversial given that it involves asymmetric inheritance of polarity determinants. However, recent work, as well as a condition of the original proposal, shows that the division plane is not pre-determined by the cell itself, but rather by its neighbors (Johnson and Ziomek, 1981; unpublished results from the Hiiragi Group).

Blastomere isolation experiments have been used to argue against pre-patterning in other systems (e.g. Dreisch's sea urchins; Dreisch, 1892; Schematic 5). Mouse blastomere isolation and differential contractility experiments have convincingly provided evidence contradicting the pre-patterning model and supporting the conditional specification models but cannot distinguish between the inside-outside and cell polarity models (Korotkevich et al., 2017; Maitre et al., 2016; Tarkowski, 1959; Tarkowski and Wróblewska, 1967; Schematic 6). Instead, these results point more towards a merge of the two conditional models. Such a joint model, while inherently more complicated due to a necessary balancing act between multiple active mechanisms feeding into a single end-state, fittingly displays the immense regulatory potential of self-organized systems.

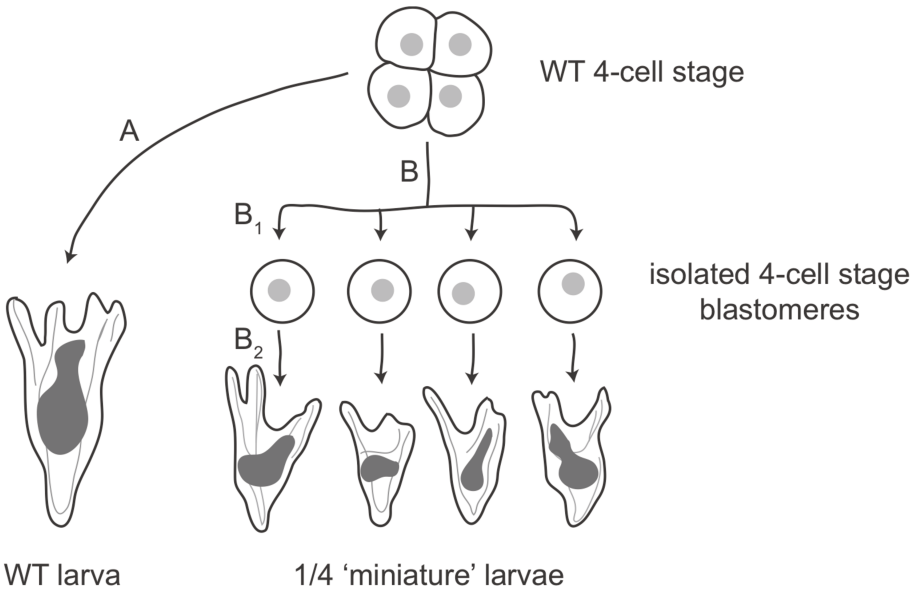

Schematic 5. Sea urchin blastomere isolation experiments (path B or B_1,B_2) exhibit the process of conditional specification as the resultant 'miniature' larvae are morphologically similar to WT larvae (path A) except in size.

Classically, conditional specification is thought to be mediated through cell-cell contact, that is to say a cell's fate is determined by interactions with neighboring cells (e.g. paracrine signaling or differential adhesion profiles). However, recent years have shown that alterations to the external environment (e.g. extracellular matrix stiffness) are capable of influencing or altering an uncommitted cell's differentiation path (reviewed by Kumar et al., 2017; Engler et al., 2005). Fitting with a joint conditional model, recent research has made it clear that cell polarity (apico-basal), cell-cell adhesion and cell position (inner v. outer) play important roles in cell lineage establishment and maintenance within the early mouse embryo (Korotkevich et al., 2017; Maitre et al., 2016; Stephenson et al., 2010). This is particularly well documented for the first lineage segregation event during preimplantation mouse development (trophectoderm-inner cell mass differentiation; described in detail in the paragraphs). While these findings have greatly advanced the knowledge of mechanisms at play during conditional specification, much remains to be understood as it is not yet clear if any single form of cell-cell or cell-niche environment has a dominating effect over others.

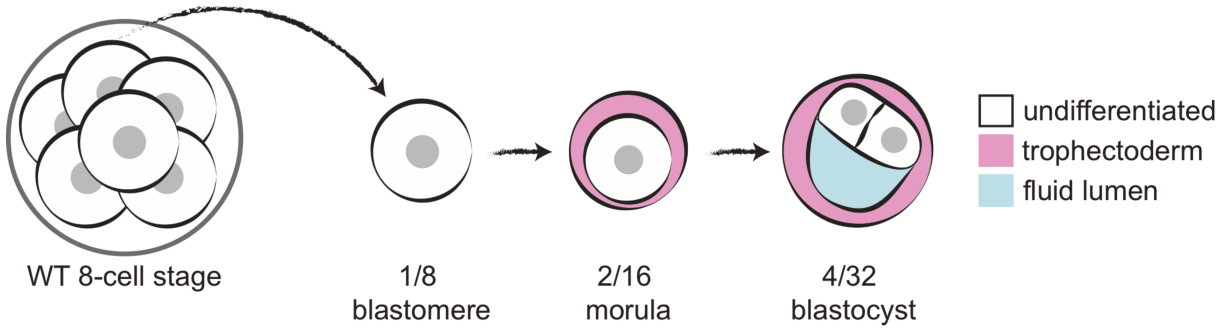

Schematic 6. Isolated blastomeres from an 8-cell stage mouse embryo recapitulate wild-type molecular and morphological changes associated with morula to blastocyst transition.

The culmination of preimplantation stages is formation of a blastocyst containing three spatially segregated cell lineages and an abembryonically localized fluid lumen (Schematic 7). The molecular specification of the three cell lineages – trophectoderm (TE), epiblast (EPI) and primitive endoderm (PrE) – occurs sequentially over two rounds of lineage establishment, but are not directly coincident with morphogenetic changes (Artus et al., 2011; Chazaud et al., 2006; Rossant and Tam, 2009). Preceding the first lineage segregation a major morphogenetic change, known as compaction, must first occur. The second lineage segregation event occurs in parallel with a second morphogenetic change of the embryo – the emergence of the blastocyst fluid lumen.

Compaction of the 8-cell embryo is a process through which the contact-free surface area of the embryo is minimized and the cell-cell interface area is maximized (Maître et al., 2015). A compacted embryo is referred to as a morula. This process is driven by periodic cortical contractility and changes in surface tension at cell-cell and cell-medium interfaces (Maître et al., 2015). Though compaction precedes the first lineage segregation event, it is tightly linked to changes in cell adhesion and the acquisition of apical polarity that are known to impact fate specification when disrupted (Hirate et al., 2013; Korotkevich et al., 2017; Stephenson et al., 2010). Additionally, the mechanisms driving compaction are biophysical and alter each cell's immediate environment. The inclusion of mechanical signals as well as biochemical signals greatly increases the pool of potential conditional fate specification mediators leading into the 16-cell stage.

Asymmetric inheritance of the apical domain and differential contractility between daughter cells of the 16-cell stage embryo result in apolar inner cells that upregulate inner cell mass (ICM) markers and polarized outer cells that upregulate TE markers (Anani et al., 2014; Korotkevich et al., 2017; Maître et al., 2016; Nishioka et al., 2009; Strumpf et al., 2005). There is substantial documentation of Hippo pathway activity during TE-ICM specification (reviewed by Sasaki 2015). The pathway effectors YAP/TAZ; phospho-YAP, known to be mechosensitive, are also well documented to show TE or ICM specific expression patterns in 16-cell stage embryos that are sensitive to changes in cortical tension affecting compaction (Maître et al., 2016). Alterations of apicobasal polarity also interfere with the localization of Hippo pathway components and downstream TE-ICM specification (Hirate et al., 2013; Nishioka et al., 2009). Collectively, investigations of Hippo signaling, polarity regulation and changing physical forces during the 8- and 16-cell stages reveal that differentiation to the molecular identify of either TE or ICM is likely achieved through feedback and crosstalk of multiple mechanisms, both biochemical and biophysical. The natural followup question would then be, 'Does the same hold true for the second lineage segregation event?,' which has received far less attention regarding potential biophysical inputs.

Subsequent cleavage rounds to 32, 64 and 128-cell stages see the establishment of the EPI and PrE cell lineages. The 16- to 32-cell cleavage cycle maintains the apicobasal polarity and TE-ICM differentiation established during the 8- and 16-cell stages. During the 32-cell stage, ICM cells are stochastically biased toward either EPI or PrE identity on a molecular level (Chazaud et al., 2006; Guo et al., 2010; Kang et al., 2013; Ohnishi et al., 2014; Schrode et al., 2014). These biases are either reinforced or changed during the remainder of pre-implantation development depending on cell rearrangements and final cell position within the ICM, such that the EPI cells are situated between TE and PrE cells, which align along the luminal surface (Frankenberg et al., 2011; Plusa et al., 2008; Saiz et al., 2013).

Both the compacted 8- and 16-cell stages are referred to as morula stages and are reached at the end of the second embryonic day (E2.5-E3.0). The morphogenetic transition from morula to blastocyst occurs over the remainder of the pre-implantation timeline (E3.0-E4.5). Throughout the literature, it is common to find statements along the lines of, 'Blastocyst formation occurs at the 32-cell stage...' However, as will be presented and discussed at length during later chapters, these statements, while convenient, lack precision. Similar to compaction, blastocyst lumen formation is initiated prior to EPI-PrE specification; in contrast, while compaction is completed before TE-ICM specification, blastocyst lumen morphogenesis continues to form and expand as EPI-PrE specification occurs. Because of these differences in the timing of completion of each event, molecular or morphogenetic, the first two lineage segregation events are not directly comparable.

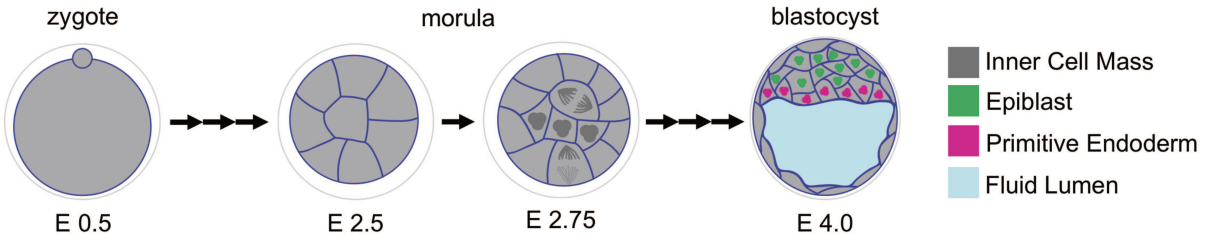

Schematic 7. Cell fate specification in mouse preimplantation development.

Before delving into the underlying molecular programming of blastocyst lumen formation and EPI-PrE specification, it is important to summarize the steps that achieve proper morula morphogenesis, without which blastocyst morphogenesis cannot occur. Some of these points will become more detailed later in the chapter. An embryo capable of proceeding to the blastocyst stage must first successfully:

1. Blastomeres initiate apico-basal polarization at the 8-cell stage so that the outer cells of the 16-cell stage embryo (fated to become TE cells) will have apical domains interacting with the extracellular environment and basolateral domains forming the adherens-based cell-cell adhesion (Ziomek and Johnson, 1980; Stephenson et al., 2010; Korotkevich et al., 2017).

2. The 8-cell stage embryo undergoes compaction through which intercellular spaces within the embryo are eliminated (Ziomek and Johnson, 1980).

3. Post-compaction, the morula develops a 'permeability seal' which is principally composed of a tight junction network that also determines the boundaries between apical and basolateral domains of the outer cells (Eckert and Fleming, 2008).

4. Division to the 16-cell stage yeilds the first inner cells (fated to become the ICM) arise through asymmetric divisions and differential cortical contractility so that the inner cells are naive to contact with the external environment and the plasma membrane is completely apolar in composition (Korotkevich et al., 2017). This is also the point at which differences in subcellular phosphoYAP localization, indicative of differences in mechanoreception, is observed (Maître et al., 2016).

5. After the tight junctional complexes within the permeability seal are mature, the embryo has the capacity to initiate fluid accumulation. The precise timing of this action varies between embryos; it is typically during the transition from 16- to 32-cell stage (unpublished data; Fernández and Izquierdo, 1980).

2.2 Molecular Specification of Inner Cell Mass Lineages

Many studies have been conducted to investigate the molecular identity of the EPI and PrE lineages and how they emerge from a single progenitor population. While there are intersection points of pathways involved in the specification of both lineages (e.g. ERK signaling), this section will be focused more specifically on the main regulators of PrE specification identified thus far. The full timeline of PrE maturation, from initial transcriptional biases through epithelialization, has been nicely reviewed by Hermitte and Chazaud (2014). Given the scope and aims of this project (see **Project Motivation and Central Questions**), the information presented here will only briefly extend into the process of PrE epithelialization in a later section.

The most prominently discussed regulator of PrE specification is FGF4. In has been known for several decades that in cases of perturbed FGF signaling through the loss of FGF4 or FGFR2 mouse embryos do not undergo proper morphogenesis beyond pre-implantation stages (Arman et al., 1998; Feldman et al., 1995). FGF4-FGFR1/2 signaling is both paracrine and autocrine during ICM differentiation into EPI and PrE (Kang et al., 2017; Molotkov et al., 2017). It has been shown to control the proportioning of EPI and PrE cells within the ICM (Krawchuk et al., 2013) as well as to be required for the restriction of PrE factors, such as Gata6, during later blastocyst development stages (Kang et al., 2013; Yamanaka et al., 2010).

FGF4-FGFR1/2 signaling feeds into the ERK signaling cascade, which often ends with transcription factor regulation (e.g. Gata6 or Nanog; Lanner and Rossant, 2010). ERK signaling cascade events within the developing ICM have been heavily investigated (Bessonnard et al., 2014; Frankenberg et al., 2011; Lanner and Rossant, 2010; Meng et al., 2018; Messerschmidt and Kemler, 2010; Nichols et al., 2009). By modulating Gata6, which is downstream of Erk1/2 in the signaling pathway, the timing of PrE fate specification can be modulated (Schrode et al., 2014). One study displayed that phosphorylation of Gata6 by Erk1/2 mediates an ICM cell's exit from a pluripotent state towards PrE commitment (Meng et al., 2018). This is consistent with results showing that Erk1/2 inhibition promotes a continued pluripotent state (Nichols et al., 2009).

Expanding on these findings, multiple circuits have been proposed for how FGF4/MAPK, ERK signaling and critical transcription factors are regulated to produce robust EPI-PrE specification events (Bessonnard et al., 2014; Schröter et al., 2015). The debate between a bi- or tri-stability regulatory networks as well as balances between cell autonomous and non-autonomous mechanisms are still ongoing. Setting these aside, the end states of multiple scenarios is clear and consistent across investigations: loss of either FGF4, FGFR1 or FGFR2 results in loss of the PrE lineage (Kang et al., 2013; Kang et al., 2017; Krawchuk et al., 2013; Molotkov et al., 2017), Nanog is required for PrE specification through EPI maintenance (Messerschmidt and Kemler, 2010) and Gata6 activity leads to exit from a pluripotent ICM state (Meng et al., 2018; Schrode et al., 2014). These signaling cascades result in the robust emergence of two molecularly distinct and differentiation initiated cell populations from the single ICM population: pluripotent FGF4 producing, EPI cells marked by high Nanog expression and the FGF4-receiving PrE cells marked by high Gata6 expression that have exited pluripotency.

In many cases FGF4/MAPK/ERK investigations and transcriptional studies point towards a unifying idea of how EPI and PrE programming occurs. However, knowledge on the molecular level has yet to be resolved with studies that have described which cells are producing FGF4 (EPI cells; Bessonnard et al., 2014) and in which domains PrE and TE cells express the corresponding receptors (FGFR2; Haffner-Krausz et al., 1999; Salas-Vidal and Lomelí, 2004). This is even further complicated when it is considered that FGFR1 is a pan-ICM receptor (Kang

et al., 2017; Molotkov et al., 2017). Additional questions arise when certain phenotypes are apparently dependent on either the distance of a receiving tissue from the source of the ligand or differential expression of the receptor across space within a tissue (Arman et al., 1998; Rassoulzadegan et al., 2000). These unresolved possibilities leave a substantial gap in the understanding of how signaling cascades are interpreted spatial scales exceeding a cell's immediate neighbors (i.e. Does ubiquitous ligand diffusion occur or some mechanism of ligand/receptor sequestration to subdomains within the embryo?).

2.3 Spatial Organization of Epiblast and Primitive Endoderm Lineages

At the end of pre-implantation, the two ICM lineages – EPI and PrE – have well-defined and exclusive spatial niches within the blastocyst (Schematics 7,8). While this is widely accepted within the field of pre-implantation development, very few studies have made it a point of central focus. In fact, even when it is acknowledged, this information is usually stated as a qualitative observation by which to stage the development of an embryo. Furthermore, the molecular mechanisms of EPI-PrE spatial niche formation (i.e. the resolution of initially intermingled precursors into spatially segregated tissues) are still unknown. While there have been a few attempts (ongoing and unpublished work in the Hiiragi Group and others; Meilhac et al., 2009), clean lines of investigation for mechanism identification are lacking. This is in part due to an insufficiency of applicable tools to dynamically and concurrently track molecular specification and spatial position. However, the main obstacle faced by studies attempting to identify a mechanism is the inability to answer whether the spatial pattern is determined through active cell movement, passive cell repositioning or molecular reprogramming.

A study investigating the role(s) of Rho-kinase/ROCK signaling within the preimplantation embryo reported the prolonged intermingling of EPI and PrE cells upon pharmacological inhibition of ROCK activity (Laeno et al., 2013). Other studies reported that ROCK inhibition prevents blastocyst lumen formation (Kawagishi et al., 2004) and simultaneously compromises the proportioning of TE and ICM cells (Laeno et al., 2013). These findings, particularly the prolonged intermingling of EPI and PrE cells in embryos with reduced luminal volume, are intriguing with regard to if and how the two processes, EPI-PrE spatial segregation and lumen expansion may be linked. However, ROCK inhibition has been shown to perturb several processes within the cell and is therefore insufficient to answer these questions. Therefore, more precise methods of perturbation are necessary to determine significant mechanisms at play.

Successful blastocyst morphogenesis (i.e. proper spatial partitioning of blastocyst cell lineages and lumen formation) permits the embryo to proceed to peri- and post-implantation stages of embryonic development (E4.5 onwards). Apparent failure to spatially segregate ICM lineages

(i.e. position the PrE on the surface of the blastocyst lumen) leads to embryonic lethality is the earliest post-implantation stages (E5.0; Moore et al., 2015; Stephens et al., 1995; Yang et al., 2007). These studies rely exclusively on the genetic knockout of either adhesion or selective cargo membrane redistribution machinery. The results suggest that the cell-cell adhesion or adhesion remodeling is important for the EPI-PrE spatial segregation progress. A recent study has shown that Cdh1 zygotic knockout embryos are capable of EPI-PrE segregation (Filimonow et al., 2019). Combined, these studies display that some unidentified aspect of ICM cell-cell interactions (i.e. membrane organization) feeds into the process of cell repositioning. With recent advancements in live imaging with increased spatial and temporal resolution along with fluorescent reporter lines, this provides an interesting line of investigation that could now be followed to help the elucidation of sorting mechanisms.

FGF4 signaling is necessary to maintain the two lumen-adjacent lineages (TE and PrE; Feldman et al., 1995; Goldin and Papaioannou, 2003). As the TE is the tissue which facilitates implantation and interaction with the uterine environment and the PrE is the tissue which delivers nutrients to the developing EPI, it is clear that proper timing of the morphogenesis (spatial domains) and maintenance (molecular regulation) of TE and PrE lineages during blastocyst morphogenesis is critical. Recent studies have revealed that FGF4 signaling through the shared receptor of EPI and PrE cells (FGFR1), is crucial to establishing the molecular identity of the two lineages (Kang et al., 2017; Molotkov et al., 2017). The differential reception of FGF signaling by all of the blastocyst cell lineages does bring to mind the function of morphogen gradients in conditional cell fate specification (Gilbert 2000). It may be possible that the differential expression of both FGF ligands and receptors creates a complex signaling pattern which in turn leads to well-defined spatial niches for each blastocyst lineage. However, as the spatial information for FGFR1 expression in ICM lineages (e.g. polarized membrane localization) as well as the kinetic and diffusive information for FGF4 is severely limited, such hypotheses have not been addressed.

2.4 Apicobasal Polarity and Shape Change during Blastocyst Formation

Once embryos have achieved morula maturation (see steps presented at the beginning of the chapter), the embryo can begin to undergo the global morphological changes associated with blastocyst formation. Chiefly, this is the formation of the Embryonic-Abembryonic axis (Em-Ab axis). This axis is defined by the isolation of the ICM to the embryonic pole of the embryo, which occurs through the emergence of the blastocyst lumen (Garbutt et al., 1987). More specifically, early phases of fluid accumulation result in multiple fluid pockets that preferentially localize at the base of TE cells before coalescing to form the abembryonic pole of the Em-Ab axis (Schematic 8; Figure 1A; Dumortier et al., 2019; Garbutt et al., 1987; Motosugi et al., 2005). This process, as with most tissues that undergo *de novo* lumen formation, is

tightly linked to the embryo's apicobasal polarity program. However, the molecular regulation of apicobasal polarity in the mouse blastocyst is not as well understood as in other systems (e.g. MDCK cysts) due to the differences previously mentioned (See **Introduction I: Lumen Formation and Function in Development**).

The apical domain of TE cells continues to face the external environment of the embryo throughout the process of blastocyst morphogenesis. This polarity organization is inverted to the morphology of a typical cyst where the apical side is facing the lumen (Bryant and Mostov, 2008). Inner cells exposed to the lumen do not undergo polarization and epithelialization until the very end of preimplantation development (E3.75-E4.0; Gerbe et al., 2008; Saiz et al., 2013), and therefore have not yet been considered to contribute to luminal polarity during blastocyst stages. Studies have revealed the necessity of polarity and position are involved in the coordination of lumen formation (Eckert et al., 2004; Stephenson et al., 2010). Tight regulation and maintenance of the established apico-basal polarity and tight junctions within the TE cells are required for blastocyst lumen formation and expansion regulation (Eckert et al., 2004; Madan et al., 2007; Moriwaki et al., 2007). Touched upon in the previous section, ROCK inhibition perturbs morula and blastocyst morphology (Duan et al., 2014; Kawagishi et al., 2004; Laeno et al., 2013). The detrimental effects of ROCK inhibition on the morula to blastocyst transition include perturbations of apicobasal polarity (Kono et al., 2014). Formation and maintenance of this polarity is in part regulated by Atp1, a Na^+/K^+-ATPase, that is also heavily involved in fluid accumulation and is discussed in the following section (Violette et al., 2006). While these studies have not revealed why the TE polarity remains inverted throughout the process of blastocyst formation, they do collectively provide a wealth of evidence to the importance of membrane asymmetry (i.e. membrane polarization) for the morula to blastocyst transition, without which lumen formation does not initiate (Korotkevich et al., 2017).

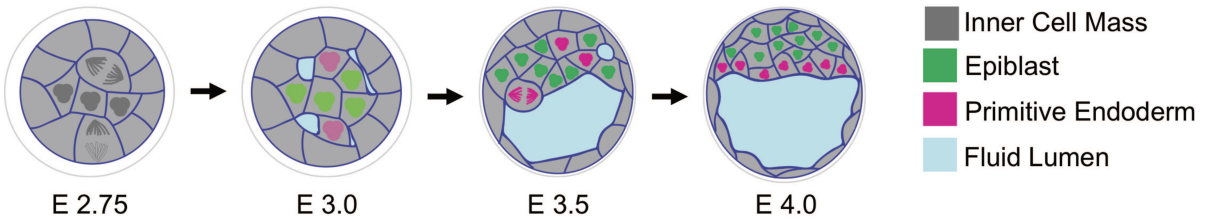

Schematic 8. Lumen morphogenesis in blastocyst development.

2.5 Blastocyst Lumen Formation

The formation and expansion of the blastocyst lumen is concurrent with the specification of EPI and PrE lineages (Rossant and Tam, 2009). Several studies were conducted on the regulation of fluid accumulation in the blastocyst lumen and found that lumen expansion could be stimulated through various means such as increasing cAMP levels or the introduction of TGF or EGF signals (Dardik and Schultz, 1991; Manejwala et al., 1986). Theses modulation effects are indicative of active (i.e. energy expensive) mechanisms of fluid accumulation. Aquaporins (transmembrane water channels) were also found to have apical or basolateral polarized expression domains (Barcroft et al., 2003), which reiterated the close link between apicobasal polarity and fluid accumulation.

The most substantial finding in regards to fluid accumulation mechanism identification has thus far been that the major driver of fluid accumulation within the embryo is thought to be Atp1 as it forms an osmotic gradient across TE cells through its polarized basolateral expression (Wiley, 1984; Watson, 1992; Watson and Barcroft, 2001). However, a complete understanding of the behaviors of Atp1 is still lacking given that genetic studies, some of which knocked out subunits of supposed importance to the process of fluid accumulation, show conflicting results (see Schematic 9 as an example; Barcroft et al., 2004; Jones et al., 1997; Madan et al., 2007). It should be noted that all genetic knockout studies relating to Atp1 function in mouse blastocyst formation have utilized single isoform mutant mouse lines. However, a two-isoform heterozygous knockout line was constructed for the purposes of studying its role in cardiac calcium regulation, which could be used in future studies to eliminate the possibility of isoform compensation ($\alpha 1, \alpha 2$; James et al., 1999).

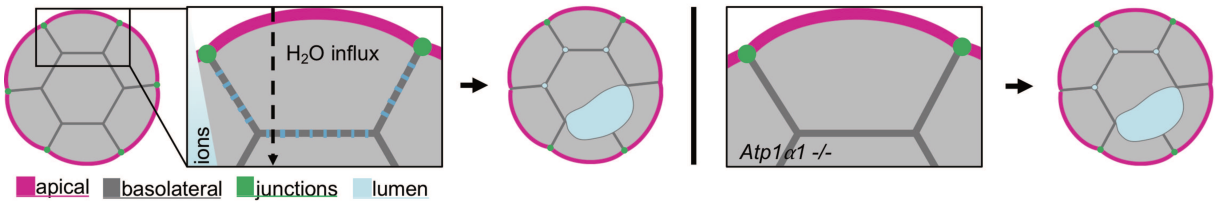

Schematic 9. *Atp1α1 -/-* embryos form morphologically normal blastocyst lumina (Barcroft et al., 2004).

Several electron microscopy studies have been conducted to investigate changes in cytoplasmic organization throughout mouse preimplantation development (Aziz and Alexandre, 1991; Calarco and Brown, 1969;Fleming and Pickering, 1985; Wiley and Eglitis, 1980; Wiley and Eglitis, 1981). Collectively, these studies reported the blasolateral localization of cytoplasmic vesicles that are proposed to undergo secretion and mitochondria. The interpretation of these studies led to the proposal that localization of lipid droplets near basolateral mitochondria could act as an ATP source for Atp1 activity (Fleming and Pickering, 1985; Wiley and Eglitis, 1981). While it has not been confirmed due technical limitations at the time of study, the studies reporting basolateral cytoplasmic vesicles propose that their secretion is important for blastocyst lumen formation (Aziz and Alexandre, 1991; Fleming and Pickering, 1985; Wiley and Eglitis, 1980).

In 16-cell stage morulae, presumptive TE cells appear to have significantly more dilute cytoplasm than that of presumptive ICM cells (Calarco and Brown, 1969). Cytoplasmic vesicles were observed at the basolateral membranes of blastomeres in pre-cavitation morulae (Calarco and Brown, 1969; Wiley and Eglitis, 1980). This observation was confirmed by other studies (Aziz and Alexandre, 1991; Fleming and Pickering, 1985; Wiley and Eglitis, 1981). In 16-cell stage embryos, secondary lysosomes also accumulate in the basal cytoplasm (Fleming and Pickering, 1985). Whether these are distinct from the cytoplasmic vesicles proposed to be important for lumen formation is unclear, yet also unlikely given the different functionalities of the organelles. Incubation of morulae with colcemid apparently disrupted the release of these vesicles as well as preventing lumen formation (Wiley and Eglitis, 1980).

The observations of these electron microscopy studies provide highly interesting possibilities for active mechanisms of fluid accumulation. The dilute TE cytoplasm points towards differential osmotic properties to pull liquid (i.e. water) into the embryo from the extraembryonic environment, which is in line with the polarized localization of aquaporins and Atp1. In parallel, the multiple reports of basal cytoplasmic vesicles offer an additional mechanism that, while likely under independent regulation, could act in concert with osmotic mechanisms of fluid accumulation. With the advances in live imaging resolution, these two possibilities can now be investigated in depth.

Chapter 3

Project Motivation and Central Questions

Thus far, little is known about the function(s) of the blastocyst lumen. Despite the temporal correlation of EPI-PrE specification and lumen formation, the potential function of the lumen to regulate fate specification and cell positioning have yet to be investigated. As stated in **Introduction I: Lumen Formation and Function in Development** it has been shown that failed tubulogenesis causes altered fate allocation ratios due to changes in microenvironments (Kesavan et al., 2009). Throughout the course of this project, the early phases of blastocyst lumen formation and expansion were examined in relation to PrE cell initial specification and migration with an aim to better understand the interplay between cell fate specification and blastocyst morphogenesis.

The central motivation of this project was to address if, and by extension how, fluid lumina (i.e. the morphogenesis of lumina into their final geometry (form or shape) within tissues) has an impact of the processes of cell fate specification and cell positioning within developing tissues. To investigate this, the specification of epiblast (EPI) and primitive endoderm (PrE) cell lineages within the mouse blastocyst (see Schematic 7 for lineage positioning) was chosen as a model. As stated in the previous chapter, the initial specification of EPI and PrE appears to be concurrent with the onset of fluid accumulation when viewed within the timeline of embryonic days (see Schematic 8).

The central questions of the project are:

1. Does the initiation, resolution and expansion of fluid lumina within the pre-implantation mouse embryo affect the specification of the EPI and PrE cell lineages and/or the subsequent spatial segregation of EPI and PrE cells?

2. If there is an affect of lumen morphogenesis on EPI and PrE lineages, what is the mechanism?

In deciding how to analyze and interpret the data acquired throughout this project, questions regarding the relationship(s) between tissue morphogenesis (i.e. geometry and spatial position) and fate acquisition (i.e. molecular identity) occurred:

1. If the position of a cell relative to a noncellular entity within a tissue impacts the cell's molecular profile, how can the development of the noncellular entity and the cell be integrated?

2. If two processes are concurrent, and one appears to influence the other but has independent timing, which developmental timeline is dominant?

NOTE:

A manuscript relating to the results of the first central question (effect identification) was written and submitted to *Developmental Cell* in March 2019. The revised manuscript and reply letter were submitted in June 2019; however, the preprint corresponding to the original submission can be found on *bioRχiv* (575282; doi: https://doi.org/10.1101/575282). The main chapters of this thesis (Chapters 1-7, 9-11) reflect the structure of the revised manuscript with an expanded introduction. The appendices of this thesis contain unpublished experimental datasets and notes on source code.

Chapter 4

Results I: Characterization of Blastocyst Lumen Formation

Given the multipoint origin of the blastocyst lumen (Motosugi et al., 2005) and the persistent formation of the blastocyst lumen in *Atp1α1 -/-* mice (a Na^+/K^+-ATPase subunit; Barcroft et al., 2004), cell-level behaviors of the first moment of extracellular fluid accumulation at high spatial resolution over multiple timescales were examined (Figure 1A-C). In addition to the previously reported multiluminal stage (Motosugi et al., 2005), the unbiased appearance of microlumina arranged in a 'string of pearls' like morphology at cell-cell interfaces throughout the embryo that progressively undergo coalescence over 2-3 hours (Figure 1B) was observed.

Given the multipoint origin of the blastocyst lumen (Motosugi et al., 2005), I examined the first moments of extracellular fluid accumulation at high spatial resolution over multiple timescales (Figure 1A-C). In addition to the previously reported multiluminal stage, I observed the unbiased appearance of microlumina arranged in a 'string of pearls' like morphology at cell-cell interfaces throughout the embryo that progressively undergo coalescence over 2-3 hours (Figure 1B). A thorough description of the coalescence of the microlumina as a function of Ostwald ripening was conducted by another group contemporaneously (Dumortier et al., 2019). Because of this, the results presented in this chapter are focused on the identification of a secondary mechanism of fluid accumulation.

In embryos at a stage just prior to measurable separation of cell membranes due to fluid accumulation (approximately 84hrs post-hCG, E3.0), I observed large, cortically-localized, actin-coated vesicles along the basolateral membranes of outer cells and ubiquitously along the membranes of apolar, inner cells (Figure 1C, top panel; Movie S1). These vesicles are actively secreted into intercellular space in approximately 60 seconds (Figure 1C, bottom panel; Movie S2). The presence and dynamic behavior of these vesicles persists through the early phases of luminal coalescence and expansion (E3.0-E3.25); however, such vesicles are no longer observable in embryos in which the lumen has expanded to occupy at least 50% of the total embryo volume (approximately 96hrs post-hCG, E3.5; Figure 1E, Figure S1). Actin coated vesicles in E3.5

embryos are significantly smaller than those in E3.0 embryos; they form cytoplasmic clusters, and no observable secretion events occur at the same time scale as that of E3.0 vesicles (Figure 1E,S1).

4.1 Widespread Secretion of Cytoplasmic Vesicles into Intercellular Space Drives Early Fluid Accumulation.

The capability of both *Atp1α1 -/-* and pharmacologically Atp1 inhibited embryos to form morphologically normal lumina indicates the action of a secondary, and Atp1 independent, mechanism of fluid accumulation.In embryos at a stage just prior to measurable separation of cell membranes due to fluid accumulation (approximately 84hrs post-hCG, E3.0), large, cortically-localized, actin-coated vesicles along the basolateral membranes of outer cells and ubiquitously along the membranes of apolar, inner cells were observed (Figure 1C, top panel). These vesicles are actively secreted into intercellular space in approximately 60 seconds (Figure 1C, bottom panel). The presence and dynamic behavior of these vesicles persists through the early phases of luminal coalescence and expansion (E3.0-E3.25); however, such vesicles are no longer observable in embryos in which the lumen has expanded to occupy at least 50% of the total embryo volume (approximately 96hrs post-hCG, E3.5; Figure 1E, Figure S1). Actin coated vesicles in E3.5 embryos are significantly smaller than those in E3.0 embryos; they form cytoplasmic clusters, and no observable secretion events occur at the same time scale as that of E3.0 vesicles (Figure 1E,S1; summarized in Schematic 10).

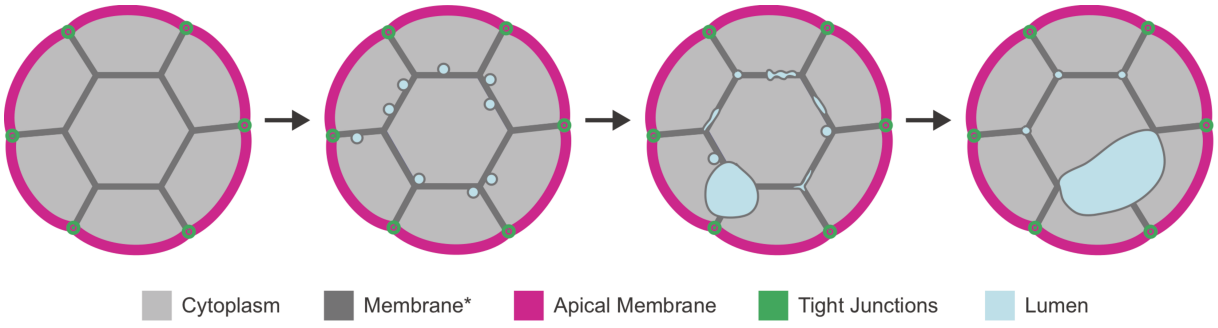

Schematic 10. The ordered emergence of vesicles, microlumina and coalescence events during blastocyst morphogenesis.

4.2 Actin Mediated Secretion is Independent of Atp1 Action

To determine if vesicle release is linked to the Atp1 driven mechanism of fluid accumulation, I incubated embryos with ouabain, a well-known inhibitor of Atp1 activity (Bagnat et al., 2007; Manejwala et al., 1989), for two hours prior to fluid accumulation onset. I observed that the vesicle release mechanism is still present in embryos cultured with ouabain (Figure 1F, top panel; Figure 1E; Movie S3). The time it takes a single vesicle in Atp1 inhibited embryos to be secreted appears similar to that of WT embryos (Figure 1F, bottom panel; Movie S4). These results suggest that vesicle secretion as a fluid accumulation mechanism is independent of Atp1.

4.3 Inhibition of COPII Machinery Impacts Luminal Volume

To discern if vesicle release makes a measurable contribution to total luminal volume, embryos from early (E3.0-E3.5) and late (E3.5-E4.0) stages of lumen expansion were incubated in media containing Brefeldin A, a well-known inhibitor of COPII machinery (Miller et al., 1992; Helms and Rothman, 1992) that does not affect cell divisions (Figure S2A) or increase the frequency of apoptotic events (Figure S2B). Titrations of Brefeldin A revealed that its inhibitory effects on luminal volume can be modulated during early lumen expansion phases (Figure 1D) in agreement with the observation of vesicle release occurring primarily during early expansion (Figure 1C, Figure S1).

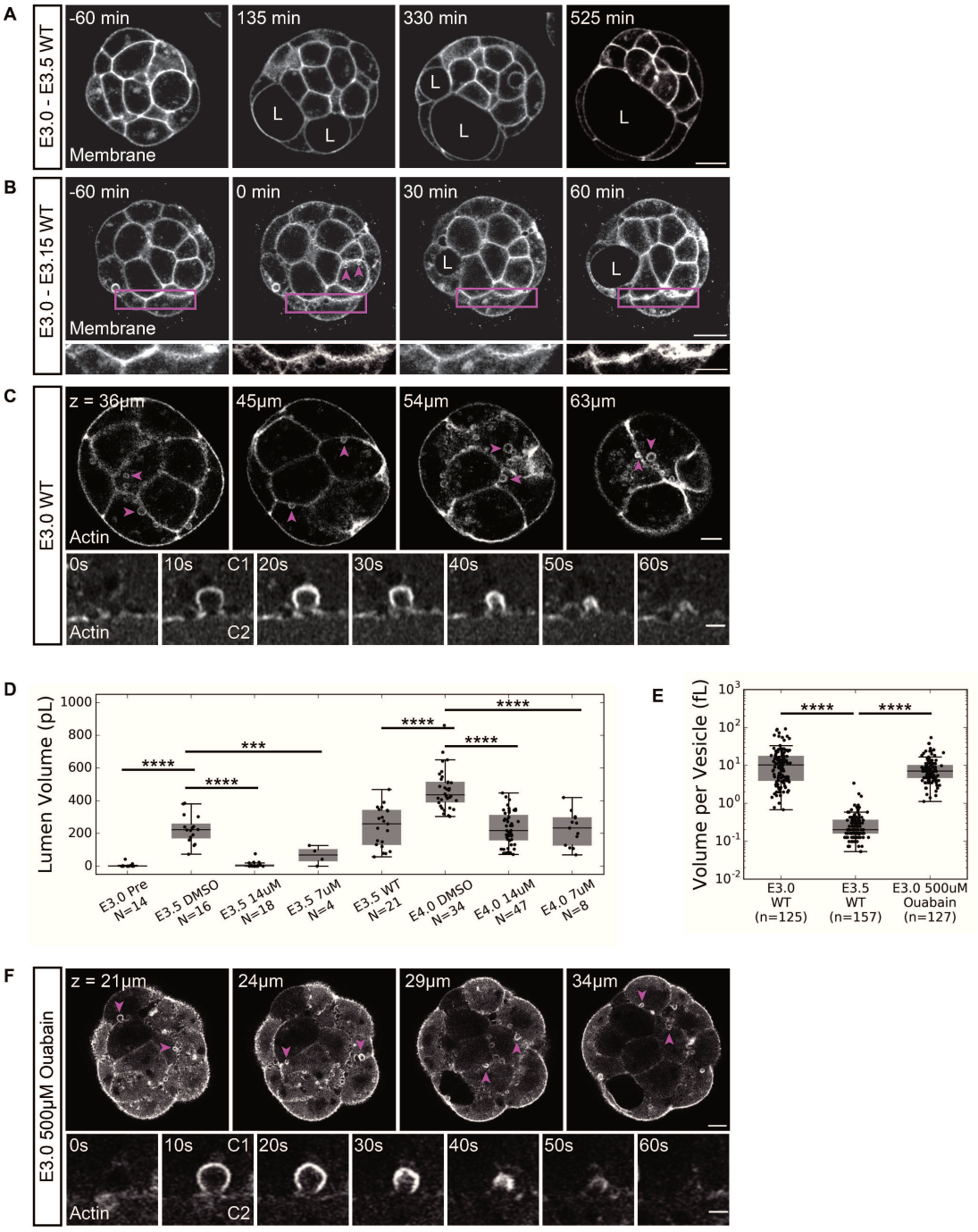
A
E3.0 - E3.5 WT
-60 min
135 min
330 min
525 min
Membrane
L
B
E3.0 - E3.15 WT
-60 min
0 min
30 min
60 min
Membrane
C
E3.0 WT
z = 36µm
45µm
54µm
63µm
Actin
0s
10s
C1
20s
30s
40s
50s
60s
C2
D
Lumen Volume (pL)
E3.0 Pre N=14
E3.5 DMSO N=16
E3.5 14uM N=18
E3.5 7uM N=4
E3.5 WT N=21
E4.0 DMSO N=34
E4.0 14uM N=47
E4.0 7uM N=8
E
Volume per Vesicle (fL)
E3.0 WT (n=125)
E3.5 WT (n=157)
E3.0 500uM Ouabain (n=127)
F
E3.0 500µM Ouabain
z = 21µm
24µm
29µm
34µm

Figure 1. Blastocyst cavities are partially derived from cytoplasmic vesicles.
(A) Time-lapse of a representative embryo expressing a membrane marker undergoing lumen formation (L marks a lumen). t = 0min when fluid accumulation is first detectable by automatic segmentation. Scale bar = 20μm. (B) Time-lapse of the first hour of fluid accumulation in an embryo expressing a membrane marker (L marks a lumen). t = 0min when 'string of pearls' microluminal structures are observed. Top row is full embryo view (magenta arrowheads highlight cytoplasmic vesicles, scale bar = 20μm). Bottom row is insets of cell-cell interfaces indicated by magenta boxes in top row highlighting the appearance of 'string of pearls'-like microlumina emergence and resolution (scale bar = 10μm). (C) Z-slices of phalloidin staining showing cortically-localized vesicles in an E3.0 embryo (top, magenta arrowheads highlight individual vesicles, scale bar = 10 μm). Time-lapse of vesicle secretion into intercellular space in a Lifeact-GFP E3.0 embryo (bottom, 'C1' marks secreting cell, 'C2' marks adjacent cell, scale bar = 2μm). (D) Box plot of volume for lumina in Brefeldin A pharmacologically inhibited embryos. (E) Box plot of volume for individual vesicles in WT embryos at E3.0 and E3.5, and ATP1 inhibited embryos at E3.0. (F) Z-slices of an E3.0 embryo expressing Lifeact-GFP showing vesicle localization under Atp1 inhibition conditions (top, magenta arrowheads highlight individual vesicles, scale bar = 10μm). Time-lapse of vesicle secretion into intercellular space under Atp1 inhibition conditions (bottom, 'C1' marks secreting cell, 'C2' marks adjacent cell, scale bar = 2μm).
***p<0.001
****p<0.0001
N = embryo
n = vesicle

Chapter 5

Results II: Apical Proteins and FGF4 Localize to Early Luminal Structures

5.1 Polarized microlumina emerge in the early blastocyst.

While the apicobasal polarity of TE cells surrounding the mouse blastocyst lumen is inverted to that of typical cysts and tubes (Alvers et al., 2014; Bryant et al., 2010 and 2014), the vesicle fusion observed in E3.0 embryos is similar to exocytosis of apical vacuolar compartments in apical cord hollowing, which is a de novo lumen formation mechanism that is conserved across species and tissues (Alvers et al., 2014; Bryant and Mostov, 2008; Sigurbjörnsdóttir et al., 2014). Critical to the initiation of apical cord hollowing is the formation of the apical membrane initiation site (AMIS) which dictates where the lumen will initiate and expand (Bryant et al., 2010; Ferrari et al., 2008). As such, I examined early lumen formation stage embryos for apical polarity phenotypes resembling reported AMIS and AMIS-like structures. Interestingly, I found that many E3.0 embryos contain microlumina enriched for the apical marker phosphorylated ERM (pERM) (43%, N = 20 of 47 embryos; Figure 2A,B). By E3.25 (90hrs post-hCG), such structures are rare as the main lumen expands and individual microlumina merge with it (Figure 2B; $p < 0.001$, two-tailed Fisher exact test). Although pERM localizes to microlumina, other apical lumen trafficking proteins, such as the small GTPase Rab11a (Alvers et al., 2014; Bagnat et al., 2007; Bryant et al., 2010; Bryant et al., 2014), are found in the subapical regions of TE cells instead of the cytoplasmic regions adjacent to microlumina (Figure S3). Interestingly, Integrin-β1 localizes to subpopulations of microlumina and nascently separated membrane domains (Figure S4A) exclusive of the pERM luminal structures (Figure S4B).

5.2 Luminal precursor structures can polarize in the early blastocyst.

While apically polarized microlumina are infrequent in E3.25 embryos, I do observe the presence of two other apically polarized structures rarely found in E3.0 embryos (Figure 2C-F). A small number of ICM cells in E3.25 embryos contain apicosome-like structures (21%, N = 19 of 92 embryos; Figure 2C,D; $p < 0.002$, two-tailed Fisher exact test), which contain apical polarity proteins and have been proposed to be luminal precursors in human pluripotent stem cell culture (Taniguchi et al., 2017). Cells containing apicosome-like structures are isolated from contact-free surfaces created by the growing lumen (Figure 2C, Movie S5). If such cells acquire sustained contact with the lumen the apicosome is released into the lumen over approximately 2-3 hours post-contact (Movie S6). Subsections of the lumen-facing membrane in a small number of E3.25 ICM cells express apical polarity markers and have a markedly shorter radius of curvature than that of the rest of the ICM-lumen interface, indicating recent fusion of either an apicosome or apically polarized microlumina (33%, N = 30 of 92 embryos; Figure 2E,F; $p < 0.0001$, two-tailed Fisher exact test).

5.3 FGF4 is detectable in early stage microlumina.

FGF4 has been shown to be essential for PrE establishment (Kang et al., 2013; Krawchuk et al., 2013; Lanner and Rossant, 2010; Yamanaka et al., 2010), and its expression is restricted to EPI cells (E3.25-E4.5) (Frankenberg et al., 2011; Ohnishi et al., 2013). Because FGF ligands have been shown to create signaling niches by localizing to microlumina (Durdu et al., 2014), I examined the localization of FGF4 protein in E3.0 embryos by injecting mRNA of *fgf4-mNeonGreen* into a single blastomere of a 4-cell stage embryo. I observe localization on the membranes of a subset of microlumina (36%, N = 7 embryos, Figure 2G), while *mNeonGreen* without the *fgf4* coding sequence does not localize to microlumina (Figure S5). The localization of FGF4 to microlumina suggests that luminal microenvironments may provide a signaling cue capable of influencing fate specification in surrounding cells.

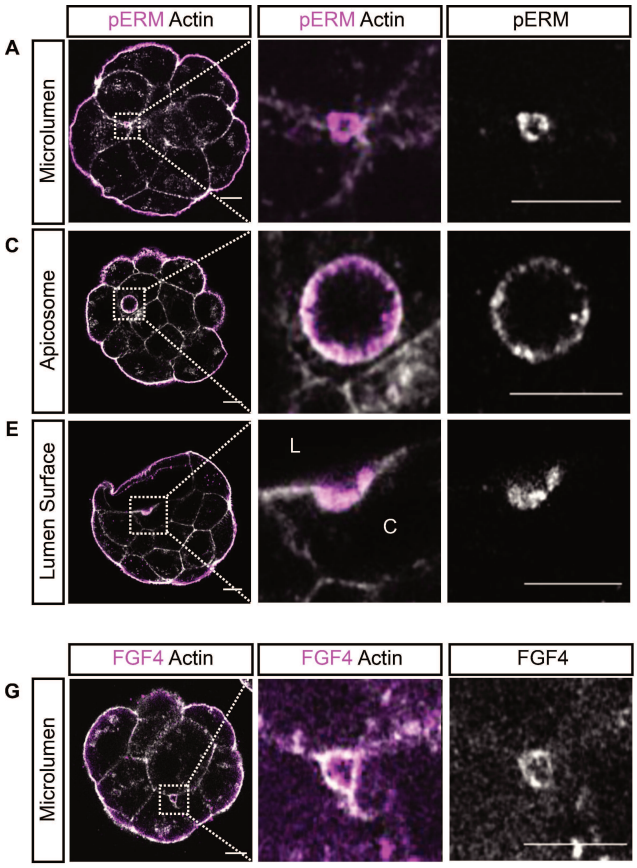
pERM Actin
pERM Actin
pERM
A
Microlumen
C
Apicosome
E
Lumen Surface
L
C
FGF4 Actin
FGF4 Actin
FGF4
G
Microlumen

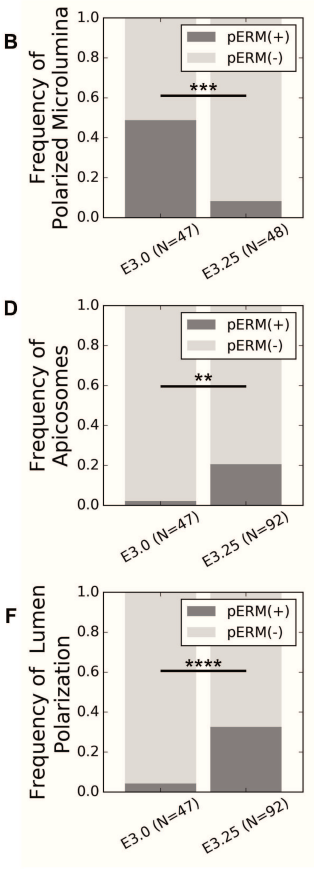
B
Frequency of Polarized Microlumina
pERM(+)
pERM(-)
***
1.0
0.8
0.6
0.4
0.2
0.0
E3.0 (N=47)
E3.25 (N=48)
D
Frequency of Apicosomes
pERM(+)
pERM(-)
**
E3.0 (N=47)
E3.25 (N=92)
F
Frequency of Lumen Polarization
pERM(+)
pERM(-)
****
E3.0 (N=47)
E3.25 (N=92)

Figure 2. Microlumina containing secreted apical domain components are transiently upregulated during early phases of fluid accumulation.
(A) Representative immunofluorescence images of an apically polarized microlumina in an E3.0 embryo. (B) Frequency of apically polarized microlumina in E3.0 and E3.25 embryos ($p < 0.001$). (C) Representative immunofluorescence image of an E3.25 ICM cell containing an apicosome. (D) Frequency of apicosome occurrence in E3.0 and E3.25 embryos ($p < 0.002$). (E) Representative immunofluorescence image of an E3.25 ICM cell in which a subsection of its membrane facing the growing lumen is apically polarized (L – lumen; C – cytoplasm). (F) Frequency of lumen polarization in E3.0 and E3.25 embryos ($p < 0.0001$). (G) Z-slice of an RNA-injected E3.0 embryo showing localization of FGF4-mNeonGreen to the membrane domains of a microlumen, representative of N = 7 embryos.
All scale bars = 10μm.
Two-tailed Fisher exact test
$^{****}p < 0.0001$
$^{***}p < 0.001$
$^{**}p < 0.01$

Chapter 6

Results III: EPI-PrE Specification and Spatial Segregation during Lumen Expansion

6.1 ICM Spatial Patterning Resolves as the Lumen Expands

During the final phases of coalescence and lumen expansion, initial transcriptional biases of ICM cells towards either EPI or PrE fate are either reinforced or changed concomitantly with spatial segregation (Chazaud et al., 2006; Frankenberg et al., 2011; Ohnishi et al., 2014). Cells that are molecularly specified to become PrE but fail to achieve correct positioning along the ICM-lumen interface in a timely manner undergo apoptosis (Plusa et al., 2008). However, it is not known precisely when the cells begin to undergo repositioning since initial position of the precursors is stochastic (Chazaud et al., 2006; Gerbe et al., 2008), and lumen formation onset is variable in terms of absolute developmental time. To determine whether spatial segregation is correlated with luminal volume, I used lineage reporters and membrane signal (Muzumdar et al., 2007) to track the emergence and positioning of EPI precursor cells (Arnold et al., 2011) and PrE precursor cells (Hamilton et al., 2003) within the ICM in relation to the expanding lumen.

6.1.1 Analysis Development Rationale

To date, studies whose main focus is the investigation of the spatial segregation of ICM lineages have not been conducted. While segregation defects have been observed (Laeno et al., 2013), they have never been quantified in reference to overall embryo orientation (position along an axis). Furthermore, few preimplantation studies involve quantification of the blastocyst lumen volume. Combined, there is a general absence of these quantifications within the field and as such a lack of appropriate quantitative analysis methods with which to analyze the datasets of

this project as it is a requirement to relate these processes to one another in order to answer the central questions.

In order to measure and track the EPI and PrE domains accurately, I first developed an analysis method that incorporates gross morphological changes occurring over the course of lumen formation and expansion. The resulting method allows us to determine the distance of each ICM lineage from the ICM-lumen interface relative to the volume of the expanding lumen and the changing morphology of the ICM by simultaneously segmenting the lumen and embryo cell mass and determining the embryonic-abembryonic axis to provide spatial orientation (Figure 3A; see Methods for details).

6.1.2 Pdgfrα (PrE) Oriented Movement

Unlike most PrE markers which are not expressed in the initial ICM population and are later upregulated in a subset of cells, Sox2, a well-known EPI marker, has been described to be expressed in all inner cells from the 16-cell stage and its expression is restricted during later stages of blastocyst development (Ohnishi et al., 2014). Because of this behavior, I chose to use Sox2::gfp as both an EPI reporter as well as a 'static' control for the analysis method.

The EPI reporter center showed no net movement toward the ICM-lumen interface and maintained a relative constant distance from the luminal surface throughout expansion (Figure 3D,E). In contrast, the PrE reporter (Pdgfr$\alpha^{\text{H2B-GFP}/+}$) center shifts toward the ICM-lumen interface as soon as coalescence begins (approximately E3.25) and continues throughout expansion (Figure 3B,C). This indicates differential sorting behavior between PrE and EPI cells, and suggests that lumen expansion may play a role in guiding EPI-PrE fate specification and spatial segregation.

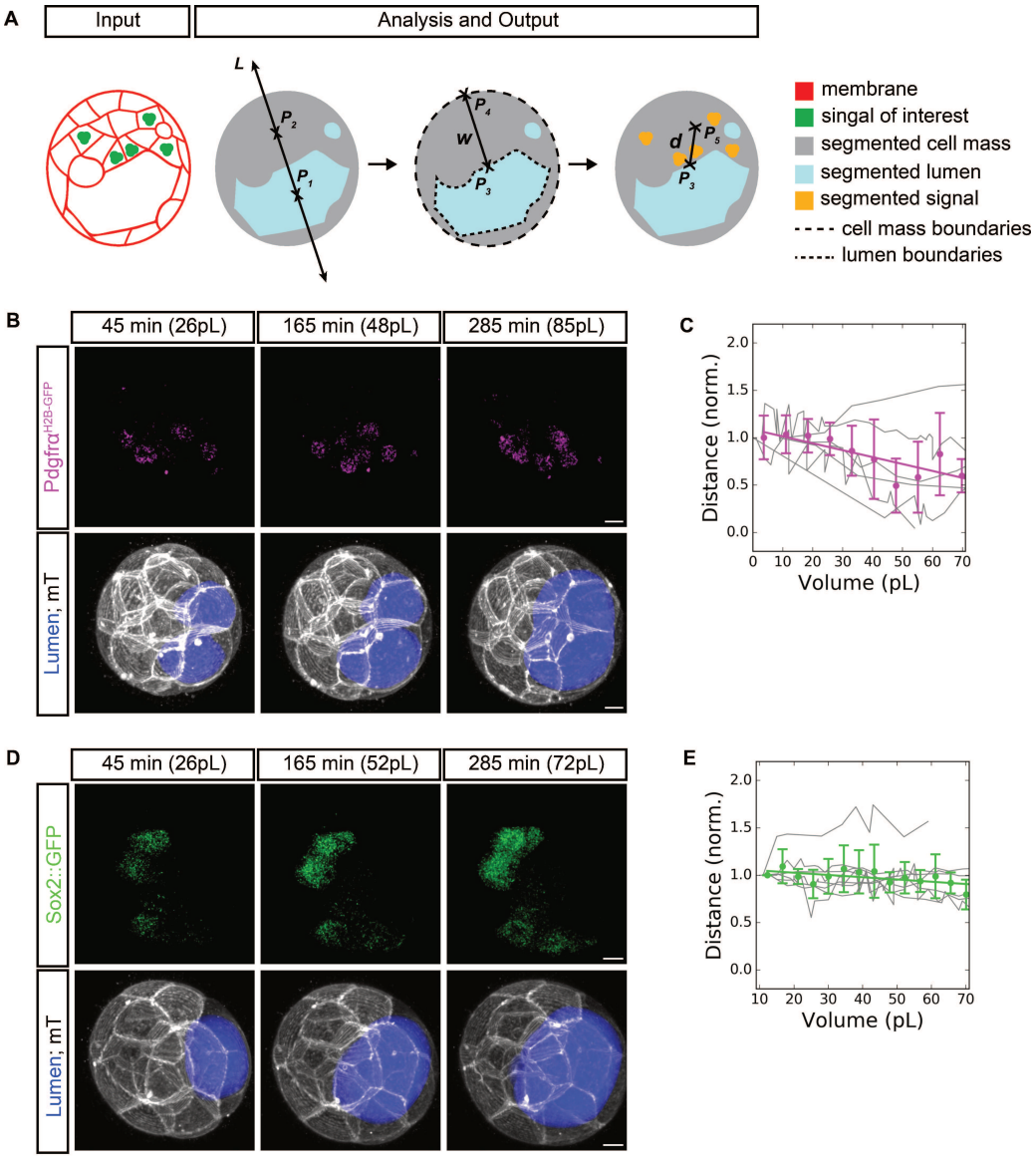
A
Input
Analysis and Output
L
P2
P1
P4
w
P3
d
P5
P3
membrane
singal of interest
segmented cell mass
segmented lumen
segmented signal
cell mass boundaries
lumen boundaries
B
45 min (26pL)
165 min (48pL)
285 min (85pL)
Pdgfra H2B-GFP
Lumen; mT
C
Distance (norm.)
Volume (pL)
D
45 min (26pL)
165 min (52pL)
285 min (72pL)
Sox2::GFP
Lumen; mT
E
Distance (norm.)
Volume (pL)

Figure 3. The Pdgfrα signaling domain approaches the luminal surface as the lumen grows in volume.

(A) Schematic 2D representation of 3D analysis method for the tracking and normalization of fate reporter expression proximity to the ICM-lumen interface. $P_{1,2,3,4,5}$ are 3D points. $\overleftrightarrow{L}$ is a 3D line ($\overleftrightarrow{P_1P_2}$ equivalent) that defines the embryonic-abembryonic axis. $\overline{w}$ is the 3D line segment ($\overline{P_3P_4}$ equivalent) that measures the ICM width. $\overline{d}$ is the 3D line segment ($\overline{P_3P_5}$ equivalent) that measures the distance from the center of mass of the signal of interest to the ICM-lumen interface. See Image Analysis for formal definitions of all geometric entities. (B) Time-lapse of an E3.0 embryo expressing a PrE reporter (Pdgfr$\alpha^{\text{H2B-GFP}/+}$; top), a membrane marker and lumen segmentation (bottom). t = 0min is defined as the first moment when a lumen can be segmented. Lumen volume (pL) is given for each time point shown. (C) Quantification of the distance of the center of Pdgfrα signaling domain to the surface of the lumen over time (N = 6 embryos, thin gray lines are traces of individual embryos, magenta dots are binned averages with vertical capped lines showing standard deviations, thick magenta line is the linear regression $y = -0.007x + 1.090$, $r^2 = 0.653$, $p < 0.005$). (D) Time-lapse of an E3.0 embryo expressing a cytoplasmic EPI reporter (Sox2::gfp; top), a membrane marker and lumen segmentation (bottom). t0 is defined as the first moment when a lumen can be segmented. Lumen volume (pL) is given for each time point shown. (E) Quantification of the distance of the center of Sox2 expression domain to the surface of the lumen over time (N = 8 embryos, thin gray lines are traces of individual embryos, green dots are binned averages with vertical capped lines showing standard deviations, thick green line is the linear regression $y = -0.002x + 1.074$, $r^2 = 0.339$, $p < 0.030$).

All scale bars = 10μm.

6.2 ICM Lineage Specification is Dependent on Luminal Expansion

6.2.1 Atp1 Inhibition Impact on EPI-PrE

Given the correlation between lumen expansion and the oriented movement of PrE progenitor cells (Figure 3D,E), I hypothesized that modulation of lumen size may impact lineage differentiation and cell positioning. To test this hypothesis, I inhibited the expansion of post-coalescence stage lumina (96-108 hours post-hCG; E3.5-E4.0) through multiple means. Embryos cultured in media containing 500μM ouabain (Wiley, 1984) show a significant decrease in luminal volume. The volume effect is titratable by changing inhibitor concentration (Figure 4A,B; Figure S6A), suggesting the effect of ouabain in reducing lumen expansion is specifically due to its action on the Atp1 channel. The inhibition of the cystic fibrosis transmembrane conductance regulator, a Cl- channel known to impact lumen expansion in other systems (Bagnat et al., 2010; Navis and Bagnat, 2015; Navis and Bagnat, 2015b), also results in reduced lumen size, although the reduction is not as significant as Atp1 inhibition (Figure S7). Notably, Atp1 inhibited embryos show significant reduction in the fluorescence levels of both EPI and PrE markers (Figure 4C) in addition to possessing a significantly lower luminal volume than that of controls without a change in the total number of cells (Figure S6B).

Analysis Development Rationale

Here, the lack of appropriate analysis methods was again confronted. In order to understand how two cell lineages, both of which are undergoing progressive changes and commitments to the lineage (i.e. the fluorescence levels of lineage markers can change dynamically), one needs to know the likelihood of a cell to have a certain expression level for each lineage at each point (coordinate) within the embryo. The chosen solution for this was to build kernel denity estimates (KDEs) for each sample and each lineage of interest within the sample. This essentially means that theoretical point density functions were computed based on the fluorescent signals within an embryo (i.e. the likelihood of every cell within the embryo to belong to an individual cell lineage can be evaluated). To confirm the fidelity of this solution, a simulation of complete overlap between lineages was computed. Maximum potential overlap ('Simulation') is defined as the scenario in which the entire ICM is equally likely to be EPI or PrE, resulting in a high overlap value.

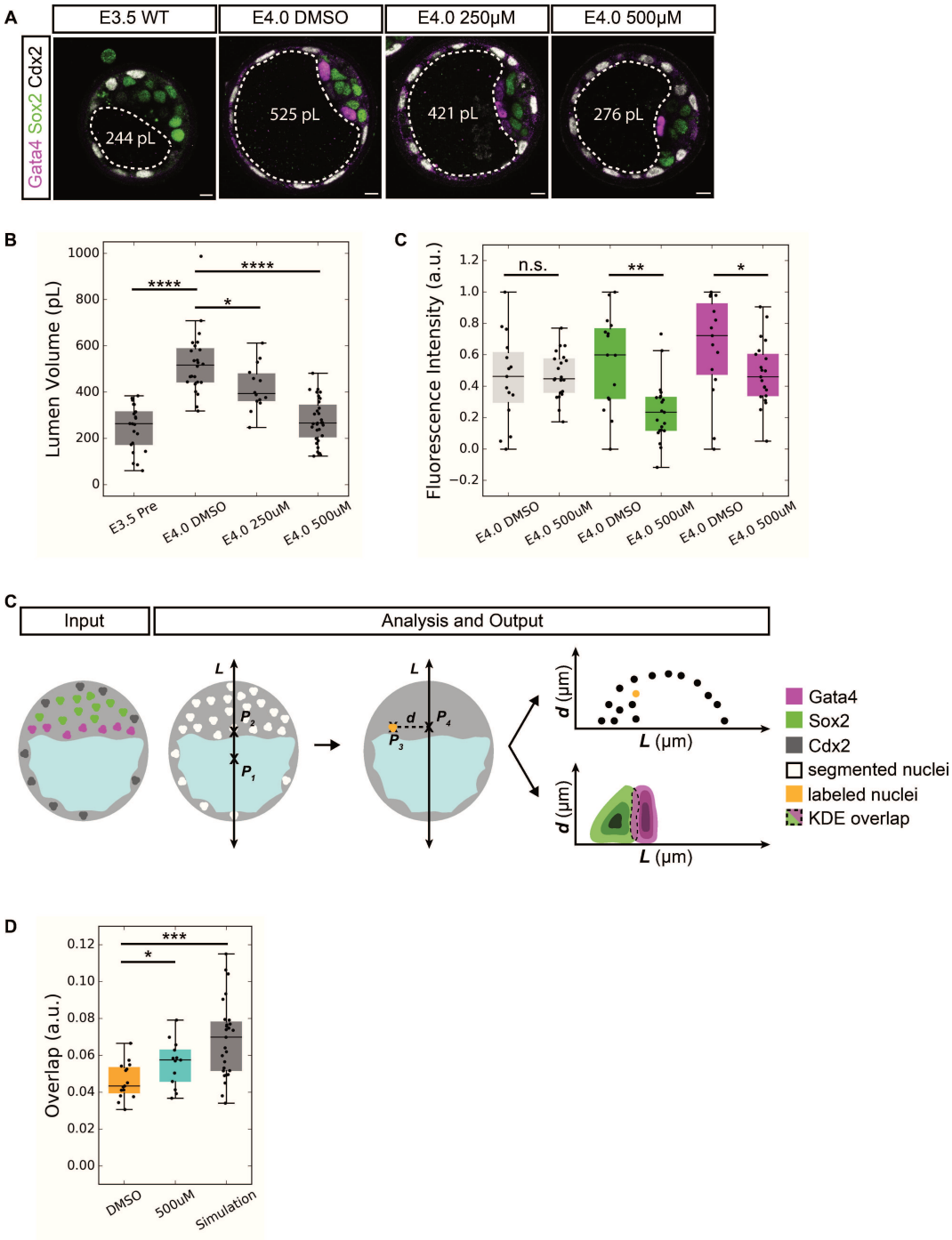
A
E3.5 WT
E4.0 DMSO
E4.0 250μM
E4.0 500μM
Gata4 Sox2 Cdx2
244 pL
525 pL
421 pL
276 pL
B
Lumen Volume (pL)
E3.5 Pre
E4.0 DMSO
E4.0 250uM
E4.0 500uM
C
Fluorescence Intensity (a.u.)
n.s.
E4.0 DMSO
E4.0 500uM
C
Input
Analysis and Output
L
d
L (μm)
d (μm)
Gata4
Sox2
Cdx2
segmented nuclei
labeled nuclei
KDE overlap
D
Overlap (a.u.)
DMSO
500uM
Simulation

Figure 4. EPI and PrE expression levels are reduced in ATP1 inhibited embryos. (A) Immunofluorescence images of TE (Cdx2), EPI (Sox2) and PrE (Gata4) fate in pre-treatment control (E3.5 WT), Atp1 inhibited (E4.0 500μM and E4.0 250μM), and end-stage control (E4.0 DMSO) embryos. Lumen boundaries outlined by dashed white line and mean lumen volume in white text. Scale bars = 10μm. (B) Boxplot of lumen volume for E3.5 WT (N = 21), E4.0 DMSO (N = 24), E4.0 250μM Atp1 inhibited (N = 14) and E4.0 500μM Atp1 inhibited (N = 31) embryos indicating that the impact on lumen volume is concentration dependent. (C) Boxplot of fluorescence levels of Cdx2 (gray), Sox2 (green) and Gata4 (magenta) in E4.0 500μM Atp1 inhibited embryos compared to E4.0 DMSO controls. (D) Schematic 2D representation of 3D analysis method for spatial segregation of ICM lineages. $P_{1,2,3,4}$ are 3D points. $\overleftrightarrow{L}$ is a 3D line ($\overleftrightarrow{P_1P_2}$ equivalent) that defines the embryonic-abembryonic axis. $\overline{d}$ is the 3D line segment ($\overline{P_3P_4}$ equivalent) that measures the perpendicular distance from the center of a cell to $\overleftrightarrow{L}$. See Image Analysis for formal definitions of all geometric entities. (D) Boxplot of spatial overlap between EPI and PrE lineages within E4.0 control (DMSO, N = 15) and E4.0 Atp1 inhibited (500μM, N =13) embryos with simulated data of maximal overlap in E4.0 WT samples (Simulation, N = 27).

$^{****}p < 0.0001$

$^{**}p < 0.01$

$^{*}p < 0.05$

6.3 Spatial Segregation of ICM Lineages is Dependent on Luminal Expansion.

6.3.1 Mechanical Inhibition of Lumen Expansion

To further examine the possible role of lumen expansion in cell fate specification and sorting, I mechanically deflated late expansion stage lumina (E3.5-E4.0) by inserting a microneedle into the lumen at the junctions of mural TE cells, and applying negative pressure to counteract expansion (Figure 5A). This action was repeated every 1-2 hours as necessary for individual embryos so that the blastocyst lumen volume did not change significantly from that of the initial E3.5 blastocysts. To ensure observations are not due to adverse effects induced by serial needle insertion, I performed a control of passive lumen deflation due to serial puncture ('Control') with no application of negative pressure. Importantly, serial needle insertion does not perturb tissue fidelity of lineage markers or embryo cell cycle progression (Figure S9, S10).

Interestingly, PrE specification levels are significantly reduced by mechanical deflation, while EPI specification levels are maintained at the level of WT embryos (Figure 5B,D). Additionally, mechanical deflation impairs the spatial segregation of EPI and PrE cells (Figure 5B,E). EPI-PrE overlap is defined as the intersection of the probability of the two populations based on spatial position in 3D and expression level of Sox2 (EPI) and Gata4 (PrE) (Figure 5C; see Methods for details).

WT v. Control v. Mechanical v. Simulation

EPI-PrE overlap of mechanically deflated embryos is more than doubled in comparison to WT controls ($\text{mean}_{\text{Mech}} = 0.053$, $\text{mean}_{\text{WT}} = 0.021$, $p < 0.0001$), but is still significantly less than that of simulated maximal overlap values ('Simulation', $\text{mean}_{\text{Simulation}} = 0.069$, $p < 0.005$). Spatial segregation analysis of controls shows a slightly higher degree of overlap between EPI and PrE domains in comparison to that of WT ($\text{mean}_{\text{Control}} = 0.028$, $p < 0.045$) while still being significantly lower than that of mechanically deflated embryos ($p < 0.007$).

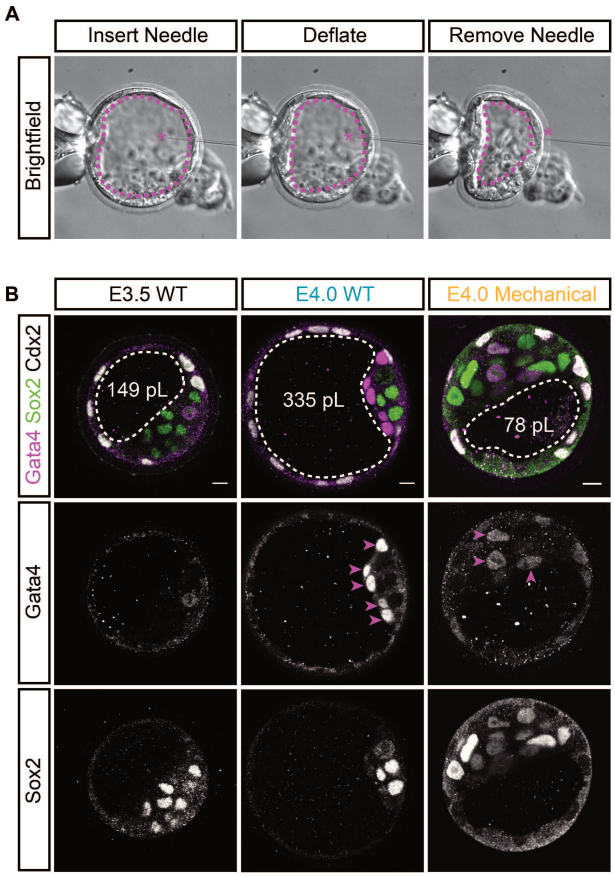
A
Insert Needle
Deflate
Remove Needle
Brightfield
B
E3.5 WT
E4.0 WT
E4.0 Mechanical
Gata4 Sox2 Cdx2
149 pL
335 pL
78 pL
Gata4
Sox2

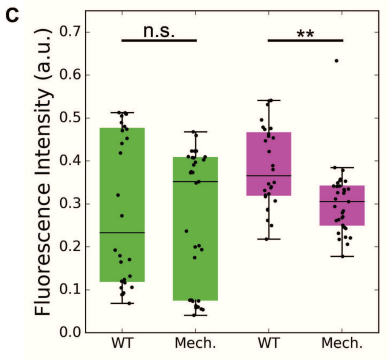
C
Fluorescence Intensity (a.u.)
n.s.
**
WT
Mech.
WT
Mech.

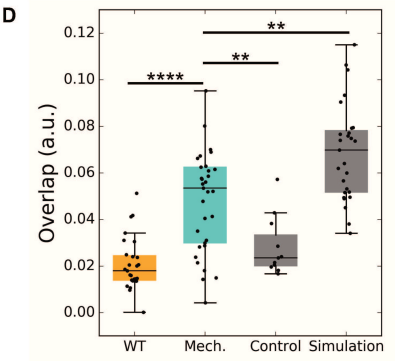
D
Overlap (a.u.)
****
**
**
WT
Mech.
Control
Simulation

Figure 5. PrE specification and spatial segregation of ICM lineages is impaired by mechanical inhibition of lumen expansion.

(A) Brightfield images of mechanical deflation. Magenta asterisk marks the needle tip. Dotted magenta line indicates lumen boundary. (B) Immunofluorescence images of EPI (Sox2) and PrE (Gata4) fate in pre-manipulation control (E3.5 WT), E4.0 post-manipulation control (E4.0 WT) embryos and E4.0 mechanically inhibited (E4.0 Mechanical). Magenta arrowheads indicate the position of cells expressing high levels of Gata4 within the ICM. White dotted line indicates lumen boundaries. Average lumen volume in white text. Scale bars = 10μm. (C) Boxplot of fluorescence levels of Sox2 (green) and Gata4 (magenta) in mechanically inhibited ('Mech', N = 33) and post-manipulation control ('WT', N = 28) E4.0 embryos. (D) Boxplot of spatial overlap between EPI and PrE lineages within post-manipulation control ('WT', N = 27), mechanically inhibited ('Mech', N = 33), E4.0 procedural control ('Control', N = 11) and E4.0 simulation of complete overlap in WT conditions ('Simulation.', N = 27).

$****p < 0.0001$

$**p < 0.01$

n.s. = not significant

6.4 Potential role of luminal FGF4 in EPI-PrE specification.

As pharmacological and mechanical deflation experiments cannot distinguish the mechanical and biochemical influences of the lumen on EPI-PrE development, I next altered the luminal contents in early expansion phase embryos (E3.0-E3.5) without significantly effecting change in luminal volume or embryo cell number (Figure S11) in order to investigate the potential role of the lumen as a signaling niche. I chose to enhance and inhibit FGF4 signaling through luminal deposition (see Methods) of FGF4 protein and an FGFR1 inhibitor (Yamanaka et al., 2010), respectively; PBS deposition was used as a control. Embryos with luminally deposited FGF4 (FGF4-I; 500ng/mL FGF4 with 1μg/mL heparin) exhibit Gata4 and Sox2 expression levels significantly higher than that of control embryos (Figure 6A,B). In comparison, embryos with luminally deposited PD173074 (PD-I; 200nM) exhibit significantly lower Gata4 levels than that of control (Figure 6B). Note that the differences in luminal volume between FGF4-I and PD-I embryos with that of the PBS- I control embryos is not significant (Figure 6C), suggesting that the impact on cell fate is driven by changes in luminal contents rather than changes in lumen size. While the reduction of Gata4 levels of PD-I embryos is similar to the changes reported in globally inhibited embryos (Yamanaka et al., 2010), the increased expression levels of both Sox2 and Gata4 in FGF-I embryos differs from global treatments, which show conversion of the entire ICM to PrE at the expense of the EPI population (Kang et al., 2013; Yamanaka et al., 2010). The increased expression of both EPI and PrE markers in FGF4-I embryos suggests the importance of local availability of fate specifying factors within the embryo.

To further dissect the mechanical or biochemical role of the lumen, I tested if luminal deposition of FGF4 can rescue the reduced EPI-PrE molecular specification levels in embryos with reduced lumen size (Figures 4,5). I performed FGF4 luminal deposition and cultured the injected embryos in media containing ouabain (FGF4- OUA; 250μM), the Atp1 inhibitor previously used (Figures 1,4). PBS deposition and subsequent Atp1 inhibition (PBS-OUA) was used as a control in addition to standard DMSO controls. FGF4-OUA embryos show a significant increase in the specification of both EPI (Sox2) and PrE (Gata4) lineages in comparison with that of PBS-OUA controls (Figure 7A,B). These changes in cell fate specification are decoupled from lumen expansion given that FGF4-OUA luminal volume remains as small as that of PBS-OUA (Figure 7C). These results show that luminal deposition of FGF4 can at least partially rescue EPI-PrE specification in embryos with reduced lumen expansion. Taken together, our findings reveal a potential biochemical function of the lumen to impact ICM lineage specification and maturation.

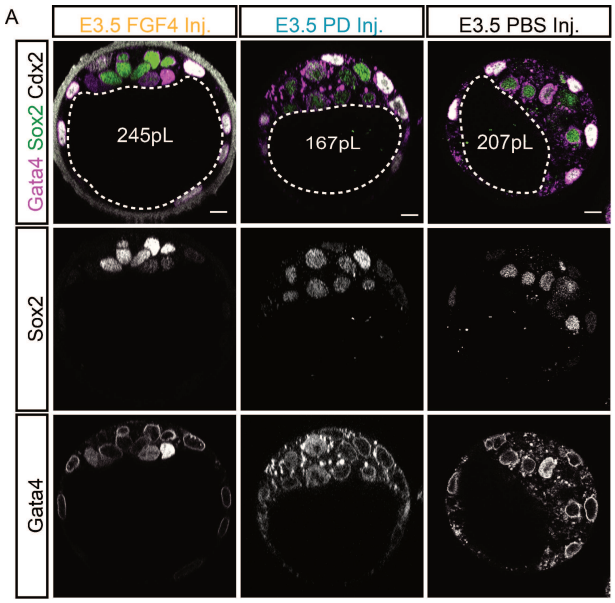
A
E3.5 FGF4 Inj.
E3.5 PD Inj.
E3.5 PBS Inj.
Gata4 Sox2 Cdx2
245pL
167pL
207pL
Sox2
Gata4

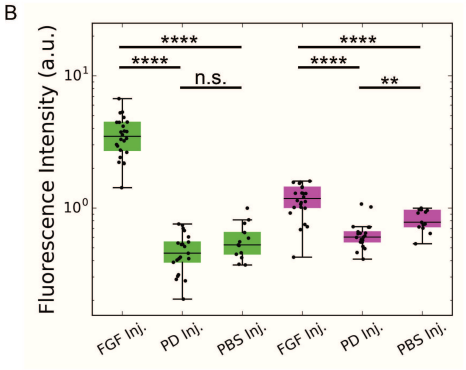
B
Fluorescence Intensity (a.u.)
****
****
n.s.
****
****
**
FGF Inj.
PD Inj.
PBS Inj.
FGF Inj.
PD Inj.
PBS Inj.

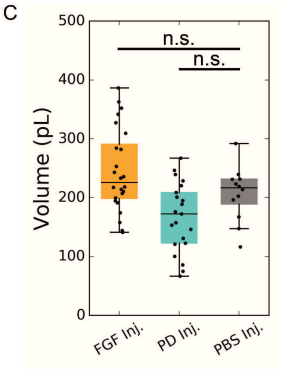
C
Volume (pL)
n.s.
n.s.
FGF Inj.
PD Inj.
PBS Inj.

Figure 6. Luminal perturbation of FGF4 signaling impacts molecular specification of EPI and PrE lineages.

(A) Immunofluorescence images of EPI (Sox2) and PrE (Gata4) fate in E3.5 post-FGF4 deposition (E3.5 FGF4 Inj.), E3.5 post-PD173074 deposition (E3.5 PD Inj.) and E3.5 post-PBS deposition (E3.5 PBS Inj.). White dotted line indicates lumen boundaries. Average lumen volume in white text. Scale bars = 10μm. (B) Boxplot of fluorescence levels of Sox2 (green) and Gata4 (magenta) in E3.5 post-FGF4 deposition (FGF4 Inj., N = 24), E3.5 post-PD173074 deposition (PD Inj., N = 21) and E3.5 post-PBS deposition (PBS Inj., N = 13) embryos. (C) Boxplot of luminal volume in E3.5 post-FGF4 deposition (FGF4 Inj., N = 24), E3.5 post-PD173074 deposition (PD Inj., N = 21) and E3.5 post-PBS deposition (PBS Inj., N = 13).

$****p < 0.0001$

$**p < 0.01$

n.s. = not significant

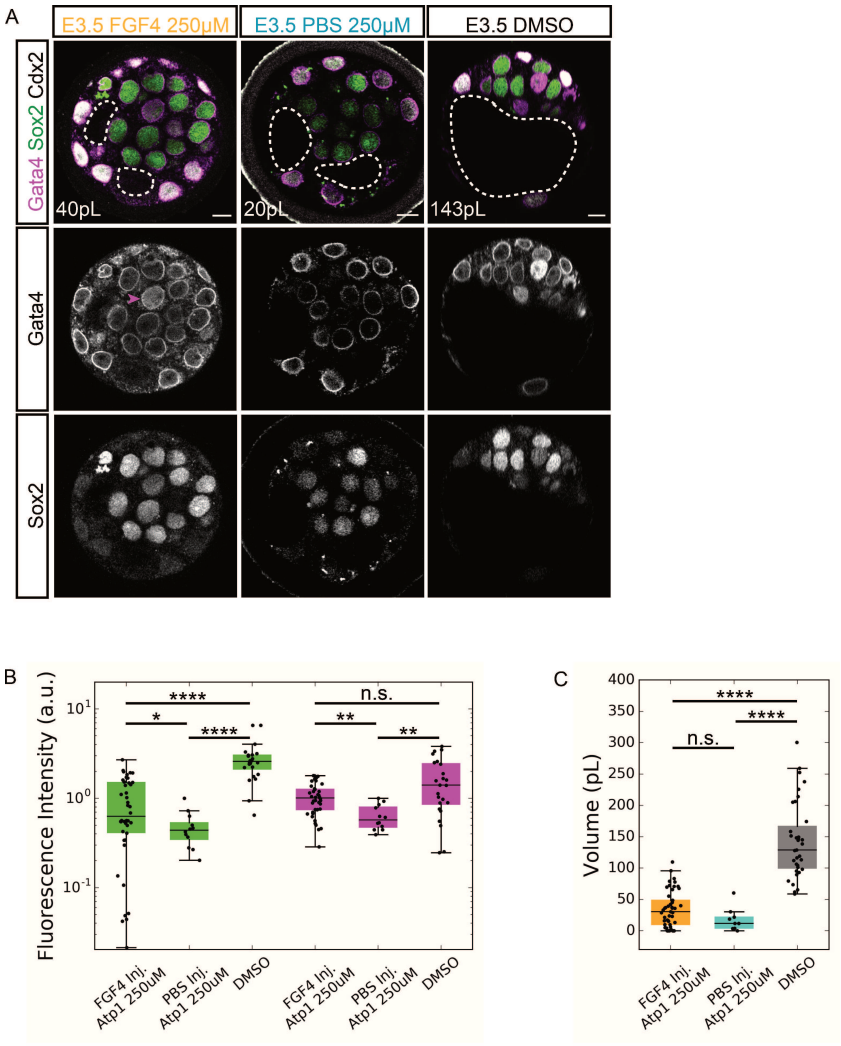
A
E3.5 FGF4 250μM
E3.5 PBS 250μM
E3.5 DMSO
Gata4 Sox2 Cdx2
Gata4
Sox2
40pL
20pL
143pL
B
Fluorescence Intensity (a.u.)
****
*
****
n.s.
**
**
FGF4 Inj. Atp1 250uM
PBS Inj. Atp1 250uM
DMSO
C
Volume (pL)
****
****
n.s.

Figure 7. Luminal deposition of FGF4 partially rescues EPI-PrE specification in ATP1-inhibited embryos.

(A) Immunofluorescence images of EPI (Sox2) and PrE (Gata4) fate in E3.5 post-FGF4 deposition and Atp1 inhibition (E3.5 FGF4 250μM), E3.5 post-PBS deposition and Atp1 inhibition (E3.5 PBS 250μM) and E3.5 control embryos (E3.5 DMSO). White dotted line indicates lumen boundaries. Average lumen volume in white text. Magenta arrowhead indicates cell with high Gata4 expression relative to neighboring cells. Scale bars = 10μm. (B) Boxplot of fluorescence levels of Sox2 (green) and Gata4 (magenta) in E3.5 post-FGF4 deposition and Atp1 inhibition (250μM FGF4 Inj., N = 42 embryos), E3.5 post-PBS deposition and Atp1 inhibition (250μM PBS Inj., N = 12) and E3.5 control embryos (DMSO, N = 12). (C) Boxplot of luminal volume in E3.5 post-FGF4 deposition and Atp1 inhibition (250μM FGF4 Inj., N = 49 embryos), E3.5 post-PBS deposition and Atp1 inhibition (250μM PBS Inj., N = 9) and E3.5 control embryos (DMSO, N = 38).

*$p < 0.05$

**$p < 0.01$

****$p < 0.0001$

n.s. not significant.

Chapter 7

Formal Discussion

Collectively, the data presented here reveal a new mechanism of blastocyst lumen formation and its role in facilitating the specification and positioning of the ICM lineages. I have shown that all cells of the embryo, not only the trophectoderm, can contribute to lumen initiation and growth through a vesicle secretion mechanism (Figure 1), in agreement with previous studies (Wiley and Eglitis, 1980 and 1981; Fleming and Pickering, 1985; Aziz and Alexandre, 1991). The apicosome-like structures observed in E3.25 embryos (Figure 2C) show that ICM cells isolated from contact-free surfaces can generate luminal precursor-like structures (Taniguchi et al., 2015 and 2017), which is in line with our observation that all cells of the embryo contribute to lumen formation.

The presence of apically polarized microlumina in E3.0 embryos (Figure 2A) along with the widespread vesicle release (Figure 1C) reveal notable parallels between blastocyst lumen formation mechanisms and apical cord hollowing. Furthermore, the morphology and secretion dynamics of the vesicles reported here are markedly similar to those present in systems that require regulated secretion of contents from large vesicles into a lumen (Miklavc et al., 2012; Rousso et al., 2016; Segal et al., 2018; Tran et al., 2015). However, the localizations of Rab11 (Figure S3) and Integrin-β1 (Figure S4) during the onset of fluid accumulation suggest that the molecular mechanisms of blastocyst lumen formation are differentially regulated than that of typical apical cord hollowing. If molecules such as morphogens or chemokines are secreted through this mechanism, this could provide a causal link between fluid accumulation and fate specification and/or cell migration (Durdu et al., 2014). In addition, if vesicles contain highly concentrated osmolytes or cell-adhesion modifying molecules (e.g. Integrin-β1 or extracellular matrix cofactors, Figure S4) secretion would facilitate downstream lumen expansion as seen in other systems (Takeda et al., 2000; Strilic et al., 2010).

I have shown that immediately following coalescence of microlumina into a singular lumen, PrE biased ICM cells begin directional movement toward the ICM-lumen interface (Figure 3). When lumen expansion is perturbed, PrE maturation and repositioning is disrupted (Figure 4,5), suggesting a causal role of lumen expansion in guiding EPI-PrE cell fate specification and

spatial sorting, which is crucial for tissue organization in downstream embryonic development (Moore et al., 2014; Morris et al., 2002; Yang et al., 2007). These results indicate that spatial segregation of ICM cell lineages initiates earlier than previously thought (Chazaud et al., 2006; Gerbe et al., 2008) and depends on morphological changes within the embryo.

The net movement of PrE cells to the luminal surface in accordance with lumen expansion (Figure 3-5) is reminiscent of chemokine-guided migration (Boldajipour et al., 2008; Bussman and Raz, 2015; Dona et al., 2013). Spatial segregation between PrE and EPI cells suggests their differential reception of luminal cues (Figure 3). The presence of FGF4 in microlumina (Figure 2), its expediting effect on fate specification when luminally deposited (Figure 6) and partial rescue of the impact of reduced luminal volume (Figure 7) may suggest an instructive role of FGF4 accumulated in the lumen. One such scenario is that as the lumen expands luminal FGF4 concentration increases to guide ICM differentiation. While future studies to profile the luminal contents will be necessary for exploring this hypothesis in depth, I have taken a first step to attempt to decouple the potential biochemical and mechanical roles of the lumen in EPI-PrE specification (Figure 6,7).

In addition to signaling molecules present in the fluid, the constantly changing physical microenvironment within the blastocyst on account of lumen emergence, coalescence and expansion may also impact tissue remodeling through changes in cell adhesion and cell shape (Dumortier et al., 2019; Durdu et al., 2014; Engler et al., 2006; Mammoto et al., 2013). It has been shown that in epithelial systems multi-luminal phenotypes due to incomplete coalescence can alter the ratios of cell types within tissues and disrupt tissue function (Bagnat et al, 2007; Bryant et al., 2010; Chou et al., 2016; Kesavan et al., 2009). Recent work shows that lumen expansion plays an important role in controlling embryo size and spatial allocation of TE and ICM cells (Chan et al., 2019). In this study, I extend this finding to the second lineage segregation event, by testing the ability of biochemical means to compensate for the effects of reduced luminal size on the specification of the epiblast and primitive endoderm lineages (Figure 7). I find that biochemical changes to luminal composition are sufficient to initiate the molecular specification of EPI and PrE (Figures 6,7).

Taken together, these data suggest that lumen expansion may provide the niche in which chemical and physical cues are integrated in order to guide the self-organized patterning of the ICM in the blastocyst. Further studies will need to be conducted in order to understand the mechanisms and interplay underlying lumen formation, cell polarization and fate specification during blastocyst morphogenesis.

Chapter 8

Conclusions and Perspectives

In the proceeding sections, the statements made will be of a combined nature. I will offer my view on how the findings of this project can be extended beyond blastocyst morphogenesis as well as begin to introduce the lines of investigation that have been designed, initiated but not yet concluded to address the second central question (see **Project Motivation and Central Questions**).

8.1 Lumen Morphogenesis as a Timer

Embryonic development is virtually always referred to in terms of absolute (chronological) time (e.g. 'The blastocyst is formed on embryonic day 3.'). While this is of course useful because it offers a certain level of unification within the field of developmental biology, I believe it to be insufficient in the context of morphogenesis. Although it has only been properly quantified in a single case to my knowledge, blastocyst lumen formation during preimplantation development does not correlate with the cell cycle (Fernández and Izquierdo, 1980). While I can confirm this finding anecdotally, rigorous quantification of this as well as the proposal of alternative 'morphogenetic timers' are necessary to further this line of thinking.

For blastocyst lumen formation, both permeability seal maturation and absolute time since fertilization (both of these are more variable between embryos than cell cycle time) have been proposed as alternative timers as a signal for fluid accumulation to initate (Fernández and Izquierdo, 1980). Permeability seal maturation as a timer is lightly supported by differences in expression onset and localization of ZO-1 α isoforms (Sheth et al., 1997). As tight junctions are multiprotein complexes, it is likely that an individual component (e.g. the ZO-1 α^+ isoform; Sheth et al., 1997) comprises a rate limiting assembly step that may act as a timer. While it is known that a certain level of tight junction maturation is required for lumen formation, thereby making it a good timer candidate, the principle of a rate limiting assembly step as a timer for morphogenesis is applicable to any essential protein complex (e.g. cofactor binding or transmembrane channel assembly) for a mophogenetic process to initiate.

In the context of EPI-PrE lineage commitment, I would propose luminal maturation (i.e. luminal coalescence and expansion rates) to be a much more faithful timer of when a blastocyst will reach maturity (i.e. the blastocyst achieves EPI-PrE spatial segregation as well as singular luminal expansion). A lumen timer would compensate for variability between embryos while still providing standardization and a method of comparison through volume matching.

8.2 Adhesion Remodeling

It is very tempting to draw parallels between the actin-mediated vesicle release identified and described here with that of systems like the *Drosophila melanogaster* salivary gland (Miklavc et al., 2012; Rousso et al., 2016; Segal et al., 2018; Tran et al., 2015). While the idea that these vesicles are secreting large volumes of contents that will impart some biochemical functional capacity to the growing lumen (e.g. FGF4 with bulky cofactors such as heparin), other possibilities are equally plausible.

Adhesion remodeling has been shown repeatedly within polarized tissue that undergo reorientation due to changes in the microenvironment or are preparing for lumenogenesis (Desclozeaux et al., 2008; Dumortier et al., 2019). Adhesion remodeling involves the orchestration of several subcellular pathways (principally the secretory pathway and directed transport of recycling endosomes) as well as cell- and tissue-level communication to allow for a seamless redirection of apicobasal membrane domains and tissue morphology (Bryant et al., 2014). Proteins like Podocalyxin (Pdx), which is a sialoglycoprotein, are typically localized to the apical membranes of epithelial tissues containing lumina, and its trafficking during epithelialization has been studied with great detail (Mrozowska and Fukuda 2016). Pdx has also been shown to act as an anti-adhesion molecule due to its highly negative surface charge (Takeda et al., 2000). The secretion and accumulation of Pdx leads to membrane repulsion and separation. This allows the apical domains to become 'slick' surfaces that allow luminal substances to pass without being trapped by adhesions (Strilić et al., 2010). As high negative surface charge is a property common to sialic acids, it is possible that other proteins like Pdx may be contained in the vesicles reported at the basolateral and apolar membranes of the mouse morula.

Thinking along the lines of adhesion remodeling to facilitate fluid accumulation for blastocyst lumenogenesis offers a platform of unification between this study and that of Dumortier et al., 2019, which shows Cdh1 remodeling during microluminal stages. As can be found in **Appendix I: Current Experiments and Reasoning**, the membrane repulsion does not appear to be driven by Pdx secretion from the actin-coated vesicles. However, there is an interesting preliminary result showing that Integrin-β1 localizes to nascently separating membrane domains at what are presumably basolateral and/or apolar sites. This combined with the pERM localization to early microlumina and apicosome-like structures implies that the process of membrane separation during blastocyst initiation may indeed be highly complex and involve adhesion re-

modeling through multiple pathways (classical polarity, adherens and integrins).

Providing additional interest in adhesion remodeling during blastocyst morphogenesis, another recent study proposes that Cdh1 is not required for the spatial segregation of EPI and PrE precusor cells from the initial salt-and-pepper pattern to sorted and distinct domains (Filimonow et al., 2019). While this is an indeed an attractive frame of thought, it requires much further investigation to fully understand how embryos lacking differential adhesion between mixed populations are able to spatially segregate. It is important to note that the results presented by Filimonow et al. do not involve the spatial tracking of individual PrE precursor cells. Tracking in live imaging datasets is essential in order to distinguish between active movement and repositioning of molecularly specified PrE precursors from deep within the ICM to the surface of the blastocyst lumen or molecular reprogramming of cells based on their position in cases of altered adhesion. Some attempts at single cell tracking have been conducted in early blastocysts during approximately EPI-PrE spatial segregation phases (unpublished results from the Hiiragi Group; Meilhac et al., 2009). These results indicate that active movement of cells is involved in the repositioning of cells within the ICM, but have not yet distinguished the mechanism(s) underlying the movements.

Accurate dissection of the contributions of each type of adhesion and/or anti-adhesion will require substantial investigation; however, I believe it to be a promising direction toward understanding the nature of basolateral lumen formation. Extending the potential involvement of β1 integrins and apical polarity proteins, there is substantial evidence that several of the same membrane domain remodeling proteins utilized for PrE polarization in preimplantation stages are also essential for the maintenance of EPI and PrE spatial niches throughout implantation stages (Gerbe et al., 2008; Leheste et al., 2002; Lighthouse et al., 2011; Stephens et al., 1995). Some conditional genetic knockouts of potential remodeling regulators already exist, but have yet to be applied to preimplantation stages (Lighthouse et al., 2011; Moore et al., 2014; Nakayama et al., 2013; Stephens et al., 1995). I believe that utilizing these mouse lines in combination with fluorescent reporters of adherins and integrins may reveal previously unknown differential adhesion profiles. Then, dependent on the results, parallels from migrational polarity could be applied to the process of EPI-PrE spatial segregation. On the other hand, a lack of differential adhesion scaffolds are identified from such investigations would point towards a physically based mechanism of spatial segregation (e.g. differences in tissue mechanics).

8.3 Potential Mechanical Influences of the Blastocyst Lumen

The results presented here largely address how lumen expansion (i.e. change in luminal volume) impacts fate specification and positioning. To more conclusively assess how lumen geometry

influences its encapsulating cells and subsequent tissue layers, a significant amount of quantitative assessment remains to be conducted. Blastocyst expansion rates and luminal pressure changes over the course of blastocyst maturation have been measured (Chan et al., 2019; Dumortier et al., 2019). In addition to global measurements such as these and sphericity, I believe it will be necessary to evaluate local changes in lumen geometry (e.g. curvature) to further the understanding of how TE and PrE cells interact with the lumen. Hopefully, this approach, along with similar quantification of cell shape changes in the TE and PrE, will begin to provide insight into if and how luminal growth feeds into the process of fate specification by regulating shape of cell and tissue scales.

Measurements of local shape change in combination with information on the distribution of extracellular matrix components could also be used to advance our understanding of how individual blastocyst lineages respond to forces generated by the developing lumen. *In vitro* approaches have been used to follow liver canaliculi morphogenesis in scenarios of varying anisotropic intercellular mechanical tension due to changes in adhesion or extracellular matrix interaction (Li et al., 2016). The importance of substrate mechanical properties (e.g. stiffness) and shape in cell fate differentiation is now well-established (Engler et al., 2006; Kumar et al., 2017). Given that the blastocyst is becoming a more easily tractable system with rapid advancements in image analysis, it may be a promising direction to combine previously implemented biophysical tools (e.g. micropipette aspiration; Maître et al., 2012,2015,2016) with force inference (for inaccessible regions of the embryos, e.g. ICM-ICM or ICM-lumen interfaces) and quantitative fluorescence information of adhesion and/or extracellular matrix deposition. In theory, this would allow for initial correlations between geometric and force measurements with membrane composition information.

8.4 Luminal Signaling

From the viewpoint of apical polarization and epithelialization, the spatial arrangement of cell lineages within the blastocyst is intriguing. It has been shown by former students of the group that TE cells can only maintain a single apical domain (unpublished data from Ekaterina Korotkevich). This offers an explanation as to why TE cells maintain their apical domain toward the external (uterine) environment throughout blastocyst morphogenesis and implantation. The PrE cells do not undergo epithelialization until the very end of preimplantation stages (reviewed int Hermitte and Chazaud, 2014). The positioning of the apical domain when this occurs is logical as it forms at the only contact-free surfaces that the cells know. What is intriguing about the regulation of TE and PrE cells once they have reached this position and maturation, both lineages require FGF4 to be maintained, and the receptor (FGFR2) is localized to TE and PrE contact-free surfaces along the blastocyst lumen (Salas-Vidal and Lomelí, 2004). This combined with the localization of FGF4 to microlumina (Figure 2) and previous

studies describing the possibility of microlumina to act as signaling niches through FGF ligand sequestration (Durdu et al., 2014) begs the question of whether or not the blastocyst lumen is a complex microenvironment that not only provides structure to the embryo (shape) but also facilitates essential singaling behaviors. Disentangling the two functions will by no means be simple, but it will be necessary if the true purpose of the blastocyst lumen is to be elucidated.

The results presented in Figure 6 represent preliminary tests to understand if local changes in FGF4 availability will differentially impact the blastocyst cell lineages. While the increase in EPI and PrE marker fluorescence in FGF4-I embryos is very intriguing, no dynamics of the changes have been measured. It would be exciting to repeat this experiment with timelapse imaging of EPI and PrE reporters. These datasets could be analyzed using the same pipeline implemented in Figure 3. Not only would this reveal the temporal dynamics of the changes in EPI-PrE specification under FGF4-I conditions, but it would also answer if PrE biased cells reposition faster than the WT situation or if the cells in closest proximity to the new FGF4 source undergo reprogramming. The later result of this experiment would also aid in beginning to understand the more dominant molecular impacts on EPI-PrE spatial segregation (i.e. Is EPI-PrE spatial segregation due to passive consequences of differential tissue material properties, or is it active rearrangement due to a chemotaxis-like mechanism?).

If it is at some point it is conclusively determined that the blastocyst lumen does act a signaling niche, this will offer a second developmental context in which such microenvironments are formed and influence critical decisions regarding fate specification and cellular behavior. This would naturally lead to the questions such as: How prevalent are such mechanisms throughout embryonic development? How is this balanced with other, more physical, functions of lumina (Schematic 11)? While it is still very much so early days in terms of these possibilities, I believe it harbors a great deal of potential for future studies.

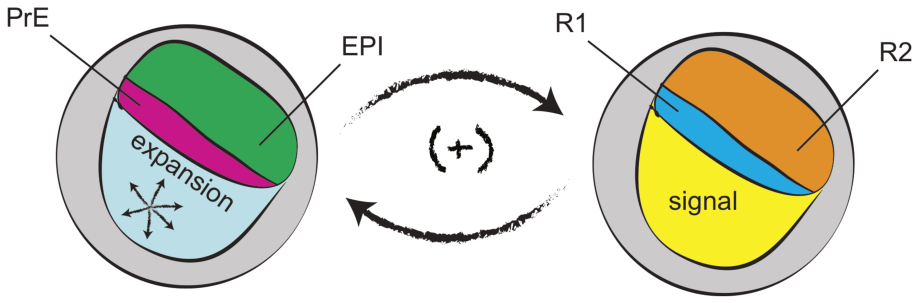

Schematic 11. Is EPI-PrE organization mediated by mechanosensitive responses to lumen expansion (left), a differentially received biochemical signal contained in the lumen (right) or a combination of the two potential mechanisms?

8.5 Quantitative Analysis Tools for Progressive Fate Specification

While it is not a biological finding, there is a simple, but significant difference between the quantitative analysis methods developed and implemented during this project and those used in past studies of EPI-PrE specification. Previous studies showing a failure of EPI-PrE spatial segregation, such as Laeno et al., 2013, have reported that the proportioning of EPI and PrE cell numbers remains constant despite the prolonged spatial overlap. However, ICM cells were classified as either EPI or PrE, and more definitive measures of quantification were not pursued. Harsh thresholding of signals or binary classification poses a risk of biasing results if datasets in fact possess intermediate states (i.e. double positive cells expressing both EPI and PrE markers at lower levels). Although datasets can appear binary to the human eye, a computer may interpret the same 8-bit tiff image to possess multiple populations.

Thankfully, it is not necessary to binarize objects of interest to belong to a single population. By incorporating a neutral signal that marks all objects of interest (i.e. DAPI in the case of nuclei), objects can be segmented and unbiasedly assessed for a degree of expression for multiple markers (i.e. Sox2 and Gata4 for EPI and PrE lineages). The spatial segregation analysis used here to assess the intermingling of EPI and PrE lineages under experimental conditions (Figures 4,5; see **Materials and Methods** and **Appendix II: Analysis Pipelines**) does not rely on thresholding or binary classification of cell lineage. Though it cannot be confirmed without repeating experiments from the published study (Laeno et al., 2013), I believe that if binarized EPI-PrE datasets were reanalyzed using the unbiased approach discussed here, the results may fit closely with those reported here.

8.6 A Closing Note

It is my hope that the approaches used and developed throughout this project can be extended to other developmental models of lumen morphogenesis. As I am sure it is clear, there is still a great deal of work to be done before a comprehensive understanding of the function(s) of the blastocyst lumen is achieved. I have greatly enjoyed this project. There are few others working on this aspect of preimplantaion development. I sincerely hope that these lines of investigation are followed through as I firmly believe that to understand how tissues develop and become functional organ systems if is necessary to study both the cells, noncellular entities and the interactions of the two.

Chapter 9

Materials and Methods

9.1 Experimental Model and Subject Details

9.1.1 Animal Work

All animal work was performed in the Laboratory Animal Resources (LAR) Facility at European Molecular Biology Laboratory (EMBL) with permission from the institutional veterinarian (ARC number TH110011). LAR Facilities operate according to international animal welfare guidelines (Federation for Laboratory Animal Science Associations guidelines and recommendations). All experimental mice were maintained in specific pathogen-free conditions on a 12-12-hour light-dark cycle and used from 8 weeks of age.

9.1.2 Embryo Recovery and Culture

To obtain pre-implantation embryos, female mice were superovulated by intraperitoneal injection of 5 or 7.5 international units (IU) of pregnant mare's serum gonadotropin (Intervet, Intergonan) followed by 5 or 7.5 IU of human chorionic gonadotropin (hCG; Intervet, Ovogest 1500) 48 hours later. Hormone injection dosage was batch dependent and determined by LAR services. Superovulated females were mated with male mice directly after hCG injection. Embryos were flushed from dissected oviducts and uteri of female mice after super-ovulation and mating with male mice. Embryos were flushed from dissected oviducts and uteri at 48, 72, 78, 84, 96 and 108 hours post-hCG using KSOMaa with Hepes (Zenith biotech, ZEHP-060). After flushing, embryos were washed in KSOMaa with Hepes, transferred to 10μL drops of KSOMaa (Zenith biotech, ZEHP-050) covered with mineral oil (Sigma, M8410) on either a tissue culture dish (Falcon, 353001) or petri dish (Falcon, 351008) and then cultured at 37°C in a CO_2 incubator (Thermo Scientific, Heracell 240i) with 5% CO2.

9.1.3 Transgenic Lines and Genotyping

The following mouse lines were used in this study: (C57BL/6xC3H) F1 as WT, mTmG (Muzumdar et al., 2007), Lifeact-EGFP (Reidl et al., 2010), PdgfrαH2B-GFP (Hamilton et

al., 2003) and Sox2-GFP (Arnold et al., 2011). Standard tail genotyping procedures were used to genotype mice (for primers and PCR product sizes see Table S1).

9.2 Method Details

9.2.1 Pharmacological Inhibition

Ouabain (Sigma, O3125) was resuspended in DMSO (Sigma, D2650) at a stock concentration of 100mM. For working concentrations of 500μM, 250μM and 100μM the stock concentration was diluted in KSOMaa. Brefeldin A (Sigma, B6542) was resuspended in DMSO at a stock concentration of 1.4mM. For working concentrations of 14μM and 7μM the stock concentration was diluted in KSOMaa. CFTR Inhibitor-172 (Santa Cruz Biotechnologies, sc-204680) was resuspended in DMSO at a stock concentration of 1mM. For working concentrations of 10μM and 5μM the stock concentration was diluted in KSOMaa. Embryos were incubated with the appropriate working concentration of ouabain, Brefeldin A, CFTR Inhibitor-172 or an equivalent DMSO concentration in μ-Slide chambered coverslips (Ibidi, 81506) for a 12-hour period before fixation in 4% PFA (see Immunofluorescence Staining).

9.2.2 Serial Mechanical Deflation

Embryos were mounted on epifluorescence microscope (Zeiss, Observer.Z1) equipped with temperature-controlled incubation chamber and visualized using transmitted light. A micromanipulator (Narishige, MON202-D) with a glass holding needle (Harvard Apparatus, GC100T-15) was used to stabilize the embryo while a fine-tipped glass needle attached to a second micromanipulator was used to actively deflate the lumen by penetrating the mural TE at the junction of two cells and manually applying negative pressure. This action was repeated multiple times during the experimental window.

As a procedural control, the deflation needle was inserted at the junction of two mural TE cells in the same manner as experimental embryos and subsequently removed while maintaining a net zero difference in pressure between the lumen and the deflation needle throughout the entire duration of the procedure.

9.2.3 Luminal Deposition

Embryos were mounted and stabilized in the same fashion as for Serial Mechanical Deflation (see above). An injection needle containing either a recombinant FGF4 protein solution (500ng/mL FGF4 with 1μg/mL heparin), an FGFR1 inhibitor solution (200nM PD173074) or PBS (as a control) was inserted between mural TE cells into a developing lumen. Positive pressure was then applied to deposit the solution in the lumen.

9.2.4 Cloning and *In Vitro* Transcription

The CDS of *fgf4* without a stop codon was cloned into a Gateway middle entry clone and then used in an LR reaction with a 5' entry clone containing an SP6 site and a 3' entry clone containing the CDS of *mNeonGreen* (Shaner et al., 2013) with a polyA site. Standard pGEM cloning was used to create a control plasmid with mNeonGreen with a T7 site.

9.2.5 mRNA Injection

Linearized plasmid was used as the template for an *in vitro* transcription reaction from an Invitrogen mMessage SP6 kit (AM1340M). mRNA injections were performed on the same microscope and with the same micromanipulators as described earlier (see Serial Mechanical Deflation). mRNA was injected into a single blastomere of 4-cell stage embryos at a concentration of 200ng/μL using a needle (Harvard Apparatus, G100TF-15) attached to an injector (Eppendorf, FemtoJet).

9.2.6 Immunofluorescence

Fixation and Permeabilization

Embryos were fixed with 4% PFA for 15 minutes at room temperature and subsequently permeabilized with PBS (0.5% Triton-X) for 20 minutes at room temperature before transferring to blocking buffer (PBS with 0.1% Tween-20; 5% BSA) for at least 4hrs at 4oC. Embryos were incubated with primary antibodies diluted in blocking buffer overnight at 4oC. After washing with blocking buffer, embryos were incubated with secondary antibodies diluted in blocking buffer for 2hrs at room temperature. Finally, embryos were rinsed with PBS before being mounted in a DAPI solution (PBS with 1:2000 DAPI; Invitrogen, D3571) for imaging (see Fixed Sample Imaging).

Primary Antibodies

The following primary antibodies were used in this study: rabbit anti-pERM (Cell Signaling, 3726), mouse anti-Cdx2 (BioGenex, MU392A-UC), goat anti-Sox2 (Santa Cruz Biotechnology, sc-17320), goat anti-Sox2 (R&D Systems, AF2018-SP), rabbit anti-Sox2 (Cell Signaling, 23064), rabbit anti Gata4 (Santa Cruz Biotechnology, sc-9053), goat anti-Gata4 (R&D Systems, AF2606-SP), rabbit anti-GFP (MBL, 598), mouse anti-Rab11 (BD Biosciences; 610656), rat anti-Integrin-β1 (Merck Millipore, MAB1997), goat anti-Biotinylated Gata4 (R&D Systembs, BAF2606) mouse anti-Oct3/4 (Santa Cruz Biotechnology, sc-5279) and mouse anti-Hsp47 (Enzo Life Sciences, M16.10A1).

Secondary Antibodies and Dyes

Secondary: donkey anti-goat Alexa Fluor™ 488 (Life Technologies, A-11055), donkey anti-rabbit Alexa Fluor™ 488 (Life Technologies, R37118), donkey anti-rabbit Alexa Fluor™ 546 (Life Technologies, A10040) Streptavidin Alexa Fluor™ 488 (Life Technologies, S32354) and donkey anti-mouse Cy™5 AffiniPure (Jackson Immunoresearch, 715-175-150). All secondary antibodies were used at 1:200 dilutions. DAPI was used to visualize nuclei. Rhodamine phalloidin (Invitrogen, R415) was used to visualize F-actin at a 1:200 dilution.

9.2.7 Confocal Microscopy

Fixed Sample Imaging

Either point scanning confocal imaging on an LSM-780 (Zeiss) or Airyscan Fast Mode acquisition on an LSM-880 (Zeiss) was performed for immunofluorescence staining prepared samples.

Live Imaging

Embryos were mounted in either 10μL KSOMaa drops covered with mineral oil (Sigma, M8140) on 35mm glass-bottomed dishes (MatTek, P35G-1.5-14-C), or in 15- well chambered coverslips (Ibidi, 81506) with 60μL of KSOM if part of a pharmacological inhibition experiment. For long-term imaging (timesteps $\geq$ 15 minutes), imaging was performed on an LSM-780 (Zeiss) with XY sample drift compensation (Rabut and Ellenberg, 2004). Short-term time-lapse imaging (timestep = 10 seconds) was performed on an LSM-880 using Airyscan Fast Mode acquisition. Both microscopes are equipped with custom-made temperature and gas-controlled chambers (EMBL) set to 37°C and 5% CO_2 during all experiments and C-Apochromat 40x water objectives (Zeiss).

9.3 Quantification and Statistical Analysis

9.3.1 Image Analysis

Volume Quantification

Volume quantification for time lapses was calculated from the output of a custom-written automatic membrane segmentation pipeline (Table S2). Volume threshold for segmentation was set to 1pL, 5pL, or 10pL depending on the image quality of the dataset to ensure fidelity.

For vesicles and single timepoints volume was estimated manually by measuring the vesicular or luminal circumference of the central plane in FIJI to extract the radius assuming isotropy.

Binary Luminal Structure Classification

Immunofluorescence images were examined for microlumina, apicosome-like structures and lumen-facing membranes expressing pERM. Binary scores were assigned to images on a presence (1), absence (0) basis for each structure, and the frequency of occurrence determined from the binary scores.

Center of Mass Distance to Lumen Surface

The lumen was segmented as described in Volume Quantification. The 'segmented cell mass' is taken to be the sum of all cells in the embryo such that the total embryo volume is equivalent to the sum of the 'segmented cell mass' and the 'segmented lumen.' 'Lumen boundaries' were determined from the lumen segmentation. 'Cell mass boundaries' were determined from the sum of the cell mass and lumen segmentations. Convex hulls representing the lumen and the embryo surface were created from the two boundary point sets. The center of mass of the lumen P_1 and the center of mass of the cell mass P_2 were used to determine the embryonic-abembryonic axis ($\overleftrightarrow{L}$). Lumen boundary and embryo outer boundary intersection points with $\overleftrightarrow{L}$ (P_3 and P_4 respectively) were found by recursively searching the facets of the convex hulls such that $\overline{P_3P_4}$ contains P_2 but does not contain P_1 . The ICM signal of interest was automatically segmented and the weighted center of mass (P_5) calculated. $\overline{P_3P_5}$ is taken as the absolute distance of the signal of interest to the ICM-lumen interface, which is then normalized by the absolute ICM width ($\overline{P_3P_4}$). This normalization is done to ensure no intrinsic bias due to changes in tissue morphology or size are introduced. The normalized distance for timepoint t_n in a time-lapse starting at t_0, is $(\overline{d_{t_n}}(\overline{w_{t_n}})^{-1})/(\overline{d_{t_0}}(\overline{w_{t_0}})^{-1})$ where $\overline{d} = \overline{P_3P_5}$ and $\overline{w} = \overline{P_3P_4}$. All segmentations and calculations were performed automatically using custom Python scripts (Table S2).

As the ICM width along the embryonic-abembryonic axis inherently shrinks throughout blastocyst development, the lack of global movement of all tracked signals toward the lumen confirms ICM width normalization to be a valid measure for positional normalization when examining signals within ICM populations relative to other objects along or relative to the embryonic-abembryonic axis.

Fate Specification Analysis

For immunofluorescence images, nuclei were segmented using DAPI signal as a reference. Transcription factor signal was then measured in each nucleus for all channels. From these measurements, a sum measurement was calculated for each channel and subsequently normalized to the reference DMSO control category. The entire analysis was performed using custom Python scripts (Table S2).

Spatial Segregation Analysis

Using the nuclear segmentations acquired during Fate Specification Analysis, the center of mass was calculated for each nucleus and stored as a 3D coordinate. The median and mean of each dimension from all nuclear centers of mass were calculated resulting in two 3D points of reference within the embryo, such that the median (P_1) will be within the lumen and the mean (P_2) will be within the ICM. A 3D line representing the embryonic-abembryonic axis ($\overleftrightarrow{L}$) was determined from P_1 and P_2. A 3D line segment ($\overline{d}$) is drawn from the center of mass of a nucleus (P_3) to an intersection point with $\overleftrightarrow{L}$ (P_4) such that the angle of intersection is 90_{o}. The 3D embryo can then be represented on a 2D coordinate system in which the x axis is $\overleftrightarrow{L}$ such that $x = 0$ is the minimum of all P_4 points identified and y values are the length of $\overline{d}$. After this 3D to 2D projection, the fluorescence intensity values of channels of interest were plotted along a third axis (z) against the positional information (x, y). A multidimensional kernel density estimate (KDE) is then performed to acquire a probability density map. KDEs from different channels of interest are then integrated over one another in 3D to obtain a single scalar value representing the degree of sorting between groups ('Overlap'). Maximum potential overlap values ('Simulation') are derived from the ranges of expression and domain sizes observed in WT embryos. The entire analysis was performed using custom Python scripts (Table S2).

Image Processing for Figures

Images for Figures 1A, 1B and 3 were processed with a multidimensional median filter (size = 10, scipy.ndimage). Images for Figures 1C, 1F and 2 were acquired using Zeiss Airyscan Fast Mode and processed using the corresponding automatic 3D deconvolution. Images for the membrane, Sox2::gfp and Pdgfr$\alpha^{\text{H2B-GFP}}$ of Figure 3and Movies S2 and S4 are maximum intensity Z-projections. The segmented lumen images in Figure 3 are sum projections.

9.3.2 Cell Counts

Total embryo cell numbers for Figures S2,S3 and S4 were determined from the automatic segmentation of nuclear masks (Table S2) based on DAPI signal. The results from automatic segmentations were validated manually in FIJI for a subset of images in each experimental category to check that the difference between the methods was negligible.

9.3.3 Statistical Tests

All graphs were generated and statistical analysis was performed in Python using the scipy statistics package. Two-sided Fisher exact test was used to compare the frequency of observation between two binary datasets. Kruskal-Wallis H-test for independent samples (non-parametric ANOVA) was used to test for statistical significance between populations; $^{****}p < 0.0001$

$^{***}p < 0.001$ $^{**}p < 0.01$ $^{*}p < 0.05$. Sample sizes and p-values are indicated in text, figures and figure legends. No statistical tests were used to predetermine sample sizes.

Chapter 10

References

Alvers, A.L., Ryan, S., Scherz, P.J., Huisken, J., and Bagnat, M. (2014) Single continuous lumen formation in the zebrafish gut is mediated by *smoothened*-dependent tissue remodeling. Development 141, 1110-1119.

Anani, S., Bhat, S., Honma-Yamanaka, N., Krawchuk, D., and Yamanaka, Y. (2014) Initiation of Hippo signaling is linked to polarity rather than to cell position in the pre-implantation mouse embryo. Development 141, 2813-2824.

Arman, E., Haffner-Krausz, R., Chen, Y., Heath, J.K., and Lonai, P. (1998) Targeted disruption of fibroblast growth factor (FGF) receptor 2 suggest a role for FGF signaling in pregastrulation mammalian development. Proc. Natl. Acad. Sci. U.S.A. 95, 5082-5087.

Arnold, K., Sarkar, A., Yram, M.A., Polo, J.M., Bronson, R., Sengupta, S., Seandel, M., Geijsen, N., and Hochedlinger, K. (2011) Sox2+ adult stem and progenitor cells are important for tissue regeneration and survival of mice. Cell Stem Cell 9, 317-329.

Artus, J., Piliszek, A., and Hadjantonakis, A.K. (2011) The primitive endoderm lineage of the mouse blastocyst: sequential transcription factor activation and regulation of differentiation by Sox17. Dev. Biol. 350, 393-404.

Aziz, M. and Alexandre, H. (1991) The origin of the nascent blastocoel in preimplantation mouse embryos: ultrastructural cytochemistry and the effect of chloroquine. Dev. Biol. 200, 77-85.

Bagnat, M., and Cheung, I.D., Mostov, K.E., and Stainier, D.Y.R. (2007) Genetic control of single lumen formation in the zebrafish gut. Nat. Cell Biol. 9, 954-960.

Bagnat, M., Navis, A., Herbstreith, S., Brand-Arzamendi, K., Curado, S., Gabriel, S., Mostov, K., Huisken, J., and Stainier, D.Y.R. (2010) Cse1l is a negative regulator of CFTR-dependent fluid secretion. Curr. Biol. 20, 1840-1845.

Barcroft, L.C., Offenberg, H., Thomsen, P., and Watson, A.J. (2003) Aquaporin proteins in murine trophectoderm mediate transepithelial water movements during cavitation. Dev. Biol. 256, 342-354.

Barcroft, L.C., Moseley, A.E., Lingrel, J.B., and Watson, A.J. (2004) Deletion of the Na/K-ATPase α1-subunit gene (*Atp1a1*) does not prevent caviation of the preimplantation mouse embryo. Mech. Dev. 121, 417-426.

Bessonnard, S., De Mot, L., Gonze, D., Barriol, M., Dennis, C., Goldbeter, A., Dupont, G., and Chazaud, C. (2014) Gata6, Nanog and Erk signaling control cell fate in the inner cell mass through a tristable regulatory network. Development 141, 3637-3648.

Blasky, A.J., Mangan, A., and Prekeris, R. (2015) Polarized protein transport and lumen formation during epithelial tissue morphogenesis. Annu. Rev. Cell Biol. 31, 575-591.

Bryant, D.M. and Mostov, K.E. (2008) From cells to organs: building polarized tissue. Nat. Rev. Mol. Cell Biol. 9, 887-901.

Bryant, D.M., Datta, A., Rodrigues-Fraticelli, A.E., Peranen, J., Martin-Belmonte, F., and Mostov, K.E. (2010) A molecular network for *de novo* generation of the apical surface and lumen. Nat. Cell Biol. 12, 1035-45.

Bryant, D.M., Roignot, J., Datta, A., Overeem, A.W., Kim, M., Yu, W., Peng, X., Eastburn, D.J., Ewald, A.J., Werb, Z., and Mostov, K.E. (2014) A molecular switch for the orientation of epithelial cell polarization. Dev. Cell 31, 171-187.

Boldajipour, B., Mahabaleshwar, H., Kardash, E., Reichman-Fried, M., Blaser, H., Minina, S., Wilson, D., Xu, Q., and Raz, E. (2008) Control of chemokine-guided cell migration by ligand sequestration. Cell. 132, 463-473.

Bussmann, J. and Raz, E. (2015) Chemokine-guided cell migration and motility in zebrafish development. EMBO J. 34, 1309-1318. 503, 285-289.

Calarco, P.G. and Brown, E.H. (1969) An ultrastructural and cytological study of preimplantation development of the mouse. J. Exp. Zool. 171,253-284.

Chan, C.J., Costanzo, M., Ruiz-Herrero, T., Mönke, G., Petrie, R., Bergert, M., Diz-Muñoz, A., Mahadevan, L, and Hiiragi, T. (2019) Hydraulic control of mammalian embryo size and cell fate. Nature; doi: https://doi.org/10.1038/s41586-019-1309-x

Chazaud, C., Yamanaka, Y., Pawson, T., and Rossant, J. (2006) Early lineage segregation between epiblast and primitive endoderm in mouse blastocysts through the Grb2-MAPK pathway. Dev. Cell 10, 615-624.

Chou, S.Y., Hsu, K.S., Otsu, W., Hsu, Y.C., Luo, Y.C., Yeh, C., Shehab, S.S., Chen, J., Shieh, V., He, G., Marean, M.B., Felsen, D., Ding, A., Poppas, D.P., Chuang, J.Z., and Sung, C.H. (2016) CLIC4 regulates apical exocytosis and renal tube luminogenesis through retromer- and actin-mediated endocytic trafficking. Nat. Commun. 7, 10412.

Dardik, A. and Schultz, R.M. (1991) Blastocoel expansion in the preimplantation mouse embryo: stimulatory effect of TGF-α and EGF. Development 11, 919-930.

Davidson, E.H. (1990) How embryos workd: a comparative view of diverse modes of cell fate specification. Development 108, 365-389.

De Sousa, P.A., and Kidder, G.M. (1997) Effects of brefeldin-A and monensin on organelle distribution and morphology in the preimplantation mouse embryo. Dev. Genes Evol. 206, 503-514.

Desclozeaux, M., Venturato, J., Wylie, F.G., Kay, J.G., Joseph, S.R., Le, H.T., and Stow, J.L. (2008) Active Rab11 and functional recycling endosome are required for E-cadherin trafficking and lumen formation during epithelial morphogenesis. Am. J Physiol. Cell Physiol. 295, 545-556.

Dona, E., Barry, J.D., Valentin, G., Quirin, C., Khmelinskii, A., Kunze, A., Durdu, S., Newton, L.R., Fernandez-Minan, A., Huber, W., Knop, M., and Gilmour, D. (2013) Directional tissue migration through a self-generated chemokine gradient. Nature. 503, 285-289.

Driesch, H. (1892). Entwicklungsmechanische Studien III–VI. Z wiss Zool, 55, 1-62.

Duan, X., Chen, K.-L., Zhang, Y., Cui, X.-S., Kim, N.-H., & Sun, S.-C. (2014). ROCK inhibition prevents early mouse embryo development. Histochemistry and Cell Biology, 142(2), 227–233.

Dumortier, J., Le Verge-Serandour, M., Tortorelli, A.F., Mielke, A., de Plater, L. Turlier, H., and Maitre, J.L. (2019) Fracking and Ostwald ripening position the lumen of the mouse blastoycst. bioRxiv 537985; doi: https://doi.org/10.1101/537985

Durdu, S., Iskar, M., Revenu, C., Schieber, N., Kunze, A., Bork, P., Schwab, Y., and Gilmour, D. (2014) Luminal signaling links cell communication to tissue architecture during organogenesis. Nature 515, 120–124.

Eckert, J.J. and Fleming, T.P. (2008) Tight junction biogenesis during early development. Biochim. Biophys. Acta 1778, 717-728.

Eckert, J.J., McCallum, A., Mears, A., Rumsby, M.G., Cameron, I.T., and Fleming, T.P. (2004) Specific PKC isoforms regulate blastocoel formation during mouse preimplantation development. Dev. Biol. 274, 384-401.

Engler, A.J., Sen, S., Sweeney, H.L., and Discher, D.E. (2006) Matrix elasticity directs stem cell lineage specification. Cell 126, 677-689.

Essner, J.J., Amack, J.D., Nyholm, M.K., Harris, E.B., Yost, H.J. (2005) Kupffer's vesicle is a ciliated organ of asymmetry in the zebrafish embryo that initiates left-right development of the brain, heart and gut. Development 132, 1247-1260.

Feldman, B., Poueymirou, W., Papiannou, V.E., DeChiara, T.M., and Goldfarb, M. (1995) Requirement of FGF-4 for postimplantation mouse development. Science 267, 246-249.

Fernández, M.S. and Izquierdo, L. (1980) Blastocoel formation in half and double mouse embryos. Anat. Embryol. 160, 77-81.

Filimonow, K., Saiz, N., Suwinska, A., Wyszomirski, T., Grabarek, J.B., Ferretti, E., Piliszek, A., Plusa, B., and Maleszewski, M. (2019) No evidence of involvement of E-cadherin in cell fate specification or the segregation of Epi and PrE in mouse blastocysts. PLOS ONE 14, e0212109.

Fleming, T.P. and Pickering, S.J. (1985) Maturation and polarization of the endocytotic system in outside blastomeres during mouse preimplantation development. Development 89, 175-208.

Ferrari, A., Veligodskiy, A., Berge, U., Lucas, M.S., and Kroschewski, R. (2008) ROCK-mediated contractility, tight junctions and channels contribute to the conversion of a preapical patch into apical surface during isochoric lumen initiation. J. Cell Biol. 121, 3649-3663.

Frankenberg, S., Gerbe, F., Bessonnard, S., Belville, C., Pouchin, P., Bardot, O., and Chazaud, C. (2011) Primitive endoderm differentiates via a three-step mechanism involving nanog and RTK signaling. Dev. Cell. 21, 1005-1013.

Garbutt, C.L., Chisholm, J.C., and Johnson, M.H. (1987) The establishment of the embryonic-abembryonic axis in the mouse embryo. Development 100, 125-134.

Gebala, V., Collins, R., Geudens, I., Phng, L.K., and Gerhardt, H. (2016). Blood flow drives lumen formation by inverse membrane blebbing during angiogenesis in vivo. Nat. Cell Biol. 18, 443–450.

Gerbe, F., Cox, B., Rossant, J., and Chazaud, C. (2008) Dynamic expression of Lrp2 pathway members reveals progressive epithelial differentiation of primitive endoderm in mouse blastocyst. Dev. Biol. 313, 594-602.

Gilbert, S.F. (2000) Developmental biology. Sunderland, Mass, Sinauer Associates.

Goldin, S.N. and Papaioannou, V.E. (2003) Paracrine action of FGF4 during periimplantation development maintains trophectoderm and primitive endoderm. Genesis 36, 40-47.

Guo, G., Huss, M., Tong, G.Q., Wang, C., Li Sun, L, Clarke, N.D., and Robson, P. (2010) Resolution of cell fate decisions revealed by single-cell gene expression analysis from zygote to blastocyst. Dev. Cell 18, 675-685.

Haffner-Krausz, R., Gorivodsky, M., Chen, Y., and Lonai, P. (1999) Expression of Fgfr2 in the early mouse embryo indicates its involvement in preimplantation development. Mech. Dev. 85, 167-172.

Hamilton, T. G., Klinghoffer, R. A., Corrin, P. D. and Soriano, P. (2003). Evolutionary divergence of platelet-derived growth factor alpha receptor signaling mechanisms. Mol. Cell. Biol. 23, 4013-4025.

Helms, J.B. and Rothman, J.E. (1992) Inhibition of brefeldin A of a golgi membrane enzyme that catalyses exchange of guanine nucleotide bound to ARF. Nature 360, 352-354.

Hermitte, S. and Chazaud, C. (2014) Primitive endoderm differentiation: from specification to epithelium formation. Phil. Trans. R. Soc. B 369: 20130537.

Hoijman, E., Rubbini, D., Colombelli, J., and Alsina, B. (2015) Mitotic cell rounding and epithelial thinning regulate lumen growth and shape. Nat. Commun. 6, 7355.

James, P.F., Grupp, I.L., Grupp, G., Woo, A.L., Askew, G.R., Croyle, M.L., Walsh, R.A., and Lingrel, J.B. (1999) Identification of a specific role for the Na,K-ATPase $\alpha 2$ isoform as a

regulator of calcium in the heart. Mol. Cell 3, 555-563.

Johnson, M.H. and Ziomek, C.A. (1981) The foundation of two distinct cell lineages within the mouse morula. Cell 24, 71-80.

Jones, D.H., Davies, T.C., and Kidder, G.M. (1997) Embryonic expression of the putative γ subunit of the sodium pump is required for acquisition of fluid transport capacity during mouse blastocyst development. J. Cell Biol. 139, 1545-1552.

Kang, M., Piliszek, A., Artus, J., and Hadjantonakis, A.K. (2013) FGF4 is required for lineage restriction and salt-and-pepper distribution of primitive endoderm factors but not their initial expression in the mouse. Development 140, 267-279.

Kang, M., Garg, V., and Hadjantonakis, A.K. (2017) Lineage establishment and progression within the inner cell mass of the mouse blastocyst requires FGFR1 and FGFR2. Dev Cell. 41, 1-15.

Kawagishi, R., Tahara, M., Sawada, K., Ikebuchi, Y., Morishige, K., Sakata, M., Tasaka, K., and Murata, Y. (2004) Rho-kinase is involved in mouse blastocyst cavity formation. Biochem. Biophys. Res. Commun. 319, 643-648.

Kesavan, G., Sand, F.W., Greiner, T.U., Johnasson, J.K., Kobberup, S., Wu, X., Brakebusch, C., and Semb, H. (2009) Cdc42-mediated tubulogenesis controls cell specification. Cell 139, 791-801.

Kono, K., and Tamashiro, D.A.A., and Alracon, V.B. (2014) Inhibition of RHO-ROCK signaling enhances ICM and suppresses TE characteristics through activation of Hippo signaling in the mouse blastocyst. Dev. Biol. 394, 142-155.

Korotkevich, K., Niwayama, R., Courtois, A., Friese, S., Berger, N., Buchholz, F., and Hiiragi, T. (2017). The apical domain is required and sufficient for the first lineage segregation in the mouse embryo. Dev. Cell. 40, 235-247.

Krawchuk, D., Honma-Yamanaka, N., Anani, S., Yamanaka, Y. (2013) FGF4 is a limiting factor controlling the proportions of primitive endoderm and epiblast in the ICM of the mouse blastocyst. Dev. Biol. 384, 65-71.

Kumar, A., Placone, J.K., and Engler, A.J. (2017) Understanding the extracellular forces that determine cell fate and maintenance. Development 144, 4261-4270.

Laeno, A.M.A., Tamashiro, D.A.A., and Alarcon, V. B. (2013) Rho-associated kinase activity is required for proper morphogenesis of the inner cell mass in the mouse blastocyst. Biol. Reprod. 89: doi: 10.1095/biolreprod.113.109470

Lanner, F. and Rossant, J. (2010) The role of FGF/Erk signaling in pluripotent cells. Development. 137, 3351-3360.

Leheste, J.R., Melsen, F., Wellner, M., Jansen, P., Schlichting, U., Renner-Müller, I., Andreassen, T.T., Wolf, E., Bachmann, S., Nykjaer, A., and Willnow, T.E. (2002) Hypocalcemia and osteopathy in mice with kidney-specific megalin gene defect. FASEB J. 17, 247-249.

Lighthouse, J.K., Zhang, L., Hsieh, J.C., Rosenquist, T., and Holdener, B.C. (2011) MESD is essential for apical localization of Megalin/LRP2 in the visceral endoderm. Dev. Dyn. 240, 577-588.

Madan, P., Rose, K., and Watson, A.J. (2007) Na/K-ATPase $\beta 1$ subunit expression is required for blastocyst formation and normal assembly of trophectoderm tight junction-associated proteins. J. Biol. Chem. 282, 12127-12134.

Maitre, J.L., Berthoumieux, H., Krens, S.F.G., Salbreux, G., Julicher, F., Paluch, E., and Heisenberg, C.P. (2012) Adhesion functions in cell sorting by mechanically coupling the cortices of adhering cells. Science 388, 253-256.

Maitre, J.L., Niwayama, R., Turlier, H., Nedelec, F., and Hiiragi, T. (2015) Pulsatile cell-autonomous contractility drives compaction in the mouse embryo. Nat. Cell Biol. 17, 849-855.

Maître, J.L., Turlier, H., Illukkumbura, R., Eismann, B., Niwayama, R., Nédélec, F., and Hiiragi, T. (2016) Asymmetric division of contractile domains couples cell positioning and fate specification. Nature 536, 344-348.

Mammoto, T., Mammoto, A., and Ingber, D.E. (2013) Mechanobiology and developmental control. Annu. Rev. Cell Dev. Biol. 29, 27-61.

Manejwala, F., Kaji, E., and Schultz, R.M. (1986) Development of activatable adenylate cyclase in the preimplantation mouse embryo and a role of cyclic AMP in blastocoel formation. Cell 46, 95-103.

Manejwala, F.M., Cragoe, E.J., and Schultz, R.M. (1989) Blastocoel expansion in the preimplantation mouse embryo: role of extracellular sodium and chloride and possible apical routes of their entry. Dev. Biol. 133, 210-220.

Martin-Belmonte, F., Gassama, A., Datta, A., Yu, W., Rescher, U., Gerke, V., and Mostov, K. (2007) PTEN-mediated apical segregation of phosphoinositides controls epithelial morphogenesis through Cdc42. Cell 128, 383-397.

Martin-Belmonte, F. and Mostov, K. (2008) Regulation of cell polarity during epithelial morphogenesis. Curr. Opin. Cell Biol. 20, 227-234.

Meilhac, S.M., Adams, R.J., Morris, S.A., Danckaert, A., Le Garrec, J.F., Zernicka-Goetz, M. (2009) Active cell movements coupled to positional induction are involved in lineage segregation in the mouse blastocyst. Dev. Biol. 331, 210-221.

Meng, Y., Cai, K.Q., Moore, R., Tao, W., Tse, J.D., Smith, E.R., and Xu, X.X. (2017) Pten facilitates epiblast epithelial polarization and proamniotic lumen formation in early mouse embryos. Dev. Dyn. 246, 517-530.

Meng, Y., Moore, R., Tao, W., Smith, E.R., Tse, J.D., Caslini, C., and Xu, X.X. (2018) GATA6 phosphorylation by Erk1/2 propels exit from pluripotency and commitment to primitive endoderm. Dev. Biol. 436, 55-65.

Messerschmidt, D.M. and Kemler, R. (2010) Nanog is required for primitive endoderm formation through a non-cell autonomous mechanism. Dev. Biol. 344, 129-137.

Miklavc, P., Hecht, E., Hobi, N., Wittekindt, O.H., Dietl, P., Kranz, C., and Frick, M. (2012) Actin coating and compression of fused secretory vesicles are essential for surfactant secretion – a role for Rho, formins and myosin II. J. Cell Sci. 125, 2765-2774.

Miller, S.G., Carnell, L., and Moore, H.P.H. (1992) Post-golgi membrane traffic: Brefeldin A inhibits export from distal golgi compartments to the cell surface but not recycling. J. Cell Biol. 118, 267-283.

Molotkov, A., Mazot, P., Brewer, J.R., Cinalli, R.M., and Soriano, P. (2017) Distinct requirements for FGFR1 and FGFRR2 in primitive endoderm development and exit from pluripotency. Dev Cell. 41, 511-526.

Moore, R., Tao, W., Smith, E.R., and Xu, X.X. (2014) The primitive endoderm segregates from the epiblast in β1 Integrin-deficient early mouse embryos. Mol. Cell. Biol. 34, 560-572.

Moriwaki, K., Tsukita, S., and Furuse, M. (2007) Tight junctions containing claudin 4 and 6 are essential for blastocyst formation in preimplantation mouse embryos. Dev Biol. 312, 509-522.

Morris, S.M., Tallquist, M.D., Rock, C.O., and Cooper, J.A. (2002) Dual roles for the Dab2 adaptor protein in embryonic development and kidney transport. EMBO J. 21, 1555-1564.

Motosugi, N., Bauer, T., Polanski, Z., Solter, D., and Hiiragi, T. (2005) Polarity of the mouse embryo is established at blastocyst and is not prepatterned. Genes Dev 19, 1081-1092.

Mrozowska, P.S. and Fukuda, M. (2016) Regulation of podocalyxin trafficking by Rab small GTPases in 2D and 3D epithelial cell cultures. J Cell Biol. 213, 355-369.

Muzumdar, M.D., Tasic, B., Miyamichi, K., Li, L., and Luo, L. (2007) A global double-fluorescent Cre reporter mouse. Genesis. 45, 593-605.

Nakayama, M., Nakayama, A., van Lessen, M., Yamamoto, H., Hoffmann, S., Drexler, H.C.A., Itoh, N., Hirose, T., Breier, G., Vestweber, D., Cooper, J.A., Ohno, S., Kaibuchi, K., and Adams, R.H. (2013) Spatial regulation of VEGF receptor endocytosis in angiogenesis. Nat. Cell Biol. 15, 249-260.

Navis, A. and Bagnat, M. (2015) Developing pressures: fluid forces driving morphogenesis. Curr. Opin. Genetics Dev. 32, 24-30.

Navis, A. and Bagnat, M. (2015b) Loss of cftr function leads to pancreatic destruction in larval zebrafish. Dev. Biol. 399, 237-248.

Nichols, J., Silva, J., Roode, M., and Smith, A. (2009) Suppression of Erk signalling promotes ground state pluripotency in the mouth embryo. Development 136, 3215-3222.

Nishioka, N., Inoue, K.I., Adachi, K., Kiyonari, H., Ota, M., Ralston, A., Yabuta, N., Hirahara, S., Stephenson, R.O., Ogonuki, N., Makita, R., Kurihara, H., Morin-Kensicki, E.M., Nojima, H., Rossant, J., Nakoa, K., Niwa, H., and Sasaki, H. (2009) The Hippo signaling pathway components Lats and Yap pattern Tead4 activity to distinguish mouse trophectoderm from inner cell mass. Dev. Cell 16, 398-410.

Ohnishi, Y., Huber, W., Tsumura, A., Kang, M., Xenopoulos, P., Kurimoto, K., Oles, A.K., Arauzo-Bravo, M.J., Saitou, M., Hadjantonakis, A.K., and Hiiragi, T. (2014) Cell-to-cell expression variability followed by signal reinforcement progressively segregates early mouse

lineages. Nat. Cell Biol. 16, 27-37.

Plusa, B., Piliszek, A., Frankenberg, S., Artus, J., and Hadjantonakis, A.K. (2008) Distinct sequential cell behaviours direct primitive endoderm formation in the mouse blastocyst. Development 135, 2081-3091.

Rassoulzadegan, M., Rosen, B.S., Gillot, I., and Cuzin, F. (2000) Phagocytosis reveals a reversible differentiated state early in the development of the mouse embryo. EMBO J. 19, 3295-3303.

Reidel, J., Flynn, K.C., Raducanu, A., Gärtner, F., Beck, G., Bösl, M., Bradke, F., Massberg, S., Aszodi, A., Sixt, M., and Wedlich-Söldner, R. (2010) Lifeact mice for studying F-actin dyanmics. Nat. Methods 7, 168-169.

Rodriguez-Boulan, E. and Macara, I.G. (2014) Organization and execution of the epithelial polarity programme. Nat. Rev. Mol. Cell Biol. 15, 225-242

Rossant, J. and Tam, P.P.L. (2009) Blastocyst lineage formation, early embryonic asymmetries and axis patterning in the mouse. Development 136, 701-713.

Rousoo, T., Schejter, E.D., and Shilo, B.Z. (2016) Orchestrated content release from Drosophila glue-protein vesciles by a contractile actomyosin network. Nat. Cell Biol. 18, 181-190.

Salas-Vidal., E. and Lomelí, H. (2004) Imaging filopodia dynamics in the mouse blastocyst. Dev. Biol. 265, 75-89.

Saiz, N., Grabarek, J.B., Sabherwal., N., Papalopulu, N., and Plusa, B. (2013) Atypical protein kinase C couples cell sorting with primitive endoderm maturation in the mouse blastocyst. Development 140, 4311-4322.

Sasaki, H. (2015) Position- and polarity-dependent Hippo signaling regulates cell fates in preimplantation mouse embryos. Semin. Cell Dev. Biol. 47-48, 80–87.

Schrode, N., Saiz, N., Di Talia, S., and Hadjantonakis, A.K. (2014) GATA6 levels modulate primitive endoderm cell fate choice and timing in the mouse blastocyst. Dev. Cell 29, 454-467.

Schindelin, K. Arganda-Carreras, I., Frise, E., Kaynig, V., Longair, M., Pietzsch, T., Preibisch, S., Rueden, C., Saalfeld,S., Schmid, B., Tinevez, J.Y., White, D.J., Hartenstein, V., Eliceiri, K., Tomancak, P., and Cardona, A. (2012) Fiji: an open-source platform for biological-image

analysis. Nat. Methods 9, 676-682.

Schröter, C., Rué, P., Mackenzie, J.P., and Aria, A.M. (2015) FGF/MAPK signaling sets the switching threshold of a bistable circuit controlling cell fate decisions in embryonic stem cells. Development 142, 4205-4216.

Segal, D., Zaritsky, A., Schejter, E.D., and Shilo, B.Z. (2018) Feedback inhibition of actin on Rho mediates content release from large secretory vesicles. J. Cell Biol. 217, 1815-1826.

Shaner, N.C., Lambert, G.G., Chammas, A., Ni, Y., Cranfill, P.J., Baird, M.A., Sell, B.R., Allen, J.R., Day, R.N., Israelsson, M., Davidson, M.W., and Wang, J. (2013) A bright monomeric green fluorescent protein derived from *Branchiostoma lanceolatum*. Nature Methods 10, 407-409.

Sheth, B., Fesenko, I., Collins, J.E., Moran, B., Wild, A.E., Anderson, J.M., and Fleming, T.P. (1997) Tight junction assembly during mouse blastocyst formation is regulated by late expression of ZO-1 α^+ isoform. Development 124, 2027-2037.

Sigurbjörnsdóttir, S., Mathew, R., and Leptin, M. (2014) Molecular mechanisms of *de novo* lumen formation. Nat. Rev. Mol. Cell Biol. 15, 665-676.

Sobajima, T., Yoshimura, S., Iwano, T., Kunii, M., Watanabe, M., Atik, N., Mushiake, S., Morii, E., Koyama, Y., Miyoshi, E., and Harada, A. (2015) Rab11a is required for apical protein localisation in the intestine. Biol. Open 4, 86-94.

Stephens, L.E., Sutherland, A.E., Klimanskaya, I.V., Andrieux, A., Meneses, J., Pedersen, R.A., Damsky, C.H. (1995) Deletion of β1 integrins in mice results in inner cell mass failure and peri-implantation lethality. Genes Dev. 9, 1883-1895.

Stephenson, R.O., Yamanaka, Y., and Rossant, J. (2010) Disorganized epithelial polarity and excess trophectoderm cell fate in preimplantation embryos lacking E-cadherin. Development 137, 3383-3391.

Strilić, B., Eglinger, J., Krieg, M., Zeeb, M., Axnick, J., Babál, Müller, D.J., and Lammert, E. Electrostatic cell-surface repulsion initiates lumen formation in developing blood vessels. (2010) Curr. Biol. 20, 2003-2009.

Strumpf, D., Mao, C.A., Yamanaka, Y., Ralson, A., Chawengsaksophak, K., Beck, F., and Rossant, J. (2005) Cdx2 is required for correct cell fate specification and differentiation of trophectoderm in the mouse blastocyst. Development 132, 2093-2102.

Takeda, T., Go, W.Y., Orlando, R.A., and Farquhar, M.G. (2000) Expression of podocalyxin inhibits cell-cell adhesion and modifies junctional properties in Madin-Darby canine kidney cells. Mol. Biol. Cell. 11, 3219-3232.

Taniguchi, K., Shao, Y., Townshend, R.F., Tsai, Y.H., DeLong, C.J., Lopez, S.A., Gayen, S., Freddo, A.M., Chue, D.J., Thomas, D.J., Spense, J.R., Margolis, B., Kalantry, S., Fu, J., O'Shea, K.S., and Gumucio, D.L. (2015) Lumen formation is an intrinsic property of isolated human pluripotent stem cells. Stem Cell Rep. 5, 954-962.

Taniguchi, K., Shao, Y., Townshend, R.F., Cortex, C.L., Harris, C.E., Meshinchi, S., Kalantry, S., Fu, J., O'Shea, K.S., and Gumucio, D.L. (2017) An apicosome initiates self-organizing morphogenesis of human pluripotent stem cells. J. Cell Biol. 216, 3981-3990.

Tarkowski, A. K. (1959) Experiments on the development of isolated blastomeres of mouse eggs. Nature 184, 1286–1287.

Tarkowski, A. K. and Wróblewska, J. Development of blastomeres of mouse eggs isolated at the 4- and 8-cell stage. J. Embryol. Exp. Morphol. 18, 155–180 (1967).

Tran, D.T., Masedunskas, A., Weigert, R., and Hagen, K.G.T. (2015) Arp2/3-mediated F-actin formation controls regulated exocytosis in vivo. Nat. Commun. 6, 10098.

Violette, M.I., Madan, P., and Watson, A.J. (2006) Na^+/K^+-ATPase regulates tight junction formation and function during mouse preimplantation development. Dev. Biol. 289, 406-419.

Watson, A.J. (1992) The cell biology of blastocyst development. Mol. Reprod. Dev. 33, 492-504.

Watson, A.J. and Barcroft, L.C. (2001) Regulation of blastocyst formation. Front. Biosci. 6, 708-730.

Wennekamp, S., Mesecke, S., Nédélec, F., and Hiiragi, T. (2013) A self-organization framework for symmetry breaking in the mammalian embryo. Nat. Rev. Mol. Cell Biol. 14, 452-459.

Wiley, L.M. and Eglitis, M.A. (1980) Effects of colcemid on cavitation during mouse blastocoele formation. Exp. Cell Res. 127, 89-101.

Wiley, L.M. and Eglitis, M.A. (1981) Cell surface and cytoskeletal elements: cavitation in the mouse preimplantation embryo. Dev. Biol. 86, 493-501.

Wiley, L.M. (1984) Cavitation in the mouse preimplantation embryo: Na/K-ATPase and the origin of nascent blastocoele fluid. Dev. Biol. 105, 330-342.

Yamanaka, Y., Lanner, F., and Rossant, J. (2010) FGF signal-dependent segregation of primitive endoderm and epiblast in the mouse blastocyst. Development. 137, 715-724.

Yang, D.H., Cai, K.Q., Roland, I.H., Smith, E.R., and Xu, X.X. (2007) Disabled-2 is an epithelial surface positioning gene. J. Biol. Chem. 282, 13114-13122.

Yang, Z., Zimmerman, S., Brakeman, P.R., Beaudoin III, G.M., Reichardt, L.F., and Marciano, D.K. (2013) *De novo* lumen formation and elongation in the developing nephron: a central role for afadin in apical polarity. Development 140, 1774-1784.

Ziomek, C.A. and Johnson, M.H. (1980) Cell surface interaction induces polarization of mouse 8-cell blastomeres at compaction. Cell 21, 935-942.

Chapter 11

Supplementary Information

11.1 Supplementary Figures

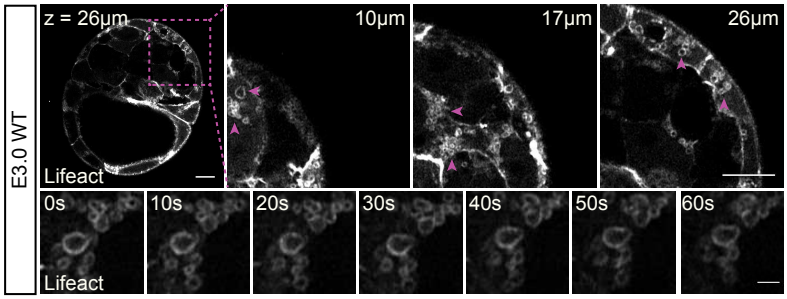

Figure S1. Cortically localized and secreted vesicles are no longer present in embryos containing an expanded lumen.
Z-slices of an E3.5 WT embryo expressing Lifeact-GFP show only cytoplasmic vesicle clusters (top row, scale bars = 10μm.). Inset (panels 2-4) delineated by magenta box (panel 1). Arrowheads (panels 2-4) highlight vesicle clusters. Time-lapse of vesicle cluster dynamics in an E3.5 WT embryo expressing Lifeact-GFP (bottom row, scale bar = 2μm). Representative of N = 24 embryos.

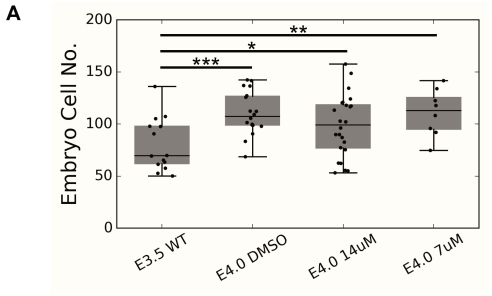

B

n.s.

Exp. / +/-	DMSO	14uM
CC-3 +	1	3
CC-3 -	14	24

Figure S2. COPII inhibition via Brefeldin A treatment does not affect total embryo cell number or induce apoptosis.
(A) Total embryo cell counts for E3.5-E4.0 COPII inhibition conditions – E3.5 WT, N = 14; E4.0 DMSO, N = 18; E4.0 7μM, N = 8; E4.0 14μM, N = 24. (B) Table showing presence (+) or absence (-) of cleaved caspace-3 signal (CC-3) in DMSO (N = 15) and COPII Inhibition (N = 27) conditions.
*$p < 0.1$
**$p < 0.01$
***$p < 0.001$
n.s. = not significant

A previous study reported that treatment of preimplantation mouse embryos with Brefeldin A results in cytokenesis failure (De Sousa and Kidder, 1997). The discrepancies between the results presented here with the previous study are likely due to differences in staging and concentration.

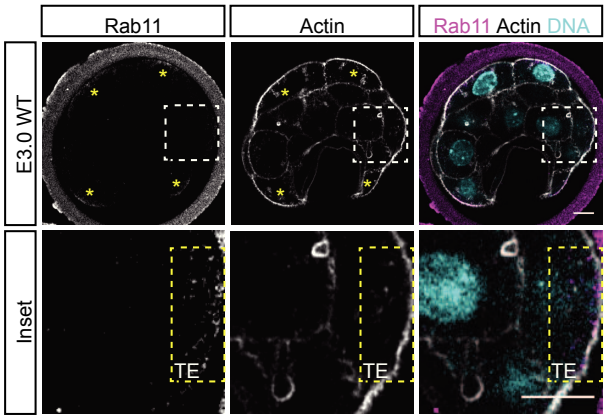

Figure S3. Rab11 localizes subapically in TE cells.
Immunofluorescence images of Rab11 in an E3.0 WT embryo. Yellow asterisks indicate TE cells in which subapical localization of Rab11 can be seen. Dashed white box outlines inset region. Dashed yellow box outlines apical and subapical region of TE cell in inset. TE cell is labeled as 'TE' within dashed yellow box of inset panels. Representative of N = 14 embryos. Scale bars = 10μm.

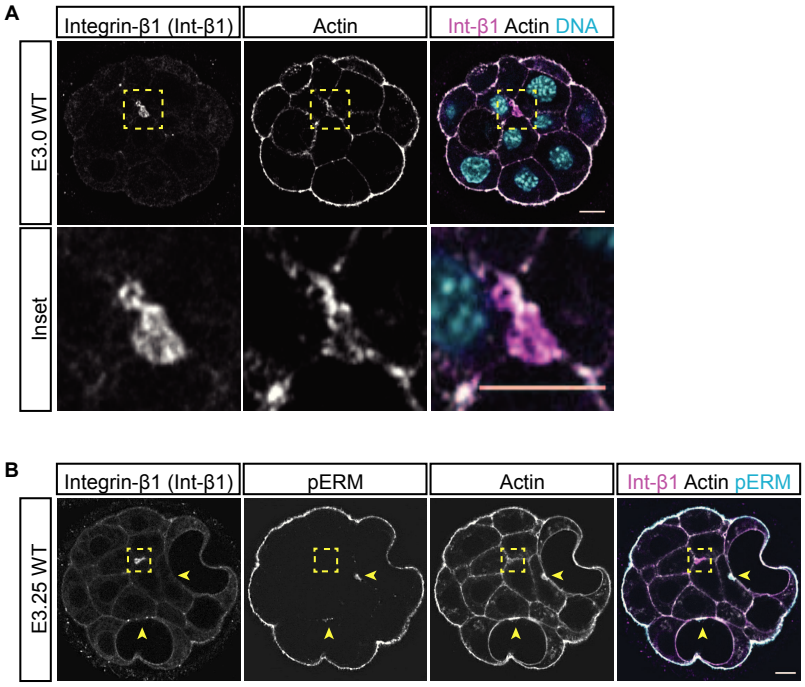

Figure S4. Integrin-β1 localizes to microlumina and nascently separated membrane domains exclusively of pERM. (A) Immunofluorescence images of Integrin-β1 in an E3.0 WT embryo. Dashed yellow box outlines inset region. Representative of N = 24 embryos. (B) Co-immunofluorescence images of Integrin-β1 and pERM in an E3.25 WT embryo. Dashed yellow box highlights Integrin-β1 localized to nascently separated membranes. Yellow arrowheads indicate pERM localized to luminal facing membrane regions. All scale bars = 10μm.

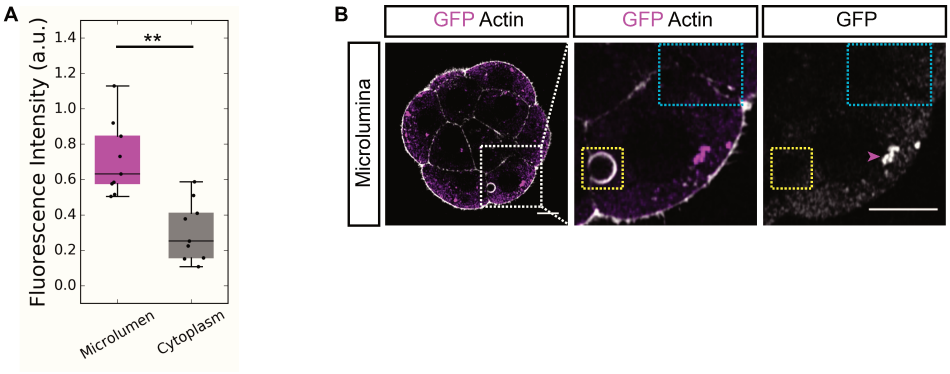

Figure S5. FGF4-mNeonGreen localizes to microlumina, while mNeonGreen does not. (A) Microluminal and cytoplasmic fluorescence levels within fgf4-mNeonGreen mRNA injected embryos ($N_{Microlumen} = 9$, $N_{Cytoplasm} = 9$). $^{**}p < 0.01$ (B) Immunofluorescence images of an E3.0 embryo injected with mNeonGreen mRNA. Blue dashed box outlines region containing multiple microlumina. Yellow dashed box outlines a presumptive fluid contributing vesicle undergoing secretion. Magenta arrowhead indicates a cluster of mNeonGreen protein adjacent to the nucleus. Representative of N = 33 embryos. Scale bars = 10μm.

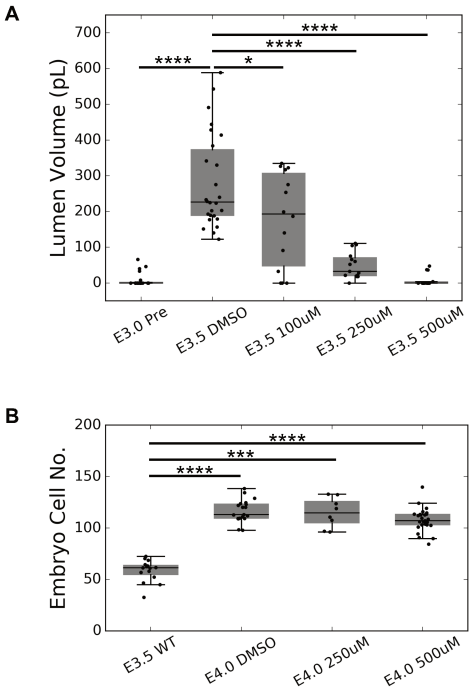

Figure S6.Inhibitory effects of ouabain are dose dependent and do not affect cell number.

(A) Volume of lumina for experimental and control embryos in E3.0-E3.5 ouabain titration inhibitions – E3.0 WT, N = 20; E3.5 DMSO, N = 26; E3.5 100μM, N = 14; E3.5 250μM, N = 15; E3.5 500μM, N = 14. (B) Total cell numbers of embryos in experimental and control groups of ouabain titration inhibitions – E3.5 WT, N = 15; E4.0 DMSO, N = 19; E4.0 250μM, N = 8; E4.0 500μM, N = 27.

*$p < 0.05$

***$p < 0.001$

****$p < 0.0001$

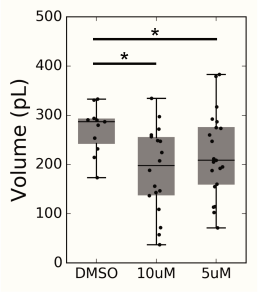

Figure S7. CFTR inhibition reduces luminal volume.
Boxplot of lumen volume in E3.0-E3.5 CFTR inhibition (10μM, N = 18 embryos; 5μM, N = 21 embryos) and control (DMSO, N = 11 embryos) conditions. *$p < 0.05$

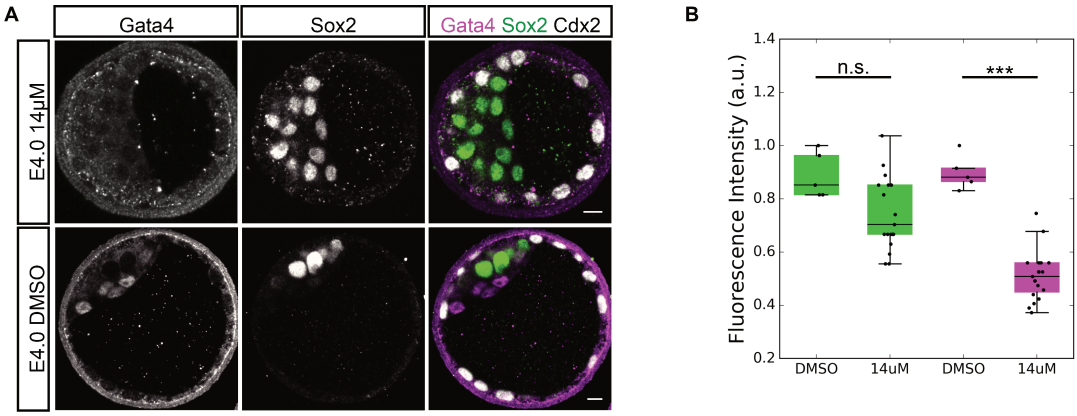

Figure S8. Brefeldin A prevents the formation of the primitive endoderm.
(A) Immunofluorescence images of EPI (Sox2) and PrE (Gata4) fate in COPII inhibited (E4.0 14μM) and control embryos (E4.0 DMSO). (B) Boxplot of Sox2 (green) and Gata4 (magenta) expression levels in COPII inhibited (14μM, N = 19 embryos) and control (DMSO; N = 5 embryos) embryos.
$***p < 0.0001$
n.s. = not significant

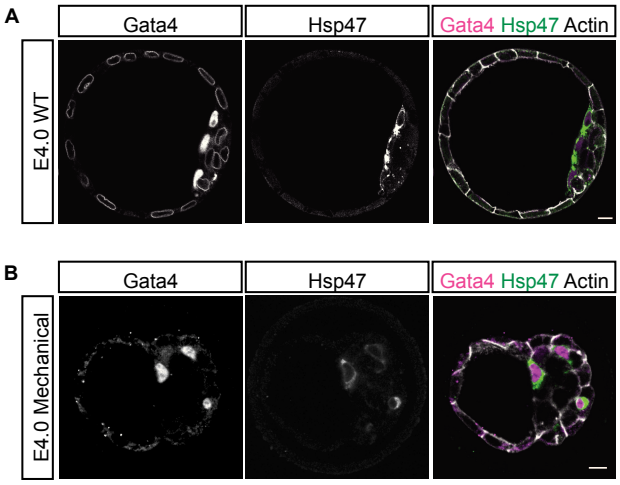

Figure S9. Gata4 is a reliable marker of PrE fate and retains tissue specificity after experimental perturbation.

(A) Immunofluorescence images of Gata4 and Hsp47 in an E4.0 WT embryo. Representative of N = 8 embryos. (B) Immunofluorescence images of Gata4 and Hsp47 in an E4.0 mechanically deflated embryo. Representative of N = 9 embryos.

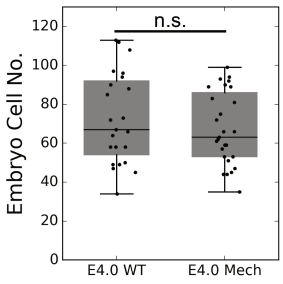

Figure S10. Serial mechanical deflation does not impact cell number.
Boxplot of total cell numbers of embryos in experimental and control groups for serial mechanical deflation – E4.0 WT, N = 23; E4.0 Mech, N = 27.
n.s. = not significant.

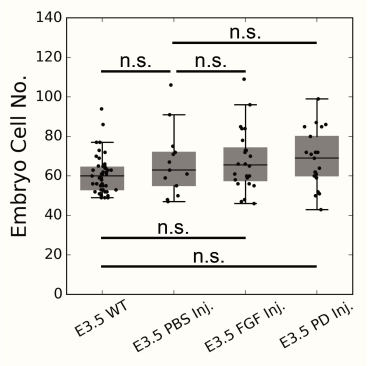

Figure S11. Luminal deposition of PBS, FGF4 protein solution or FGF inhibitor solution does not affect embryo cell number.

Boxplot of total cell numbers of embryos in experimental (E3.5 FGF Inj., N = 24 embryos; E3.5 PD Inj.; N = 21 embryos) and control (E3.5 WT, N = 47 embryos; E3.5 PBS Inj., N = 13 embryos) groups for luminal deposition.

n.s. = not significant.

11.2 Supplementary Movies

For the submission of the corresponding manuscript of this study to *Developmental Cell*, six movies were added as supplementary information. The movies can be viewed and/or downloaded here (link expires 17 August 2019):

https://oc.embl.de/index.php/s/hgEz7756psmPbD1
password: AQR-thesis-20190704

To substitute after the link expires, below are several frames from each movie above the movie legend to convey the central point of each.

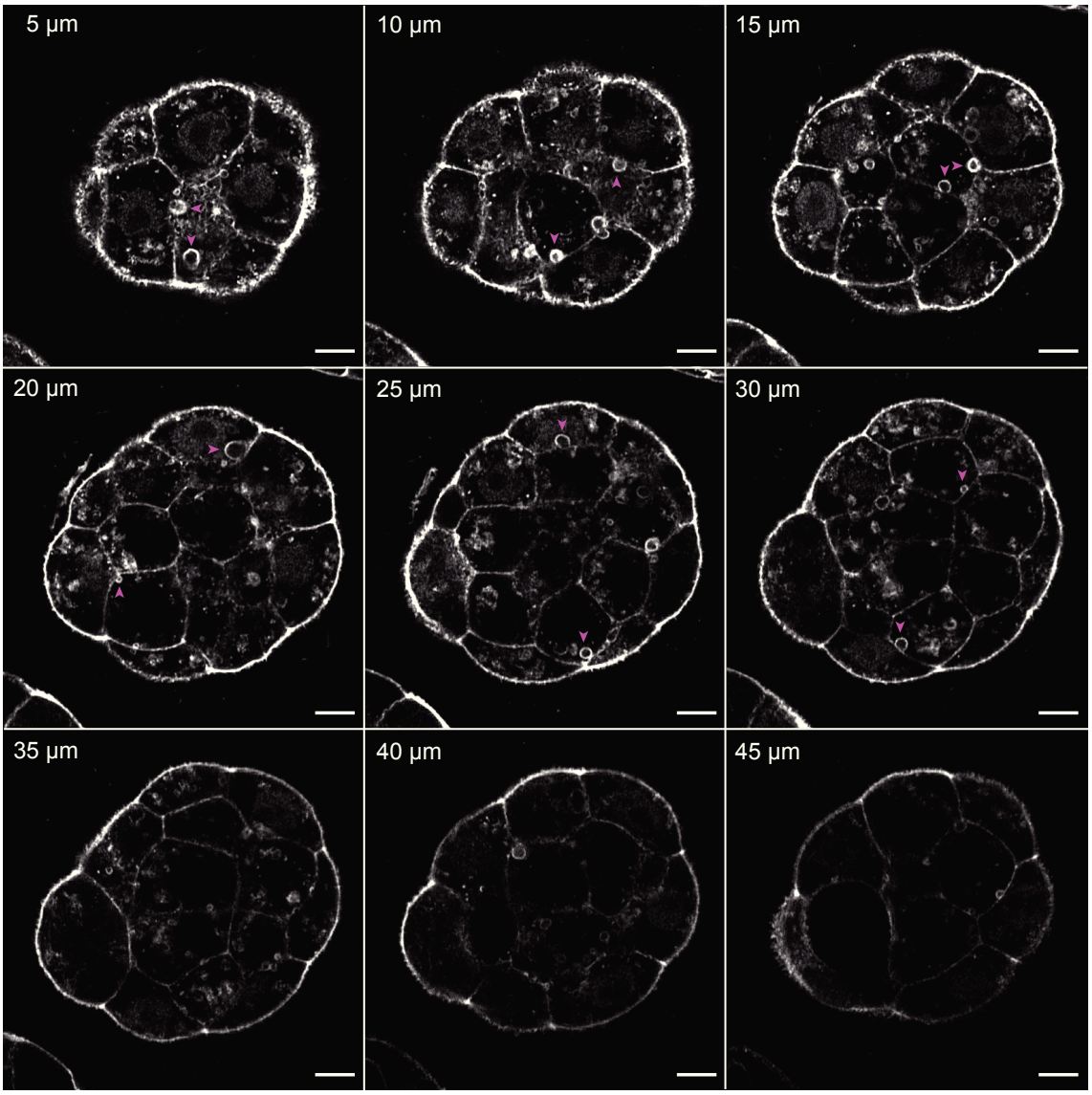

Movie S1. Vesicles localize to all basolateral and apolar membranes prior to visible extracellular fluid accumulation.
Z-stack of actin signal (phalloidin) in a WT E3.0 embryo. Magenta arrowheads highlight a subset of vesicles. Scale bar = 10μm.

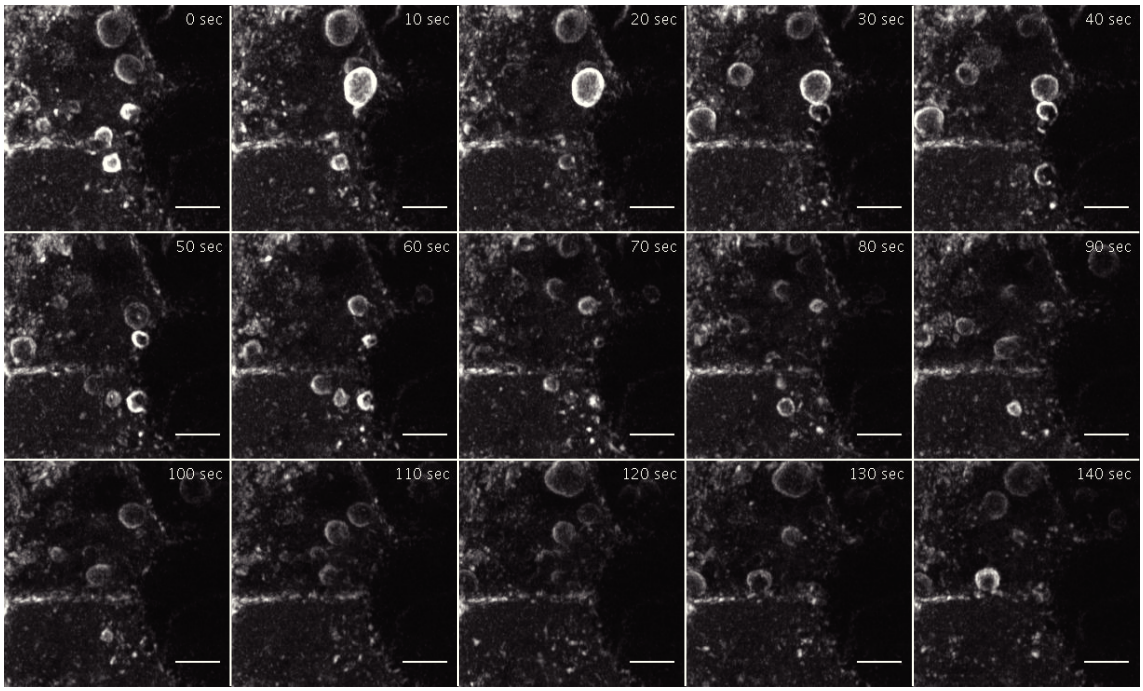

Movie S2. Vesicles are actively secreted into intercellular space.
Time-lapse (timestep = 10 seconds) of actin localization (Lifeact-GFP) during vesicle secretion in a WT E3.0 embryo. Max projection. Scale bar = 5μm.

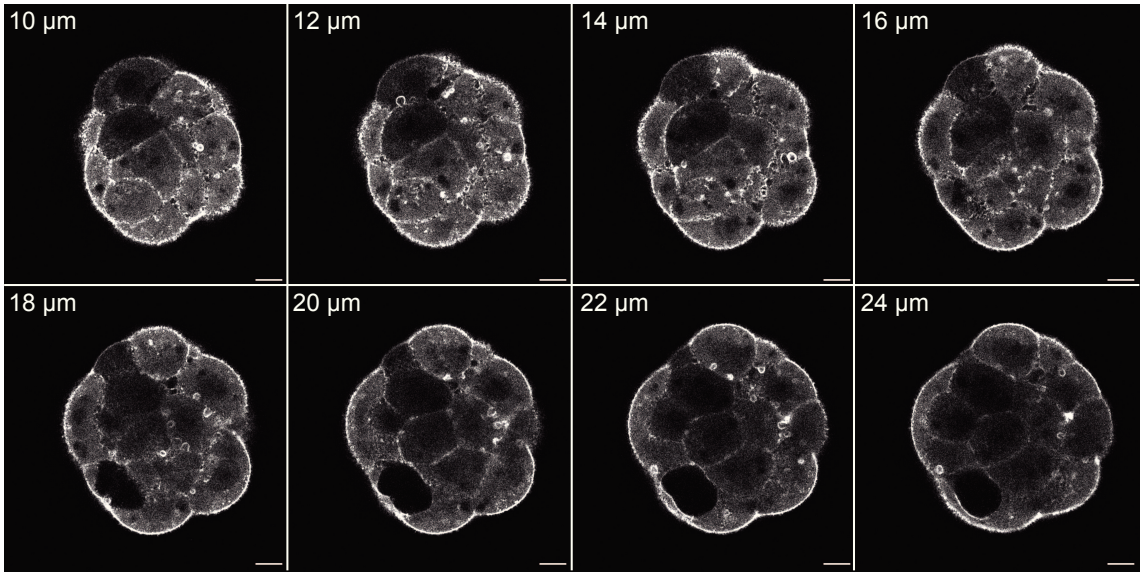

Movie S3. WT localization of vesicles is maintained in Atp1 inhibited embryos. Z-stack of actin signal (Lifeact-GFP) in an Atp1 inhibited E3.0 embryo. Scale bar = 10μm.

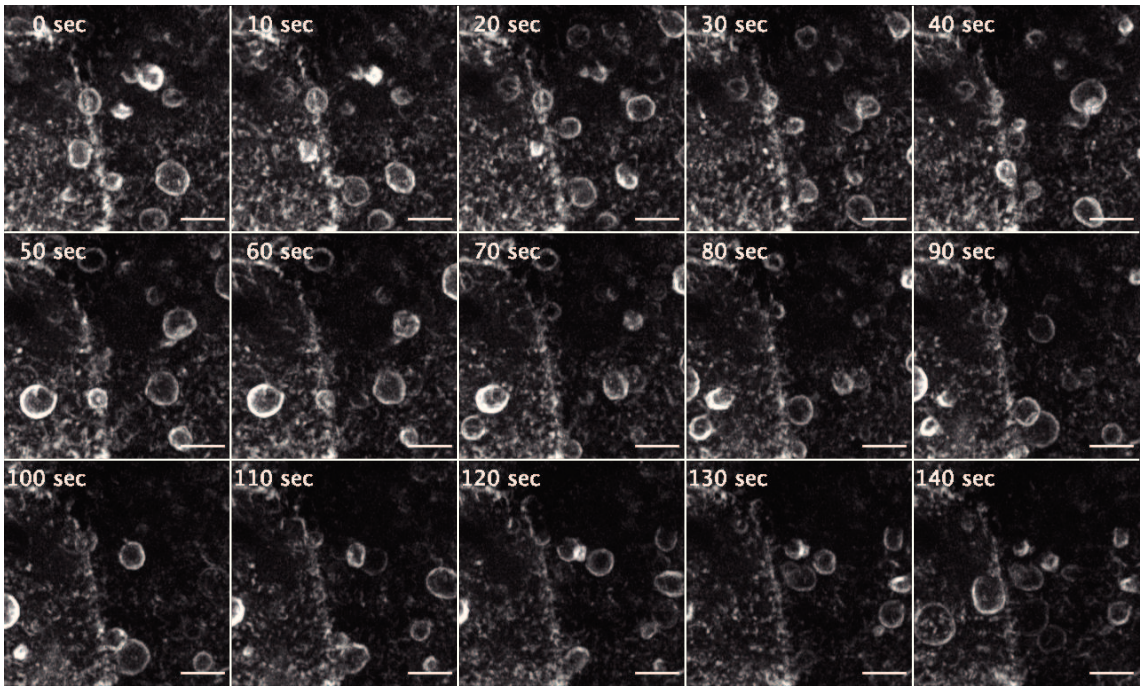

Movie S4. Vesicles continue to be secreted into intercellular space during Atp1 inhibition.

Time-lapse (timestep = 10 seconds) of actin localization (Lifeact-GFP) during vesicle secretion in an Atp1-inhibited E3.0 embryo. Max projection. Scale bar = 5μm.

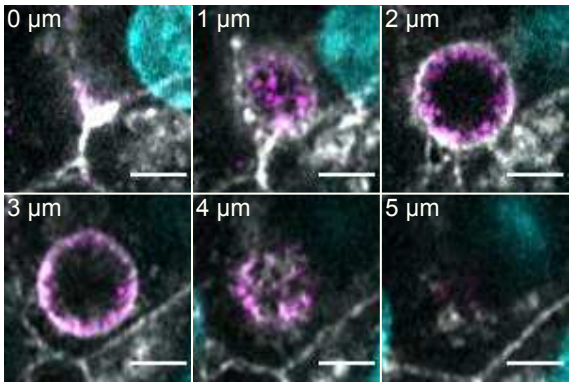

Movie S5. Apicosome-like structures are contained in cells isolated from luminal contact.

Z-stack of a cell containing an apicosome-like structure (pERM, magenta; Actin, gray; nuclei, cyan). Scale bar = 5μm.

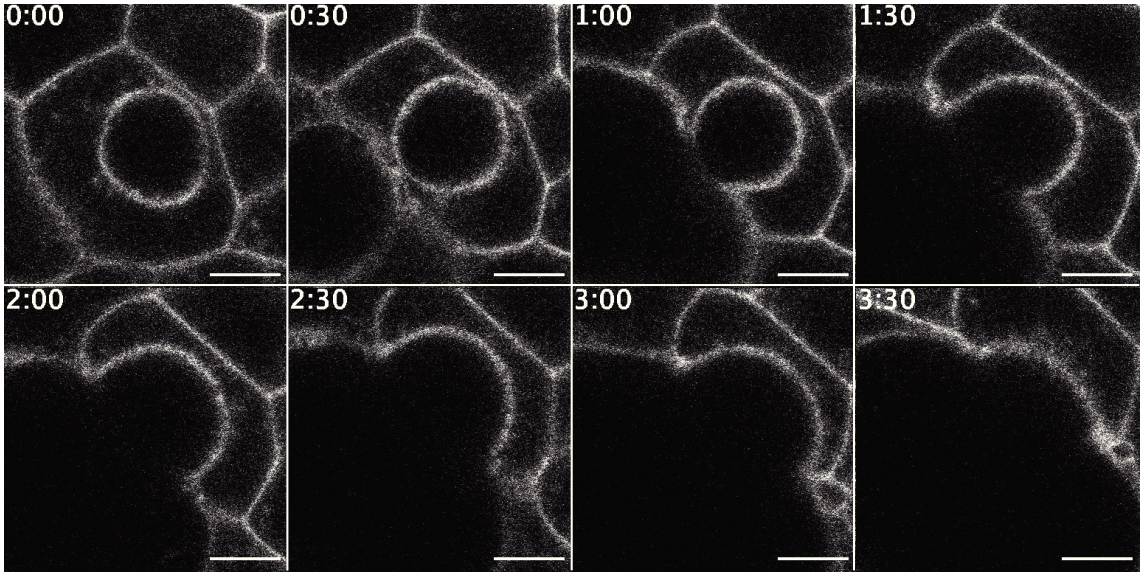

Movie S6. Apicosome-like structures are released into luminal space when the cell gains a contact-free surface.

Time-lapse (timestep = 15 minutes, hh:mm) of membrane signal (mT) in a cell releasing an apicosome-like structure into luminal space once the cell acquires a contact-free surface along the ICM-lumen interface. Scale bar = 10 μm.

11.3 Supplementary Tables

11.3.1 Genotyping Primers

Mouse Line	Primer ID	Primer Sequence	PCR Product Size (bp)
Lifeact-EGFP	LifeAct for 2 VenCeru-geno rev	TCAAGAAATTCGAAAGCATCTCAAAGG GACCATGTGATCGCGCTTCTCGTT	TG allele = 725bp
mTmG	oIMR7318 oIMR7319 oIMR7320	CTCTGCTGCCTCCTGGCTTCT CGAGGCGGATCACAAGCAATA TCAATGGGCGGGGGTCGTT	WT allele = 330bp KI allele = 250bp
Pdgfr$\alpha^{\text{H2B-GFP}}$	oIMR7801 oIMR7802 oIMR7803	CCCTTGTGGTCATGCCAAAC GCTTTTGCCTCCATTACACTG ACGAAGTTATTAGGTCCCTCGAC	WT allele = 451bp KI allele = 242bp
Sox2-GFP	GFP-qPCR2-F GFP-qPCR3-R	CACATGAAGCAGCACGACTT GAACTCCAGCAGGACCATGT	TG allele = 440bp

Analysis	Library [.Package]	[Package.] Function
Lumen Segmentation	scipy.ndimage	median_filter, binary_opening, binary_closing, label
	numpy	percentile, sum
Reporter Expression Center of Mass	scipy.ndimage	median_filter, measurements.center_of_mass
Center of Mass Distance to Lumen Surface	scipy.spatial	distance.cdist, ConvexHull
	skimage.segmentation	find_boundaries
	numpy	where
	scipy.ndimage	binary_fill_holes
	sympy.geometry	line3d.Line3D, Point3D, intersection
Fate Specification	scipy.ndimage	distance_transform_edt, label
	skimage.feature	peak_local_max
	skimage.morphology	watershed
	numpy	unique, mean, sum
Spatial Segregation	scipy.ndimage	measurements.center_of_mass
	numpy	mean, median
	sympy.geometry	line3d.Line3D, distance, perpendicular_segment, intersection
Cell Counts	scipy.ndimage	median_filter, binary_opening, measurements.label

Chapter 12

Appendix I: Current Experiments and Reasoning

12.1 Actin Nucleators

As stated in **Discussion** and **Conclusion and Perspectives**, secretion of the basal-/apolar-localized actin-coated vesicles described in this project (Figure 1) is markedly similar to that observed in systems which require regulated (actin coat compression assisted) secretion of bulky or insoluble cargo. In order to more accurately block the fusion and release of these vesicles, it would be highly beneficial to identify which actin nucleator(s) is responsible for assembling the actin coat around the vesicle. Arp2/3, a branched actin nucleator, has been shown to be necessary for the regulated secretion of *D. melanogaster* salivary glad glue protein secretion (Tran et al., 2015). Another study on actin regulation of salivary gland secretion identified Dia (a Formin family protein) to be the main actin nucleator responsible for the acting coat formation (Rousso et al., 2016). Conveniently, small molecule inhibitors of both Arp2/3 and Formins exist – CK-666 and SMIFH2, respectively. To test the relative importance of each nucleator for the formation of the actin-coat for the vesicles observed in the end-stage morula, Lifeact-GFP embryos will be incubated in media containing each inhibitor and imaged in live with the same conditions seen in Figure 1. The resulting vesicle size, secretion time and actin fluorescence intensity will then be compared between inhibitions and controls. These inhibitions can also be done on longer timescales to see if the overall lumen volume is impacted. This may provide insight into the overall contribution of the vesicles to total luminal volume.

NOTE:
While this is not currently a part of planned experimental lines of investigation, it is plausible that myosin 1b and 1c activity is involved in the secretion of the basal-/apolar-localized actin-coated vesicles. It has been shown in Aveolar Type II cells, which secrete hydrophobic lipoprotein surfactant, that myosin 1b and 1c serve as linkers of vesicle membranes to the actin coat which mediates secretion (Kittelberger et al., 2016).

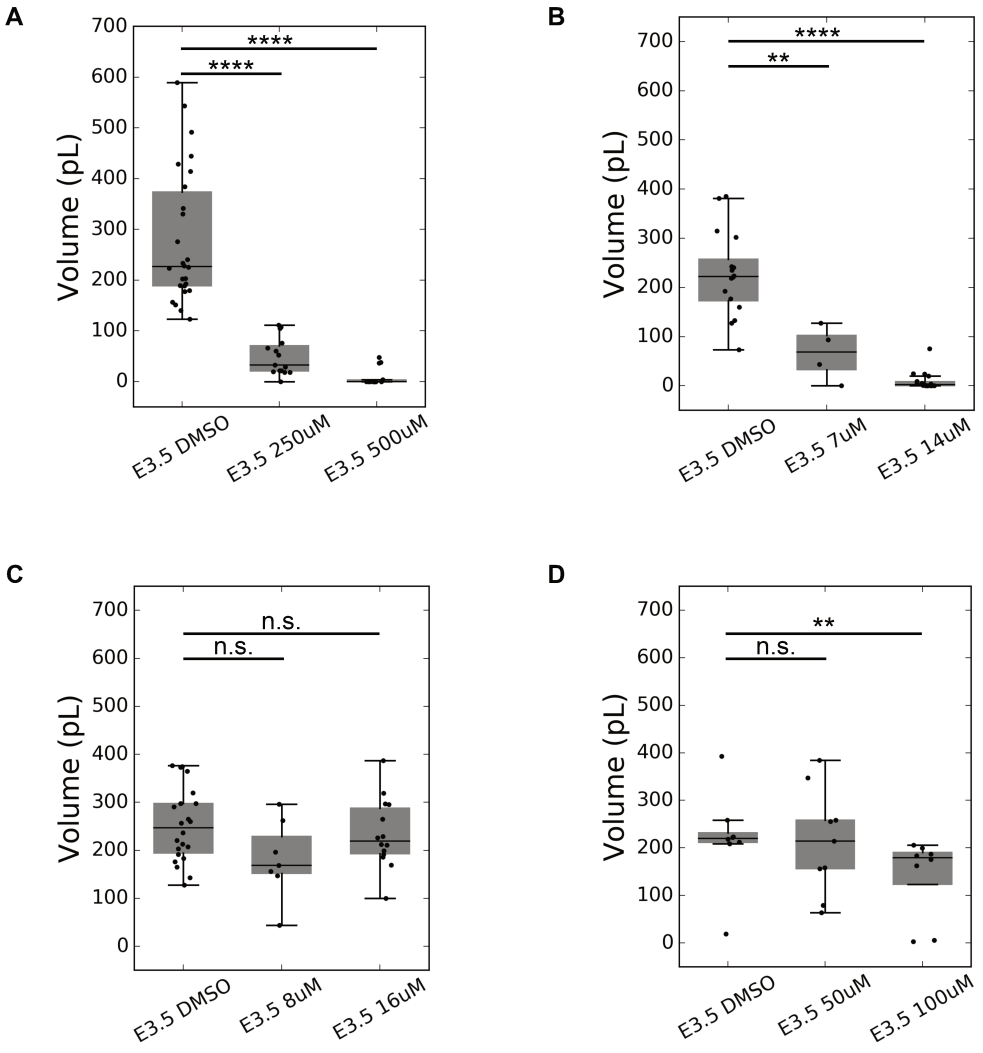

Figure A1. Inhibition of actin nucleators to block vesicle secretion in early expansion phase embryos.

(A) Boxplot of lumen volume in Atp1 inhibited (E3.5 250μM, N = 15; E3.5 500 μM, N = 14) and control (E3.5 DMSO, N = 26) embryos. (B) Boxplot of lumen volume in COPII inhibited (E3.5 7μM, N = 4; E3.5 14μM, N = 18) and control (E3.5 DMSO, N = 16) embryos. (C) Boxplot of lumen volume in Formin inhibited (E3.5 16μM, N = 14; E3.5 8μM, N = 7) and control (E3.5 DMSO, N = 22) embryos. (D) Boxplot of lumen volume in Arp2/3 inhibited (E3.5 50μM, N = 9; E3.5 100μM, N = 8) and control (E3.5 DMSO, N = 8) embryos.

$^{****}p < 0.0001$

$^{**}p < 0.01$

n.s. = not significant

N = number of embryos

12.2 Adhesion Remodeling

To begin investigating the possible role of the basal-/apolar-localized actin-coated vesicles in adhesion remodeling, Podocalyxin (Pdx) seemed the most logical place to begin as it as been shown to behave as an anti-adhesion molecule in other systems (Strilić et al., 2010; Takeda et al., 2000). Unfortunately, Pdx does not appear to localize to the vesicles or nascently separating membranes within the morula (Figure A2).

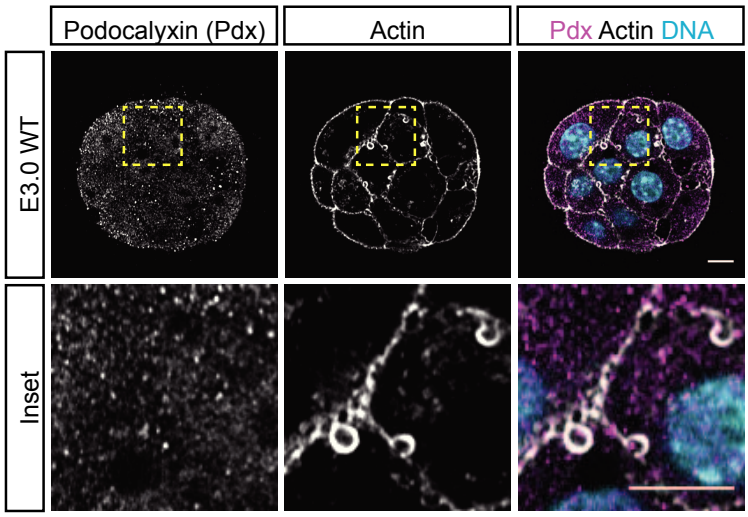

Figure A2. Podocalyxin does not localize to lumen-contributing vesicles or micro-lumina. Representative immunofluorescence images of Podocalyxin in an E3.0 WT embryo (N = 40 embryos). Top row shows full embryo. Yellow dashed box in top row outlines the 'Inset' region, which is shown in the bottom row.

Chapter 13

Appendix II: Analysis Pipelines

Throughout the duration of my PhD, I spent a significant amount of time developing image analysis methods. To include all of the source code and documentation for twenty something custom-written Python functions and the implementation of each within the thesis would require approximately fifty pages. As an alternative to this, a github repository will be created for this project in which all source code, documentation and anecdotal advice will be openly available to download for any interested parties.

The sections within this chapter can be thought of as an extension of **Materials and Methods**, some notes on the potential to extend the application of these functions and/or pipelines to other systems as well as a couple simple 'tricks' that I have found to be highly useful when working with large and/or pooled datasets.

13.1 Source Code Development and Function Descriptions

As a description of the main implementations of my functions and pipelines relevant to the results presented in earlier chapters can be found in **Materials and Methods**, additional elaboration regarding the source code should not be necessary for understanding and interpretation. However, as the development of these pipelines was of considerable importance not only for the success of the project, but also for my personal development as a scientist, I will briefly enumerate the principal functions created and their purposes:

1. **Mask Generation for Signal Type Indexing.** To avoid the inclusion of unwanted pixels when quantifying expression levels from fluorescence images, a reliable and well-characterized stain or protein can be used to create a global mask (e.g. DAPI for nuclei or Phalloidin for membranes and/or cortex). This mask can then be used to evaluate fluorescence levels of other channels (e.g. transcription factor channels indexed with a DAPI generated mask or membrane/cortex localized polarity or junctional channels indexed with a Phalloidin generated mask). This could, in principle, allow you to image

multiple proteins of interest with the same color and subsequently separate the signals based on the mask. However, this has not been optimized because it requires the previous knowledge that the proteins of interest can be imaged with the same laser power.

2. **Digital Embryo.** This is a small extension of the *Mask Generation for Signal Type Indexing*. Here, you can simply input your image of interest and your mask, and the function will return a arrays storing the x, y, z coordinates of masked objects and the corresponding indexed intensity measurements. While this is a very simple function, it is highly practical as the resulting arrays are much smaller files and will allow the speed of downstream processing and analysis to increase significantly.

3. **Symmetry Axis Determination.** As mentioned multiple times throughout the thesis, the blastocyst is oriented by the Em-Ab axis. If rotated around the Em-Ab axis, the blastocyst is symmetric. This function takes advantage of the 'weight' on one side of the axis created by the ICM. This allows the Em-Ab axis to be automatically determined by simply finding the mean (reflects ICM weight) and median (reflects overall space occupation of the embryo i.e. embryo size) points of the embryo in 3D and determines the 3D line that goes through both points. This line is representative of the Em-Ab axis and thus provides orientation.

4. **Object Centers.** An image (or array) containing the segmentation result from any signal type (i.e. nuclei, membrane, etc.) delineating boundaries is used as the input and the function will determine the x, y, z coordinates of the center of mass of each object and enumerate and store the coordinates in an array as per the object ID (integer assigned at segmentation).

5. **Axis Intersection.** Here, the dimensionality of the blastocyst from 3D to 2D begins to take place by again taking advantage of the Em-Ab axis. All that is required is the 3D line equation of the Em-Ab axis (as determined by *Symmetry Axis Determination*) and the x, y, z coordinates of the objects' (i.e. cells') centers (as determined by *Object Centers*). With these, the function projects a line segment from each object center to the Em-Ab axis such that the angle of intersection is 90^{o} (a perpendicular intersection of two linear entities). The intersection point is then stored in an array with the same order as the object IDs.

6. **Distance to Axis.** The distance of each object from the symmetry axis is determined in real space (μm) using its center of mass (*Object Centers*) and perpendicular intersection point (*Axis Intersection*). This returns a scalar value that can be used as a plotting value for a single spatial axis in downstream evaluation (x or y in *Multi-channel KDE Estimation and Integration*).

7. **Rescale to 'Origin'.** This function is to simplify visualization and downstream calculations. In the spatial axis of preference (x, y or z as in *Object Centers* and *Axis*

Intersection), the point containing the minimal value for the chosen axis is set to be the origin ($x, y, z = 0, 0, 0$). All remaining points are adjusted by the same shift so that the absolute distance between each object is retained. In parallel, the distance between the intersection point corresponding to the selected minimal point and all other objects is calculated, which is scalar and can be used as the remaining spatial axis in downstream evaluation (x or y in *Multi-channel KDE Estimation and Integration*).

8. **Multi-channel KDE Estimation and Integration.** Using the spatial dimensions determined by *Distance to Axis* and *Rescale to 'Origin'* and fluorescence values of interest (the average for each segmented object determined by iterating over the result from *Digital Embryo*), kernel density estimates (KDEs) are calculated for each protein/complex (image channel) of interest. These KDEs can then be integrated over one another. The value resulting from the integration is the likelihood that within the spatial arrangement of fluorescence values of a given sample the two specified proteins/complexes of interest will occupy the same space with those expression levels.

9. **Tissue-scale Center of Mass.** For mesoscale measurements (e.g. a segmented cell mass), this function computes the center of mass for each timepoint. As can be intuitively realized, this will find a point towards an area of higher density if the tissue is anisotropic (e.g. the point would be somewhere within the presumptive ICM in the case of a segmented cell mass from a blastocyst).

10. **Negative Space Object Segmentation.** Using a signal that clearly delineates boundaries between morphological objects, this function takes advantage of the cytoplasmic noise associated with fluorescent membrane and cortex markers. This allows cellular and noncellular entities to be segmented automatically from a single input without assigning seeds as is often necessary for cell-level segmentation.

11. **Tissue Size Normalization.** This is a useful function for tissues that are characteristically anisotropic or contain 'holes' or noncellular structures (negative space). If the boundaries of tissues or structures of interest can be determined and given as an input along with any 3D line providing orientation within the same, conditions can be set so that the specific subregions will be identified and its dimensions (e.g. height, width or length) can be quantified. This works for both single timepoint 3D images as well as limelapses.

13.2 Implemented Pipeline Constructions

This section provides detailed instructions on how to run the image analysis pipelines used in **Results III: EPI-PrE Specification and Spatial Segregation during Lumen Expansion**. Please reference the previous section and the github repository for further clarification of the calculations or transformations performed by each custom written function. Extensive

documentation of each function from an open-source library used can be found by following the links listed below:

https://docs.scipy.org/doc/numpy/
https://matplotlib.org/contents.html
https://scikit-image.org/docs/stable/
https://docs.sympy.org/latest/index.html
https://docs.scipy.org/doc/scipy/reference/
https://docs.scipy.org/doc/scipy/reference/stats.html
https://docs.scipy.org/doc/scipy/reference/tutorial/ndimage.html

13.2.1 ICM Lineage Proximity to Lumen

This analysis method was developed to be used for multi-channel, 3D (x, y, z) timelapse datasets; however, it can be used for single timepoint 3D images. This method was used to produce results presented in **Results III: EPI-PrE Specification and Spatial Segregation during Lumen Expansion** (Figure 3).

1. Segment the lumen (or other negative space object).
2. Segment signal of interest.
3. Segment embryo cell mass (or other positive space object that delineates boundary sets).
4. Calculate center of mass for segmented lumen, segmented embryo cell mass and segmented lineage marker signal weighted by fluorescence intensity.
5. Determine Em-Ab axis (symmetry axis) from segmented lumen and segmented cell mass centers of mass.
6. Determine outer boundaries of the the segmented cell mass and segmented lumen.
7. Convert cell mass and lumen outer boundaries to convex hulls.
8. Search facets of convex hulls for points contained in the Em-Ab axis.
9. Calculate ICM (subtissue) width by imposing spatial restrictions within the range of points contained in the Em-Ab axis.

13.2.2 Spatial Segregation of Cell Lineages

Unlike the method described in the previous section, this analysis method is not compatible with timelapse datasets; however, it is applicable for both 2D (x, y) and 3D (x, y, z) multi-channel, single timepoint datasets. This method was used to produce results presented in **Results III: EPI-PrE Specification and Spatial Segregation during Lumen Expansion** (Figures 4,5).

1. Segment all nuclei.

2. For each channel of interest, retain intensity values for all pixels within segmentation and average by unit of segmentation (nucleus).

3. Calculate center of mass of each unit of segmentation.

4. Calculate mean and median of segmentation.

5. Determine Em-Ab axis from mean and median points.

6. Determine intersection points of centers of mass with the axis and the distances between the center and intersection such that the angle of intersection is 90°.

7. Project embryo down into 2D from 3D using the Em-Ab axis and the distances of intersection.

8. Apply intensity values to the 2D spatial projection.

9. Calculate KDE for all channels of interest.

10. Integrate KDEs over one another to determine spatial overlap between domains.

13.3 Recognition Codes for Experimental Datasets

To aid in the speed of analyzing datasets from pharmacological inhibition experiments, each experimental category (pre-inhibition stage controls, various inhibitions and post-inhibition stage controls) was assigned a **Recognition Code**. This allowed results from multiple experiments to be grouped in a single dataset and submitted for analysis. Below is a table accounting for all of the recognition codes and the corresponding experimental category and developmental stage:

Embryonic Stage	Experimental Category	Recognition Code
E3.0	Pre-Treatment Control	11
E3.5	Ouabain 250μM	12
E3.5	Ouabain 500μM	13
E3.5	DMSO Post-Treatment Control	14
E3.5	Ouabain 100μM	15
E3.5	Pre-Treatment Control	21
E4.0	Ouabain 250μM	22
E4.0	Ouabain 500μM	23
E4.0	DMSO Post-Treatment Control	24
E4.0	Ouabain 100μM	25
E3.0	Pre-Treatment Control	31
E3.5	Brefeldin A 7μM	32
E3.5	Brefeldin A 14μM	33
E3.5	DMSO Post-Treatment Control	34
E3.5	Pre-Treatment Control	41
E4.0	Brefeldin A 7μM	42
E4.0	Brefeldin A 14μM	43
E4.0	DMSO Post-Treatment Control	44

Chapter 14

Appendix III: Additional Experimental Datasets

14.1 Fluo-4 Marks Luminal Fluid

Luminal precursors and luminal fluid in human pluripotent cells contain high concentration of calcium (Taniguchi et al., 2017). As a tool to visualize lumen formation and expansion, embryos were incubated in media containing Fluo-4 AM (Invtriogen, F14201), a cell-permeant calcium indicator, at 1μM concentration. As Fluo-4 AM only fluoresces in the presence of high concentrations of calcium ions (Ca^{2+}), the resulting signal faithfully marks microlumina as well as the dominating lumen (Figure A#).

While it was not utilized to quantify luminal fluid volume and spatial distribution in this study, it offers a useful alternative to 'negative space' segmentation or dextran labeling for future projects as a signal threshold could be simply determined and it nicely labels fluid pockets (microlumina) too small to be detected by the 'negative space' segmentation (< 1pL).

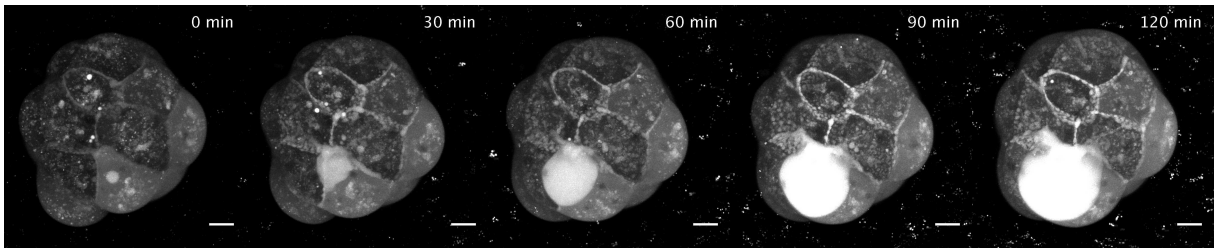

Figure A4. Fluo-4 accurately marks luminal fluid in the developing blastocyst. Scale bars = 10μm. All panels are maximum projections.

14.2 Primitive Endoderm Progression

Before developing the **ICM Lineage Proximity to Lumen** analysis method, attempts were made to show that ICM cells in closer proximity to the lumen express higher levels of Gata6 as it is widely acknowledged as an early marker of the PrE lineage (Ohnishi et al., 2013) and is essential for PrE establishment (Schrode et al., 2014). However, no such bias was found even at later blastocyst stages (>128-cell stage; Figure A5).

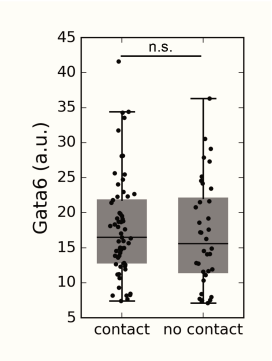

Figure A5. Gata6 immunofluorescence levels show no statistical difference between ICM cells that are in contact with the growing lumen and cells that are isolated from the lumen.

14.3 Fluid Accumulation Onset

Several timelaspe datasets of a plasma membrane reporter (mTmG) were acquired to observe the onset of fluid accumulation within the embryo. These datasets were useful in the initial observations of vesicles (Figure 1) and the development of the 'negative space' segmentation (Figure 3); however, the main use of these datasets would have been to examine the dynamics of microluminal coalescence events. As a preprint of a study from another group comprehensively study this behavior in addition to evidence of adhesion remodeling was posted to *bioRχiv* in February 2019 (537985v1), these datasets were not explored further.

14.4 Bafilomycin Induces ICM Death

Vacuolar compartments have long been speculated to contribute to lumen formation and expansion. Vacuole pressure regulators are proton pumps (Navis and Bagnat, 2015). Additionally, proton pumps, such as Atp6 (also known as vacuolar ATPases, V-ATPases or H^+-ATPases), have been shown to regulate notochord vacuole pressure (Ellis et al., 2013). The compromised

pressure regulation compromises vacuole morphology which results in impaired functional capacity to maintain tissue architecture and axis extension (Ellis et al., 2013).
To test if the large vesicles within the initiating blastocyst are regulated by Atp6 action, embryos were incubated in media containing Bafilomycin A1, which is a well-known inhibitor of H^+-ATPases (Bowman et al., 1988). Early stage incubation (E3.0-E3.5) resulted in cytoplasmic accumulation of large vesicles until the embryos undergo lysis. Late stage incubation (E3.5-E4.0) resulted in ICM-specific cell death. While these are interesting cell behaviors, cell death related phenotypes are inherently difficult to analyze. Therefore, this line of investigation ceased.

14.5 *Atp6v0a1,d1* −/− Lines

While Bafilomycin A1 inhibition (see previous section) results in cell death, there have been studies indicating the role of *Atp6* (a H^+-ATPase) in pre- and/or peri-implantation development through the maturation of the ICM (Inoue et al., 1999; Miura et al., 2003; Sun-Wada et al., 2000). Atp6 is comprised of two subcomplexes (V_0 and V_1) that can act either together as a 'full' ATPase or individually (Marshansky and Futai, 2008). Depending on subcellular localization (e.g. trans-golgi network, vesicles or plama membrane), Atp6 (V_0V_1, V_0 or V_1) has been proposed to facilitate different actions such vesicle docking to the plasma membrane or vesicle acidification (Marshansky and Futai, 2008).

In an attempt to decipher if Atp6 has a role in blastocyst lumen formation, conditional knockouts of two Atp6v0 subunits were prepared using the *loxP* and Cre recombinase system (de Vries et al., 2000): *Atp6v0a1* and *Atp6v0d1*. Unfortunately, −/− blastocysts for each line either appeared morphologically normal or displayed a complicated intracellular trapping of what is potentially luminal fluid similar to that seen in *Cdh1* −/− embryos (Stephenson et al., 2010). Due to phenotypic inconsistency, characterization of these knockouts was not pursued in order to focus on other directions of the project.

14.6 *Sec24c,d* −/− Lines

Due to the impact of Brefeldin A on luminal volume during stages when the vesicle secretion mechanism should be active (Figure 1), it was hypothesized that if secretory pathway components were perturbed genetically it may be possible to modulate this mechanism. Sec24c and d isoforms, which are COPII machinery components, have been shown to be active in early developmental stages (Baines et al., 2013; Adams et al., 2014). Conditional knockouts of these isoforms were prepared and examined for lumenogenesis phenotypes as described in the previous section. Unfortunately, these embryos showed similar phenotypic inconsistencies as the Atp6 subunit knockouts. As such, this line of investigation was not pursued further.

Chapter 15

Additional References for Appendices

Adams, E.J., Chen, X.W., O'Shea, K.S., and Ginsburg, D. (2014) Mammalian COPII component SEC24C is required for embryonic development in mice. J. Biol. Chem. doi: 10.1074/jbc.M114.566687

Baines, A.C., Adams, E.J., Zhang, B., and Ginsburg, D. (2013) Disruption of the Sec24d gene results in early embryonic lethality in the mouse. PLOS ONE 8, e61114.

Bowman, E.J., Siebers, A., and Altendorf, K. (1988) Bafilomycins: A class of inhibitors of membrane ATPases from microorganisms, animal cells and plant cells. Proc. Natl. Acad. Sci. USA 85, 7972-7976.

de Vries, W.N., Binns, L.T., Fancher, K.S., Dean, J., Moore, R., Kemler, R., and Knowles, B.B. (2000) Expression of Cre recombinase in mouse oocytes: a means to study maternal effect genes. Genesis 26, 110-112.

Ellis, K., Bagwell, J., and Bagnat, M. (2013) Notochord vacuoles are lysosome-related organelles that function in axis and spine morphogenesis. J. Cell Biol. 200, 667-679.

Inoue, H., Noumi, T., Nagata, M., Murakami, H., Kanazawa, H. (1999) Targeted disruption of the gene encoding the proteolipid subunit of mouse vacuolar H^+-ATPase leads to early embryonic lethality. Biochim. Biophys. Acta 1413, 130-138.

Kittelberger, N., Breunig, M., Martin, R., Knölker, H.J., and Miklavc, P. (2016) The role of myosin 1c and myosin 1b in surfactant exocytosis. J Cell Biol. 129, 1685-1696.

Marshansky, V. and Futai, M. (2008) The V-type H^+-ATPase in vesicular trafficking: targeting, regulation and function. Curr. Opin. Cell Biol. 20, 415-426.

Miura, G.I., Froelick, G.J., Marsh, D.J., Stark, K.L., Palmiter, R.D. (2003) The d subunit of the vacuolar ATPase (Atp6d) is essential for embryonic development. Transgenic Res. 12, 131-133.

Navis, A. and Bagnat, M. (2015) Developing pressures: fluid forces driving morphogenesis. Curr. Opin. Genetics Dev. 32, 24-30.

Navis, A. and Bagnat, M. (2015b) Loss of *cftr* function leads to pancreatic destruction in larval zebrafish. Dev. Biol. 399, 237-248.

Sun-Wada, G.H., Murata, Y., Yamamoto, A., Kanazawa, H., Wada, Y., and Futai, M. (2000) Acidic endomembrane organelles are required for mouse postimplantation development. Dev. Biol. 228, 315-325.

Summary

French

Les luminescences fluides sont des structures multicellulaires communes que l'on trouve dans un large éventail de tissus épithéliaux. La formation de novo lumen est essentielle au développement embryonnaire de nombreux organes tubaires et kystiques (c.-à-d. respiratoires, vasculaires, digestifs, excréteurs, etc.) chez les embryons vertébrés. La formation et la maturation de la lumière perturbée produisent des morphologies inappropriées qui perturbent les fonctions de base des tissus environnants.

De multiples mécanismes de formation de novo lumen existent. Le creux du cordon, un mécanisme conservé et omniprésent dans toutes les espèces et tous les systèmes d'organes, impliquait la séparation des domaines membranaires cellulaires posés de près et spécialisés, bordés par des complexes jonctionnels d'adhérence. Dans la plupart des systèmes qui utilisent le mécanisme de creusage du cordon, la lumière est amorcée entre les domaines api- ciels entourés de jonctions serrées. La formation de l'embryon préimplantatoire de souris, le blastocyste, dans lequel la lumière se forme entre les domaines basolatéraux de ses cellules externes et la masse cellulaire interne non polarisée, est distincte de cela.

Le blastocyste de souris contient trois lignées cellulaires séparées dans l'espace et une lumière liquide. Les cellules externes de l'embryon comprennent une lignée cellulaire, le trophectoderme, et forment une sphère creuse. Dans la sphère du trophectoderme, les cellules restantes de l'embryon comprennent les deux autres lignées cellulaires, l'épiblaste et l'endoderme primitif, qui sont isolés dans un hémisphère. La lumière fluide occupe l'autre hémisphère. L'endoderme primitif est situé entre l'épiblaste et la lumière liquide, formant ainsi une barrière d'isolation entre les deux entités.

La spécification du devenir des cellules peut être classée en gros selon deux mécanismes : la spécification autonome et la spécification conditionnelle. La spécification autonome, également connue sous le nom de pré-modélisation, nécessite la localisation différentielle des déterminants affectant le destin (par exemple les facteurs de transcription) à travers le zygote, qui sont à leur tour hérités de manière différenciée par les blastomères lors du clivage. La pensée derrière la spécification conditionnelle est que l'identité finalement adoptée par chaque cellule dépend de

ses interactions avec son environnement immédiat et les cellules voisines (par exemple, la signalisation paracrine ou les profils d'adhésion différentielle). Bien que le pré-modèle soit essentiel pour de nombreux organismes, d'autres organismes se fient entièrement à des spécifications conditionnelles au cours des stades embryonnaires. C'est ce qu'on appelle souvent le développement auto-organisé.

Bien qu'elle ait été proposée, l'idée d'un modèle de pré-modèle pour la spécification du devenir dans le blastocyste a été largement contredite par des expériences d'isolement (c'est-à-dire le retrait d'un seul blastomère de l'embryon précoce pour tester sa capacité de développement). Les modèles de polarité intérieure et extérieure et de polarité des cellules sont des formes de spécification conditionnelle. Les mêmes expériences d'isolement qui contredisent la spécification conditionnelle comme seule forme de spécification du devenir pour le développement des blastocystes. Des recherches récentes ont montré clairement que la polarité cellulaire (apico-basale) et la position des cellules (interne ou externe) jouent un rôle important dans l'établissement et le maintien de la lignée cellulaire chez l'embryon précoce de souris. Des études ont également révélé la nécessité de la polarité et de la position pour coordonner les changements morphogénétiques, y compris la formation de lumens.

La formation et l'expansion de la lumière du blastocyste sont concomitantes à la spécification des lignées d'épiblastes et d'endoderme primitif. Les niches spatiales bien définies de l'épiblaste et de l'endoderme primitif dans le blastocyste sont largement acceptées dans le domaine du développement préimplantatoire ; cependant, très peu d'études en ont fait un point central. L'expansion de la lumière et la ségrégation spatiale des trois lignées cellulaires sont nécessaires à la réussite de la morphogenèse des blastocystes, qui permet à l'embryon de passer aux stades suivants du développement embryonnaire.

De nombreuses études ont été menées pour étudier l'identité moléculaire des lignées d'épiblastes et d'endoderme primitif et la façon dont elles émergent d'une seule population progénitrice. Jusqu'à présent, la ou les fonctions de la lumière du blastocyste sont largement inconnues. Lumina peut servir à diverses fins, notamment induire des changements dans la forme des cellules, l'apport et l'absorption de nutriments, la rupture de la symétrie au niveau des tissus ou des organes et même la signalisation de niches, selon le tissu et le stade de développement.

Comme nous l'avons déjà dit, la morphologie de la lumière résultante perturbée entraîne une fonction tissulaire inadéquate. Un exemple intéressant de ce phénomène est l'échec de la tubulogenèse rénale, qui entraîne une modification des rapports de répartition du devenir en raison de changements dans les microenvironnements. Malgré la corrélation temporelle entre la spécification endodermique primitive de l'épiblaste et la formation du lumen, la fonction potentielle du lumen pour réguler la spécification du devenir et le positionnement cellulaire n'a pas encore été étudiée.

La motivation centrale de ce projet était de déterminer si, et par extension comment, la lumine liquide (c.-à-d. la morphogenèse de la lumine dans sa géométrie finale (forme ou forme) dans les tissus) a un impact sur les processus de spécification du sort cellulaire et de positionnement des cellules dans les tissus en développement. Tout au long de ce projet, les premières phases de la formation et de l'expansion de la lumière des blastocystes ont été examinées en relation avec la spécification initiale des épiblastes et des endodermes primitifs et le repositionnement spatial dans le but de mieux comprendre l'interaction entre la spécification du sort cellulaire et la morphogenèse des blastocystes.

Avant d'aborder les questions centrales, j'ai examiné de près les premiers moments d'accumulation de liquide dans l'embryon, j'ai observé la sécrétion de grandes vésicules cytoplasmiques dans l'espace intercellulaire. Celles-ci semblent contribuer au processus de formation des lumens et offrent un lien entre la sécrétion régulée de la cargaison et l'expansion des lumens. Bien que le contenu des vésicules n'ait pu être identifié dans le cadre de ce projet, s'il devait contenir des composés précisant le devenir (p. ex. ligands de signalisation), des molécules modifiant l'adhésion (p. ex. composants de la matrice extracellulaire) ou des osmolytes concentrés, la libération du contenu vésiculaire pourrait modifier la géométrie ou l'identité du tissu immédiatement adjacent.

Partant de la pensée que la progression de la lumière a un impact sur l'identité moléculaire des tissus adjacents, j'ai analysé les sous-domaines membranaires entourant la microlumine qui se forment pendant les étapes initiales de la formation de la lumière des blastocystes. Fait intéressant, j'ai découvert que malgré le fait que la lumière du blastocyste soit encapsulée par des membranes basolatérales et apolaires à la suite d'une coalescence et d'une expansion insuffisantes, de nombreuses microlumines présentent une localisation des composants de la membrane apicale dans les sous-domaines de la membrane. De plus, une autre population de microlumines, exclusive de celles qui contiennent des composants apicaux, présente la localisation d'une grande quantité de composants interagissant avec la matrice basolatérale extracellulaire. Cette hétérogénéité biochimique des premières structures lumineuses suggère que la régulation de la lumière des blastocystes est nettement différente de celle des autres luminescences kystiques.

La coalescence de la microlumine conduit à l'émergence d'une seule lumière dominante qui se localise sur un pôle de l'embryon et subit ensuite une expansion. Directement après une coalescence suffisante, j'observe que le début de la ségrégation spatiale épiblastique et endodermique primitive. Des études antérieures sur la spécification initiale de l'épiblaste et de l'endoderme primitif ont porté exclusivement sur les entités cellulaires impliquées dans le processus. En examinant les deux lignées par rapport à l'entité non cellulaire qui entraîne des changements morphologiques majeurs au sein de l'embryon, j'ai pu révéler la possibilité que la coordination

du positionnement spatial de l'épiblaste et de l'endoderme primitif ne se fasse pas en termes de temps absolu, astronomique, mais plutôt en fonction du temps morphogenétique.

Pour interroger la possibilité que l'expansion du lumen coordonne la spécification et la ségrégation spatiale des lignées de masse cellulaire interne, j'ai perturbé l'expansion du lumen par des moyens pharmacologiques et biophysiques. Selon l'hypothèse, les embryons perturbés par l'expansion ex- hibitaient des degrés inférieurs de spécification moléculaire de l'épiblaste et de l'endoderme primitif et un chevauchement spatial accru entre les deux lignées. Ensemble, ces résultats suggèrent que l'expansion de la lumière des blastocystes joue un rôle crucial dans l'orientation de la spécification et du positionnement du sort cellulaire.

L'un des facteurs moléculaires clés de la spécification primitive de l'endoderme est le FGF4, dont l'expression est d'abord régulée à la hausse en même temps que l'initiation luminale. En raison de la nature hétérogène de la microlumine blastocyste, j'ai examiné la localisation du FGF4 dans les embryons au stade d'apparition luminale. Le FGF4 a pu être détecté dans les domaines membranaires entourant une petite population de microlumine. Dans d'autres systèmes, il a été démontré que le FGF3 se localise à la micro-lumine et crée des niches de signalisation qui propagent des comportements tissulaires et des identités cellulaires spécifiques. Pour déterminer si la localisation luminale du FGF4 a un impact différent sur l'épiblaste et la pro- gression primitive de l'endoderme que sur les changements globaux de la signalisation du FGF4, j'ai déposé de petites quantités de solutions améliorant ou inhibant la signalisation du FGF dans la lumine du stade précoce d'expansion avec - dehors affectant le volume luminal au stade terminal. Dans des conditions améliorées, j'ai observé une augmentation de l'expression moléculaire des deux lignées de masse cellulaire interne ; dans des conditions inhibées, une diminution de l'expression des deux. Les résultats de l'amélioration des conditions lumineuses diffèrent de ceux des traitements globaux, qui entraînent une conversion complète de la masse cellulaire interne en endoderme primitif au détriment de la lignée épiblastique. Ces résultats indiquent que l'altération du contenu luminal est capable d'influencer le processus de spécification du devenir cellulaire dans le blastocyste en développement.

Bien que je n'aie pas été en mesure de démêler la contribution de l'expansion par rapport aux mécanismes basés sur le contenu luminal aux processus de spécification endodermique primaire des épiblastes et de ségrégation spatiale, il est clair qu'une formation adéquate des lumens des blastocystes est essentielle. Non seulement le lumen crée une asymétrie spatiale à l'intérieur de l'embryon en étant situé dans un seul hémisphère et en formant ainsi le premier axe d'orientation au cours du développement, mais divers stades de la progression luminale sont étroitement régulés et semblent avoir le potentiel de faciliter plusieurs décisions moléculaires au sein de l'embryon. Il est possible que le lumen fournisse à la fois des repères géométriques (expansion) et biochimiques (FGF4) qui travaillent de concert pour faciliter la spécification moléculaire et le positionnement spatial des lignées de blastocystes. Par exemple, la concentration luminale de

FGF4 peut augmenter à mesure que l'expansion se poursuit. Cela créerait un biais spatial dans la disponibilité d'un facteur clé de spécification de l'endoderme primitif que l'embryon interprète en repositionnant les cellules précurseurs de l'endoderme primitif vers le lumen. D'autres études seront nécessaires pour déterminer le profil moléculaire du contenu luminal afin de vérifier une telle hypothèse.

English

Fluid lumina are common multicellular structures found in a wide range of epithelial tissues. *De novo* lumen formation is critical to the embryonic development of many tube- and cyst-based organ system (i.e. respiratory, vascular, digestive, excretory, etc.) in vertebrate embryos. Perturbed lumen formation and maturation yields improper resultant morphologies that disrupt the basic functions of surrounding tissues.

Multiple mechanisms of de novo lumen formation exist. Cord hollowing, a conserved and pervasive mechanism across species and organ systems, involved the separation of closely opposed and specialized cell membrane domains bordered by adhesion junctional complexes. In most systems that utilize the cord hollowing mechanism the lumen is initiated between apical domains surrounded by tight junctions. Distinct from this is the formation of the mouse pre-implantation embryo, the blastocyst, in which the lumen forms between the basolateral domains of its outer cells and the unpolarized inner cell mass.

The mouse blastocyst contains three spatially segregated cell lineages and a fluid lumen. The outer cells of the embryo comprise one cell lineage, the trophectoderm, and form a hollow sphere. Within the trophectoderm sphere, the remaining cells of the embryo comprise the other two cell lineages, the epiblast and the primitive endoderm, which are isolated to one hemisphere. The fluid lumen occupies the other hemisphere. The primitive endoderm is situated between the epiblast and the fluid lumen, thereby forming an isolation barrier between the two entities.

Cell fate specification can broadly be classified under two mechanisms – autonomous specification and conditional specification. Autonomous specification, also known as pre-patterning, requires the differential localization of fate effecting determinants (e.g. transcription factors) across the zygote, which are in turn differentially inherited by the blastomeres upon cleavage. The thought behind conditional specification is that the identity eventually adopted by each cell depends on its interactions with its immediate environment and neighboring cells (e.g. paracrine signaling or differential adhesion profiles). While pre-patterning is critical for many organisms, other organisms rely entirely on conditional specification during embryonic stages. This is often referred to as self-organized development.

While it has been proposed, the idea of a pre-patterning model for fate specification in the

blastocyst has largely been contradicted through isolation experiments (i.e. the removal of a single blastomere from the early embryo to test its developmental capacity). Both the inside-outside and cell polarity models are forms of conditional specification. The same isolation experiments that contradict pre-patterning support conditional specification as the sole form of fate specification for blastocyst development. It has become clear through recent research that both cell polarity (apico-basal) and cell position (inner v. outer) play important roles in cell lineage establishment and maintenance within the early mouse embryo. Studies have also revealed the necessity of polarity and position to coordinate morphogenetic changes including lumen formation.

The formation and expansion of the blastocyst lumen is concurrent with the specification of epiblast and primitive endoderm lineages. The well-defined spatial niches of the epiblast and primitive endoderm within the blastocyst is widely accepted within the field of pre-implantation development; however, very few studies have made it a point of central focus. Both lumen expansion and spatial segregation of the three cell lineages are required for successful blastocyst morphogenesis, which permits the embryo to proceed to subsequent stages of embryonic development.

Many studies have been conducted to investigate the molecular identity of the epiblast and primitive endoderm lineages and how they emerge from a single progenitor population. Thus far, the function(s) of the blastocyst lumen are largely unknown. Lumina can serve various purposes including inducing cell shape change, nutrient delivery and absorption, tissue or organ level symmetry breaking and even signaling niches depending on the tissue and developmental stage.

As previously stated perturbed resultant lumen morphology leads to improper tissue function. An interesting example of this phenomenon is failed kidney tubulogenesis, which causes altered fate allocation ratios due to changes in microenvironments. Despite the temporal correlation of epiblast-primitive endoderm specification and lumen formation, the potential function of the lumen to regulate fate specification and cell positioning have yet to be investigated.

The central motivation of this project was to address if, and by extension how, fluid lumina (i.e. the morphogenesis of lumina into their final geometry (form or shape) within tissues) has an impact of the processes of cell fate specification and cell positioning within developing tissues. Throughout the course of this project, the early phases of blastocyst lumen formation and expansion were examined in relation to epiblast and primitive endoderm initial specification and spatial repositioning with an aim to better understand the interplay between cell fate specification and blastocyst morphogenesis.

Before addressing the central questions, I closely examined of the initial moments of fluid

accumulation within the embryo, I observed the secretion of large cytoplasmic vesicles into intercellular space. These appear to contribute to the process of lumen formation and offer a link between regulated cargo secretion and lumen expansion. While the contents of the vesicles could not be identified within the scope of this project, if they were to contain either fate specifying compounds (e.g. signaling ligands), adhesion modifying molecules (e.g. extracellular matrix components) or concentrated osmolytes, vesicular content release would alter either the geometry or identity of the immediately surrounding tissue.

Extending on the thought of luminal progression impacting the molecular identity adjacent tissues, I analyzed the membrane subdomains surrounding the microlumina that form during the initiation stages of blastocyst lumen formation. Interestingly, I found that despite the blastocyst lumen being encapsulated by basolateral and apolar membranes following sufficient coalescence and expansion many microlumina exhibit localization of apical membrane components to the membrane subdomains. Furthermore, another population of microlumina, exclusive from those containing apical components, exhibit the localization of large amount of basolateral, extracellular matrix interacting components. This biochemical heterogeneity of early luminal structures suggests that the regulation of the blastocyst lumen is markedly different than other cystic lumina.

The coalescence of microlumina leads to the emergence of a single dominating lumen that localized to one pole of the embryo and undergoes subsequent expansion. Directly following sufficient coalescence, I observe that the beginning of epiblast and primitive endoderm spatial segregation. Previous studies of the initial specification of epiblast and primitive endoderm have exclusively focused on the cellular entities involved in the process. By examining the two lineages in relation to the noncellular entity that is driving major morphological changes within the embryo, I was able to reveal the possibility that coordinating the spatial positioning of the epiblast and primitive endoderm occurs not in terms of absolute, astronomical time, but rather follows morphogenetic time.

To interrogate the possibility that lumen expansion coordinates the specification and spatial segregation of the inner cell mass lineages, I perturbed lumen expansion by pharmacological and biophysical means. In accordance with the hypothesis, expansion perturbed embryos exhibited lower degrees of epiblast and primitive endoderm molecular specification and increased spatial overlap between the two lineages. Combined, these results suggest that blastocyst lumen expansion plays a critical role in guiding cell fate specification and positioning.

One of the key molecular factors of primitive endoderm specification is FGF4, the expression of which is first upregulated contemporaneously with luminal initiation. Due to the previously noted heterogeneous nature of blastocyst microlumina, I examined the localization of FGF4 in luminal onset stage embryos. FGF4 could be detected at the membrane domains surrounding a

small population of microlumina. In other systems, FGF3 has been shown to localize to microlumina and create signaling niches that propagate specific tissue behaviors and cell identities. To determine if luminal localization of FGF4 impacts epiblast and primitive endoderm progression differentially that that of global changes to FGF4 signaling, I deposited small amounts of FGF signaling enhancing or inhibiting solutions within early expansion stage lumina without affecting the endstage luminal volume. In enhanced conditions, I observed an increase in the molecular expression of both inner cell mass lineages; in inhibited conditions, decreased expression of both. The results of luminally enhanced conditions differs from those of global treatments, which result in complete conversion of the inner cell mass to primitive endoderm at the expense of the epiblast lineage. These results indicate that alteration of luminal contents is capable of influencing the process of cell fate specification within the developing blastocyst.

While I was not able to disentangle the contribution of expansion versus luminal contents based mechanisms to the processes of epiblast-primitive endoderm specification and spatial segregation, it is clear that proper blastocyst lumen formation is key. Not only does the lumen create spatial asymmetry within the embryo by being located within a single hemisphere and thereby forming the first axis of orientation during development, but various stages of luminal progression are tightly regulated and appear to have the potential to facilitate many molecular decisions within the embryo. It is possible that the lumen provides both geometric (expansion) and biochemical (FGF4) cues that work in concert to facilitate the molecular specification and spatial positioning of the blastocyst lineages. For example, the luminal concentration of FGF4 may increase as expansion proceeds. This would create a spatial bias in the availability of a key primitive endoderm specifying factor that the embryo interprets by repositioning primitive endoderm precursor cells toward the lumen. Further studies will be necessary to determine the molecular profile of luminal contents in order to test such a hypothesis.